Loughborough University

Two-Dimensional Direction of Arrival Estimation with Time-Modulated Arrays

by

Ben Clark

A Doctoral Thesis submitted in partial fulfillment of the requirements for the award of

Doctor of Philosophy of Loughborough University

Wolfson School of Mechanical, Electrical and Manufacturing Engineering

29th April, 2019

Certificate of Originality

This is to certify that I am responsible for the work submitted in this thesis, that the original work is my own except as specified in acknowledgements or in footnotes, and that neither the thesis nor the original work therein has been submitted to this or any other institution for a degree.

.... (Signed)

BEN CLARK   (Candidate)

Dedicated to Alexandra, Friends and Family,

for all of their support along the way.

Abstract

In this thesis, the use of time-modulated arrays are considered for two dimensional direction finding systems. The work has a particular aim of providing a low cost solution with small computational overhead. A solution is provided for the one-dimensional case before it is extended to work in two dimensions, whilst new techniques are considered for the control of the array.

The work focuses on utilising the simultaneously generated sidebands caused by switching the elements of the array to obtain a direction estimate and this is achieved using the power spectrum of the array's output. The use of real-valued arithmetic delivers the low computational requirement, whilst the use of switches to implement time-modulation delivers the low cost requirement.

Methods for the control and manipulation of these simultaneous beams are also given, as are the considerations needed for implementing such an array. These techniques are derived theoretically using array equations but confirmed experimentally by utilising a novel, fully featured simulation of a time-modulated planar array with customisable properties.

Acknowledgements

I would like to thank my co-supervisors, Dr. Simon Pomeroy, Dr. Paul Lepper and particularly my supervisor Dr. James Flint for the invaluable and continuous support they have given me throughout my study. I have enjoyed my time at Loughborough University partly due to their efforts and couldn't wish for better mentors. Thanks also to Loughborough University for funding my PhD and providing me with excellent training and support throughout the nine years I have been a student.

I would also like to thank my friends and colleagues who I have spent time with during my PhD. In particular: Partheepan, Arthur, Funmi, Ozak, Tasos, Gaia, Guy, Steven and Dan have all made the last few years a great experience and each have given me good advice where I have needed it.

Finally, I would like to thank my partner Alexandra and also my family who have been very supportive throughout my time as a postgraduate.

Contents

List of Figures

List of Tables

Abbreviations

ADC	Analogue to Digital Converter
AF	Array Factor
AoA	Angle of Arrival
ASIC	Application Specific Integrated Circuit
DSP	Digital Signal Processor
ESPRIT	Estimation of Signal Parameters via Rotational Invariance Techniques
DFT	Discrete Fourier Transform
DoA	Direction of Arrival
FDA	Frequency Diverse Array
FFT	Fast Fourier Transform
FPGA	Field Programmable Gate Array
LED	Light Emitting Diode
MEMS	MicroElectroMechanical Systems
MUSIC	MUltiple SIgnal Classification
RF	Radio Frequency
SNR	Signal to Noise Ratio
TMA	Time-Modulated Array
TMLA	Time-Modulated Linear Array
TMPA	Time-Modulated Planar Array
UI	User Interface

List of Symbols

C	Fourier coefficients	—
D	total number of elements	—
$d, (d_x, d_y)$	element spacing (x or y axis)	m
f_0, f_s	frequency of target or switch cycle	Hz
k	wave number	$\mathrm{rad\,m^{-1}}$
H	total number of harmonics	—
h	harmonic index number	—
L	total number of samples	—
M, N	total number of elements x or y axis	—
m, n	element index number for the x or y axis	—
P	MUSIC spectrum	—
R	element spacing/wavelength ratio	—
S	total number of switching frames	—
s	switching frame index	—
T_s	switch cycle period	s
t	time	s
$U(t)$	switching function	—
W	complex weighting	—
w	amplitude weighting	—
X	harmonic amplitude	—
β, β_x, β_y	broadside angle (x or y axis)	°
ω	angular frequency	$\mathrm{rad\,s^{-1}}$
ϕ	azimuth angle	°
φ	element phase	rad
λ	wavelength	m
τ	relative time	s
θ	single dimensional angle, elevation angle	°

List of Symbols (Matrices)

a	steering vector	—
A	steering matrix	—
g	noise vector	—
x	array output vector	—
R	covariance matrix	—
s	signal vector	—
U	signal subspace	—
Φ	Steering diagonal matrix	—

Author's Publications

Theory and results in Chapter 3 has been published in [1] and [2]. Theory and results in Chapter 4 (Sections 4.1 to 4.2.2 and 4.3) have been published in [4].

[1] B. Clark and J. A. Flint, "Acoustical Direction Finding with Time-Modulated Arrays," *Sensors*, vol. 16, no. 12, p. 2107, December 2016.

[2] ——, "Accuracy of harmonic analysis techniques for direction of arrival estimation using time modulated arrays," in *2018 12th European Conference on Antennas and Propagation (EUCAP)*, April 2018.

[3] ——, "Using the sidebands of time modulated arrays," in *6th IET Colloquium on Antennas, Wireless and Electromagnetics*, May 2018.

[4] ——, "A Method for Forming Distributed Beams in Time-Modulated Planar Arrays," *IEEE Trans. Antennas Propag.*, vol. 66, no. 12, pp. 6958–6964, December 2018.

1 | Introduction

THE ability to project a signal that can travel through space is necessary for any system that needs information without being physically connected to its environment (e.g. through a wire). Devices commonly use electromagnetic or acoustic signals to communicate through a medium. Other devices, as well as some animals make use of these signals to locate foreign objects or to understand local geometry.

1.1 The Propagation of Signals

In order to understand the properties of an input or output waveform in the real world, it must first be sampled using a sensor. Electromagnetic signals such as radio waves or microwaves can be sensed using antennas, while acoustic signals can be sensed using microphones.

Electromagnetic and acoustic waves support the similar effects of superposition and interference when sampled at a single point in time and space. If the source of the wave is sampled sufficiently far away enough for the source of the signal to be modelled as an ideal plane wave (as demonstrated in Figure 1.1) then Equation (1.1) describes the exponential form of the travelling wave at a position y in time t:

$$s(y, t) = A_0 e^{j(ky - \omega t - \phi)} \tag{1.1}$$

where A_0 is the amplitude of the wave, k is the wave constant (equal to $\frac{2\pi}{\lambda}$ where λ is wavelength) at a specific direction, ω is the angular frequency and ϕ is the initial phase of the wave.
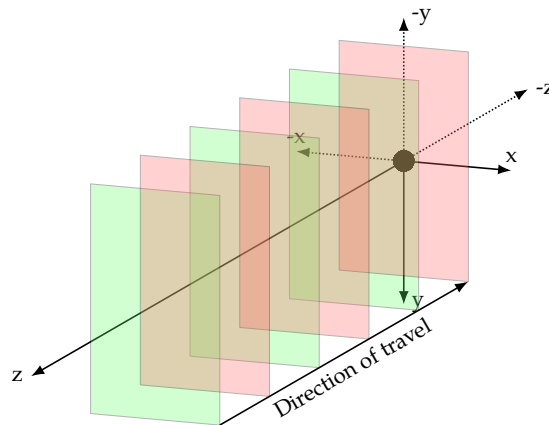
Figure 1.1: Diagram showing the plane wave propagation model, the different shaded planes represent different phases of the incoming signal.

In both types of signal, the transceivers used to propagate or sense them are usually proportional to their wavelength; the higher the signal frequency, the smaller the transceiver can be. Research into high frequency signals is increasing in interest, particularly in the fields of upcoming 5G technologies where millimetre wave signals may be used [1.1].

The identification of waveform signals has been a long-discussed topic, and one which is becoming more wide-spread as the number of devices in use that transmit signals is rapidly increasing. The prevalence of the "Internet of Things" (IoT) has driven the development of low cost sensors and actuators which have their own communication sensors built into them [1.2]. A cisco white paper reports that the number of IoT devices exceeded the human population of the world in 2008 [1.3]; even devices such as light bulbs are now available as smart devices that transmit wireless signals to an IoT driven network.

1.2   The Need for Direction Finding Systems

Following the increase in availability for devices that transmit signals, there is a greater chance that an unknown entity emits a signal that may interfere with a system. The need to know how and where a signal originated from has become a particular area of interest in this case. Direction of Arrival (DoA) (also known as Angle of Arrival (AoA)) estimation is of great importance to communication systems that need to filter

out a jamming signal propagating from an unknown direction [1.4].

Object tracking is another use case for direction finding systems. For example, it has been shown that a direction finder can be used with a variety of techniques to track patients inside a defined area [1.5].

Many techniques have been developed to identify attributes of an incoming signal such as the DoA and distance away from a target. In the previous example, multiple sensors were used in a configuration known generally as an array. Simply by adding an increased number of the same type of sensor to add to a single output stage, the system's directional response is changed as a result of differences in geometric position [1.6]. This useful property in transducer arrays mean that they are specifically studied for directional analysis or control and as such, there are a multitude of developed signal analysis techniques available to estimate the DoA of an incoming signal [1.7].

1.3   The Use of Arrays in Today's World

Many different geometric types of transducer array exist. For example, in arrays where each sensor is spaced out over a large area, it is possible to measure the Time Difference of Arrival (TDoA) and calculate a position based on the separate delayed responses from the same input signal and correlate it to each of the receivers' positions [1.8]. However, in cases where it is necessary to produce accurate DoA estimations from a single point, array networks with element spacing less than half a wavelength of the target signal are typically used [1.9].

In the case of this thesis, any set of antenna or acoustic receiver, regardless of their individual element's characteristics is defined as a sensor array. Such arrays are utilized world wide and there are many examples of arrays being utilized for directional purposes. In an extreme example, the Large acOUstic Data (LOUD) array project utilizes as many as 1020 microphones to localize or filter human voices [1.10]. At the time of writing, the largest microphone array consists of 4096 elements [1.11].

In practice, sensor arrays do not have to consist of large numbers of elements for

single applications such as DoA estimation and many examples exist for array sizes of ten elements or fewer for antennas [1.12] or acoustic transducers [1.13]. The accuracy of these cases rely on specific signal processing algorithms to extract the data from fewer sampling points, and it is usually the case that higher accuracy methods require more data or have higher computational requirement.

1.4 Problem Identification

DoA estimation is a well established theory, but due to the ever increasing availability of devices that can transmit signals there is a need to optimise the computational and financial cost requirement for direction finding systems.

Rhode & Schwarz [1.14] describe a list of requirements on direction finding systems, therefore the work in this thesis will use the following requirements as a method of measuring the effectiveness of any newly proposed direction finding techniques:

- High accuracy in determining the DoA.

- High sensitivity to small signals.

- The ability to reject noise and other interference from signals that should not be tracked.

- The ability to detect and localise a signal of short duration.

There are a plethora of approaches to spectral and DoA estimation by using arrays. The most popular algorithms make use of sub-space methods or complex arithmetic which involve a great deal of computation to produce an accurate estimation of an incoming signal; furthermore, the data of each element in the array needs to be recorded simultaneously. Systems with the specifications to perform these calculations can become expensive and therefore there is a need to reduce complexity for smaller, less complicated devices whilst maintaining the same appealing characteristics of the current technology.

The amount of research into the area of "time-modulated arrays" (TMAs) has increased recently, and their ability of generating multiple beam patterns simultaneously with only one input stage may be useful to the field of DoA estimations. There has been recent work to show that low-complexity, low power systems can be produced using TMAs [1.15]. The theories outlined in this thesis will initially focus on new methods which exploit the effects that time switching has on the data from an array of sensors.

1.5   Research Aim

The purpose of this study is to produce techniques that can be used for reducing complexity or cost in sensor arrays with a particular focus on direction of arrival estimation. Real signals can come from a two-dimensional heading (which may be represented as azimuth and elevation angles), therefore it is important to show the implications of using DoA techniques for 2D estimation.

It is also understood that array theory can be applied to electromagnetic and acoustic waves alike; however fewer publications can be found on ultrasonic arrays due to the small wavelengths associated with acoustic signals compared to the usual size of a corresponding sensor. As such, the work outlined in this thesis aims to be applicable to both Radio Frequencies (RF) and acoustic waves.

1.6   Structure of Thesis

Chapter 2 provides a background into array theory and the current state of the art for direction finding systems using arrays. The history and theory of time modulation is provided and introduces the latest concepts that implement them for direction finding theories.

Chapter 3 introduces a novel method of determining a one-dimensional DoA using time-modulated linear arrays, as well as introducing a way of reducing errors caused near null regions. The concept is explained and numeric data is provided, comparing

its accuracy and computation speed to existing techniques in the literature.

Chapter 4 introduces the use of individual element switching on time-modulated planar arrays, and extends on the previous theories of existing work and that of the previous chapters to show how 2D array weighting systems can be generated. These traits are used to derive two-dimensional DoA algorithms.

Chapter 5 focuses on the considerations needed for the implementation of the concepts explained in Chapters 3 and 4. It details examples of how a time-modulated array can be implemented, both in simulation and using different types of controller.

Finally, Chapter 6 concludes the work and details areas of future work.

1.7   Contributions of Thesis

The contributions of this work include:

- Chapter 3 introduces a novel method of determining DoA using the sidebands generated by time-modulated linear arrays, as well as introducing a way of reducing errors caused near the array's null regions. It also gives some insight into the problems arising from using fewer elements with existing techniques.

- Chapter 4 shows a novel numerical method of generating uniquely positioned sidebands with time-modulated planar arrays and extends on the novel method introduced in Chapter 3 to provide 2D DoA estimations. It is the first demonstration of a 2D estimation being achieved by using only one sensor at an instance of time with a planar array.

- Chapter 5 details the development of a novel simulation of time-modulated arrays which allows a user to implement any switching pattern and see the relevant harmonics generated. It also has some novel considerations of the effect that time controlled weighting systems have on planar arrays.

References

[1.1] T. S. Rappaport, S. Sun, R. Mayzus, H. Zhao, Y. Azar, K. Wang, G. N. Wong, J. K. Schulz, M. Samimi, and F. Gutierrez, "Millimeter Wave Mobile Communications for 5G Cellular: It Will Work!" *IEEE Access*, vol. 1, pp. 335–349, 2013.

[1.2] M. Swan, "Sensor Mania! The Internet of Things, Wearable Computing, Objective Metrics, and the Quantified Self 2.0," *J. Sens. Actuator Networks*, vol. 1, no. 3, pp. 217–253, November 2012.

[1.3] D. Evans, "The Internet of Things - How the Next Evolution of the Internet Is Changing Everything," Cisco Internet Business Solutions Group, Tech. Rep., 2011. [Online]. Available: https://www.cisco.com/c/dam/en{_}us/about/ac79/docs/innov/IoT{_}IBSG{_}0411FINAL.pdf

[1.4] K.-I. Lee, W. Kang, Y.-S. Chung, H.-G. Yang, and J. M. Kim, "A New Jammer Suppression Method in MIMO Radar Using Matrix Pencil Method and Generalized Likelihood Ratio Test," *Int. J. Antennas Propag.*, vol. 2015, pp. 1–8, 2015.

[1.5] L. Wan, G. Han, L. Shu, S. Chan, and T. Zhu, "The Application of DOA Estimation Approach in Patient Tracking Systems with High Patient Density," *IEEE Trans. Ind. Informatics*, vol. 12, no. 6, pp. 2353–2364, December 2016.

[1.6] H. Krim and M. Viberg, "Two decades of array signal processing research: the parametric approach," *IEEE Signal Process. Mag.*, vol. 13, no. 4, pp. 67–94, July 1996.

[1.7] L. Godara, "Application of antenna arrays to mobile communications. II. Beamforming and direction-of-arrival considerations," *Proc. IEEE*, vol. 85, no. 8, pp. 1195–1245, 1997.

[1.8] H. Xiong, Z. Chen, W. An, and B. Yang, "Robust TDOA Localization Algorithm for Asynchronous Wireless Sensor Networks," *Int. J. Distrib. Sens. Networks*, vol. 11, no. 5, May 2015.

[1.9] S. Haykin and K. J. R. Liu, *Handbook on Array Processing and Sensor Networks*. Wiley-IEEE Press, 2009.

[1.10] E. Weinstein, K. Steele, A. Agarwal, and J. Glass, "LOUD : A 1020-Node Microphone Array and Acoustic Beamformer," *Int. Congr. Sound Vib.*, 2007.

[1.11] Guinness World Records Limited, "Largest Microphone Array," 2014. [Online]. Available: http://www.guinnessworldrecords.com/world-records/largest-microphone-array/

[1.12] N. Karavassilis, D. E. N. Davies, and C. G. Guy, "Experimental HF circular array with direction finding and null steering capabilities," vol. 133, no. 2, pp. 147–154, 1986.

[1.13] J. Pierre and M. Kaveh, "Direction-Finding Using a Laboratory Experimental Array Testbed," in *Fifth ASSP Work. Spectr. Estim. Model.*, Rochester, NY, USA, 1990, pp. 114–118.

[1.14] Rohde & Schwarz, "Introduction into Theory of Direction Finding," *Radiomonitoring & Radiolocation*, pp. 26–49, 2010.

[1.15] R. Maneiro-Catoira, J. Brégains, J. García-Naya, and L. Castedo, "Time Modulated Arrays: From their Origin to Their Utilization in Wireless Communication Systems," *Sensors*, vol. 17, no. 3, p. 590, March 2017.

2 | Background

Iɴ order to consider what is required for a direction of arrival estimator, it is important to understand the underlying technology and how it has been used so far. This chapter discusses array theory and how arrays have previously been used to track signal sources in space. The benefit of time modulation is outlined, and suggestions for expanding on the theory are made which will be explored in further detail in the following chapters.

2.1 Conventional Arrays

If a set of transducers are placed in an array, the summation of their individual outputs has different directional characteristics when compared to one of the single elements. This change in directivity is fundamentally determined by the effects of superposition, caused by the different phase of the same signal that each sensor receives.

Consider a uniform linear array of sensors with spacing d between adjacent elements. If a plane wave impinges on the array at an angle θ relative to the array's broadside (perpendicular), each element will receive the signal at different times. This time delay can be calculated by:

$$t_d = -\frac{d \sin \theta}{c} \tag{2.1}$$

where c is the speed of the signal.

In a linear array of N elements, the signal of each output can be summed to produce a very different response based on incident angle. If the input to the array is a single

frequency signal, the overall received signal can be described by the equation

$$y(t_d, t) = \sum_{n=0}^{N-1} e^{j\omega(t + t_d n)} \tag{2.2}$$

where $n = 0$ marks the first element of the array and each adjacent element is then indexed incrementally (so that the element on the opposite side of the array to element 0 is indexed as $n = N - 1$). The first element of the array marks an arbitrary reference origin to calculate the distances of the other elements. Using Equation (2.1) the array's time domain response can be expressed as a function of the target angle:

$$y(\theta, t) = e^{j\omega t} \sum_{n=0}^{N-1} e^{jknd \sin\theta} \tag{2.3}$$

The array's relative response is maximised when $e^{j\omega t} = 1$, and removing this from Equation (2.3) also removes the equation's dependency on time, thus we have a method of calculating the directivity of a particular array. This form of the array's response is widely known as the *Array Factor* or AF.

Since each element of the array has a different associated delay depending on the angle of arrival, a set of isotropic elements has a maximum response towards the broadside of the array (where there is zero delay) and a lower response when the incident wave is received from any other angle, as shown in Figure 2.1. For consistency in array models given later in the text, a positive angle can be seen as causing a negative time delay.

2.1.1 Sidelobes and Element Weighting

It can be noticed that although the output of the system described above is maximised with broadside signals, there are approaches on the sides of the array which exhibit some (albeit much smaller than the main beam) signal strength, these sidelobes can have an impact on signal quality if the noise or interference away from the target angle is sufficiently large enough. By changing the individual gain of each element, the shape of the directivity pattern changes and specific patterns can be formed. If it is only important

(a) Array Setup

(b) Array Response
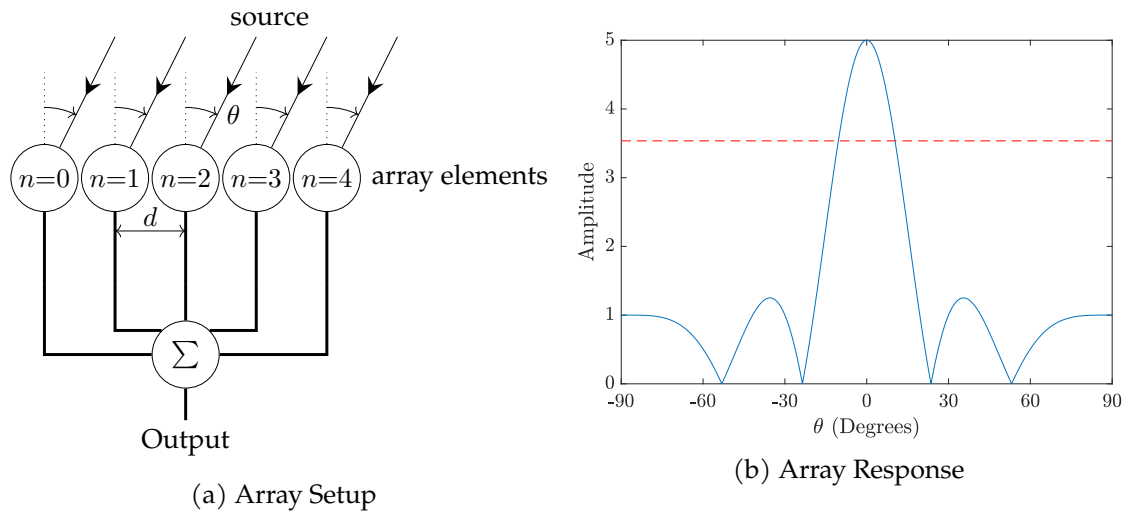
Figure 2.1: The setup (a) and output (b) of a five-element linear array of transducers. The dashed line shows the 3dB point.

to receive information from one main beam, then it is often desirable to reduce the effect of the sidelobes by adjusting the nth element's weighting w_n. The array factor equation for this situation simply becomes:

$$AF(\theta) = \sum_{n=0}^{N-1} w_n e^{jknd \sin \theta} \tag{2.4}$$

Commonly used weighting combinations known as shading patterns include the binomial, and Dolph-Chebyshev patterns [2.1]. Each of these patterns have different characteristics which are useful in different situations [2.2]. Figure 2.2 shows how a typical system achieves individual element weighting.

Binomial Weighting

Binomial shading changes the amplitude of individual elements in the array according to the binomial coefficients and signifies the relative ratio of the current for each element [2.2, 2.3]. The shading pattern minimises the sidelobes and for elements spaced out less than half a wavelength of the target signal apart, only one main beam is present. Table 2.1 shows the weighting values needed to achieve a binomially weighted 5-element array, and Figure 2.3 shows its typical Array Factor.
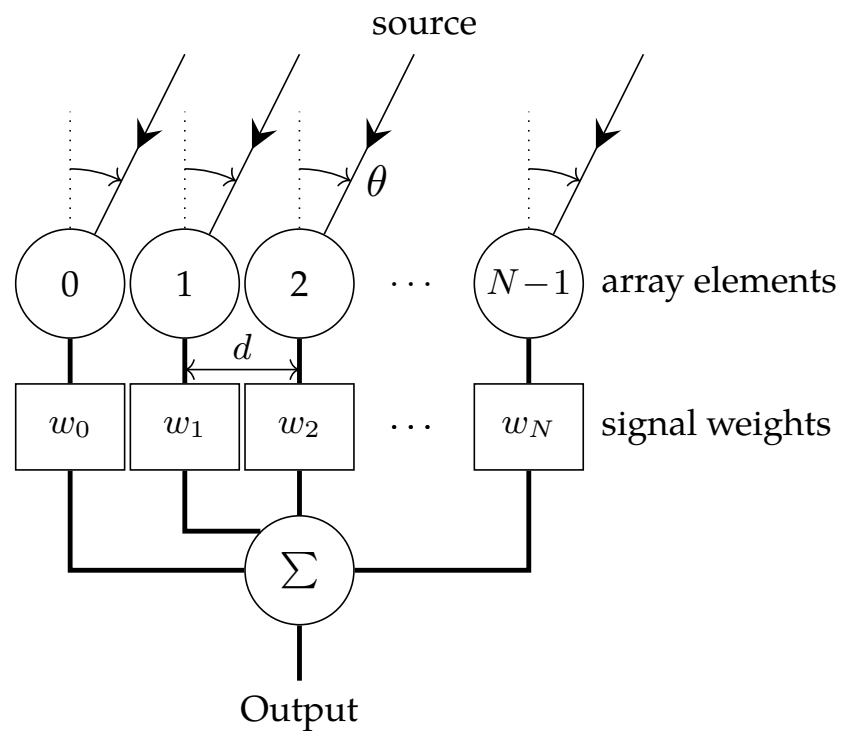
Figure 2.2: An example of an N-element conventional array with individual element weightings.

Table 2.1: The element weightings needed for a 5-element binomially weighted conventional array

w_0	w_1	w_2	w_3	w_4
1	4	6	4	1
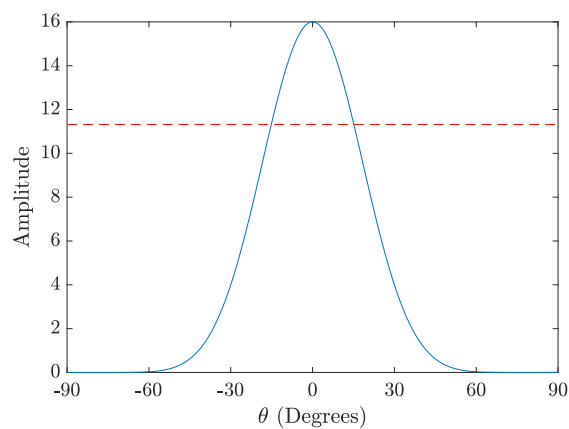
Figure 2.3: Typical response of a five-element conventional array with binomial element weightings. The red line shows the 3dB point.

Table 2.2: The element weightings needed for a five-element conventional array to obtain -20dB sidelobes

w_0	w_1	w_2	w_3	w_4
1.00	1.61	1.94	1.61	1.00

Although removing the side-lobes completely is usually seen as beneficial, the drawback of using binomial shading is that the main beam gets wider compared to that of an evenly weighted array. In the case of a five-element array the beam-width (the amount of angle above a half-power or -3dB point shown in red in Figure 2.3) is $21°$ for an evenly weighted array but approximately $31°$ for a binomially weighted array [2.3].

Dolph-Chebyshev Weighting

The Dolph-Chebyshev shading technique was produced by Dolph in 1946 [2.1] and is used for arrays in which the width of the main beam needs to remain as small as possible whilst reducing the sidelobe levels significantly. This shading factor can adjust the magnitude of the side-lobes to the same level (in contrast to an equally weighted distribution) by making use of Chebyshev polynomials to determine the weighting ratios for each element. This shading technique also allows the size of the sidelobes to be selected. In example, for a five element array the weighting distribution in Table 2.2 has been shown by Stuzman and Davis [2.4] to provide a sidelobe level of -20dB relative to the maximum possible as shown in Figure 2.4. The main beam-width for this system is approximately $24°$.

2.1.2   Phased Array Systems

The introduction of intentional delay stages at each element provides a means of introducing both magnitude and phase changes (known as complex weighting) to the array factor. As mentioned previously, manipulating the phase of each individual element φ_n (in addition to the static weighting) changes the directivity shape and direction of the
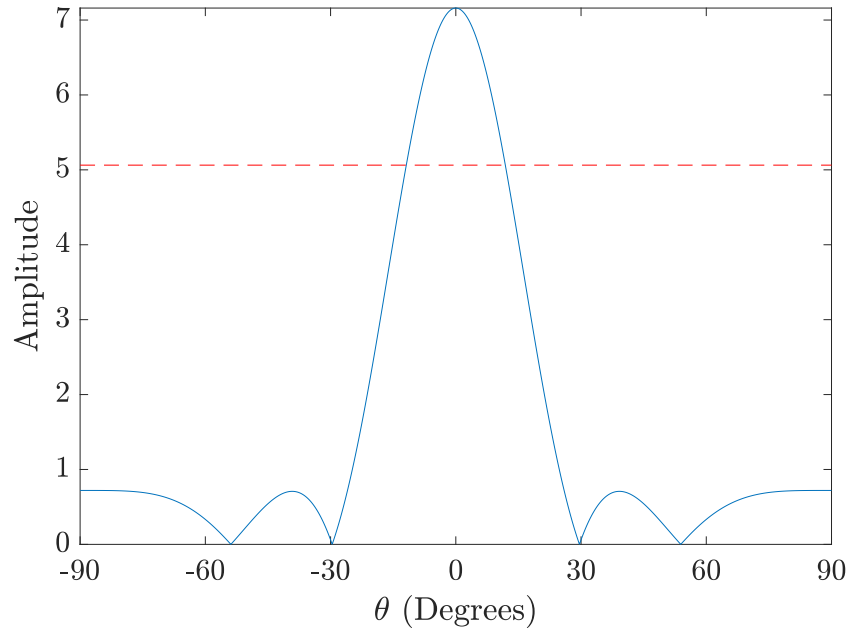
Figure 2.4: A typical response of a five-element conventional array with Dolph-Chebyshev weightings. The dashed line shows the 3dB point.

main beam, therefore Equation (2.4) becomes

$$AF(\theta) = \sum_{n=0}^{N-1} W_n e^{jknd\sin\theta} \tag{2.5}$$

where

$$W_n = w_n e^{-j\varphi_n} \tag{2.6}$$

When the selected phase change at each element is equal in magnitude (but opposite in direction) to the phase difference (of the incoming signal) experienced at each element, then the array system becomes most responsive towards the angle of incidence of the source. This process is known as *beam steering*. In mathematical terms, the array's response is maximised when the imposed phase change φ_n between adjacent transceivers matches the phase change caused by the time delay t_d.

For example, following the same array setup as in Figure 2.1, a 40 kHz acoustic signal impinging on an array at an angle of $45°$ ($\frac{\pi}{4}$ radians) will have a per-element time delay t_d of 8.83 microseconds, therefore each element will require a relative phase shift of $127.28°$ (2.22 radians) in order for the array to become most receptive in the direction of the

(a) Array Setup

(b) Array Response
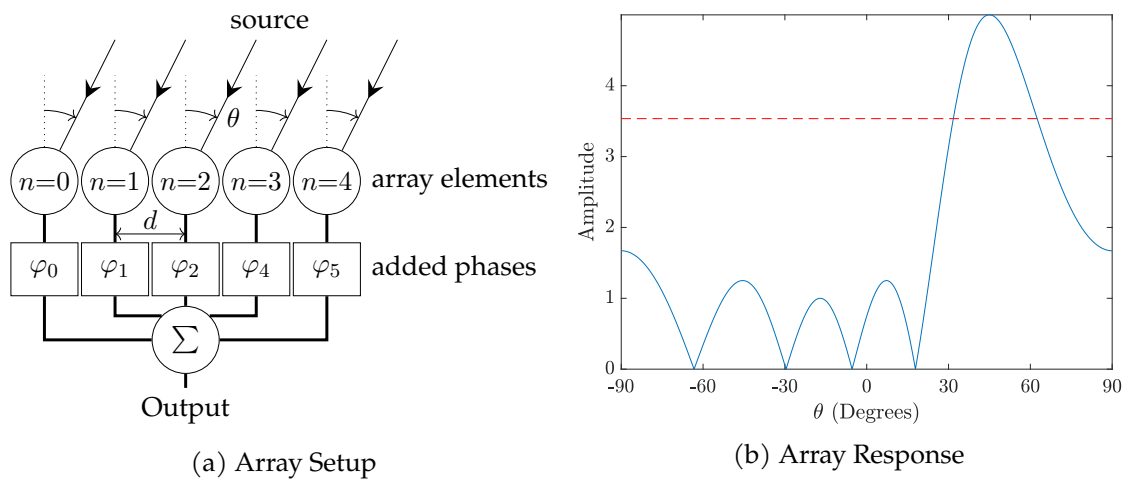
Figure 2.5: The setup (a) and output (b) of a five-element linear array of transducers with a incremental phase shift of 2.22 radians. The dashed line shows the 3dB point.

signal. This new system is shown in Figure 2.5. In antenna systems, steering the beam using time delays is preferred over complex weightings because the steering direction is not dependant on frequency [2.3].

The theory of array weighting also applies to phase shifted arrays; since the amplification of signals has no effect on the phase interference, the effect of static weightings as described in Section 2.1.1 is applied irrespective of steering caused by phase shifters. Following on from the example above, Figure 2.6 shows the directivity patterns if the same array setup were to have the binomial shading pattern applied to them. It can be noticed that all properties of the array factor without any phase shifters on individual elements are seen in the steered version also, such as the controlled level of sidelobes.

2.1.3   Null Steering

Just as the direction where the array is most responsive to incoming signals can be controlled, the directions where the array is least responsive can also be controlled. This can be useful when there is a known noise present, such as an unrelated transmitter operating on the same frequency. By controlling the complex weighting of the system it is possible to steer these nulls into a position where the array is least affected by the presence of the interference.

There has been recent work that has described methods of using optimisation meth-

(a) Array Setup

(b) Array Response
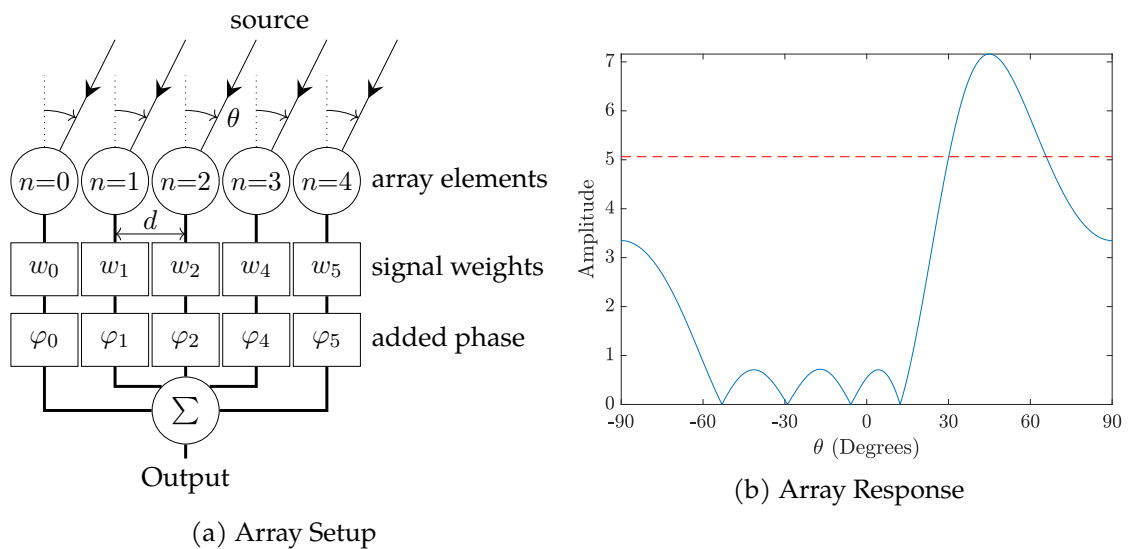
Figure 2.6: The setup (a) and output (b) of a five-element linear array of transducers with a incremental phase shift of 2.22 radians and a weighting system to produce -20dB sidelobes. The dashed line shows the 3dB point.

ods to generate multiple beam-paths with at least one null region; either by controlling the phases alone [2.5], or by changing the amplitudes and phases of each element [2.6]. This work makes use of genetic or iterative computational algorithms which progress through multiple trials of different complex weights and keep hold of the result which most closely matches the desired characteristics.

2.2   Direction Finding with Conventional Arrays

As the mobility of communicating devices increases, the demand for adaptive direction finders becomes greater. Knowing the position of a device can be critical in the areas both communications and in military applications.

In one of the most basic examples, it is possible to locate a transmitting source by means of recording the relative delay between each receiving part of a sensor network and calculating its position by means of trilateration or triangulation, providing that the location of all receivers are precisely known. In these systems, sensors are typically distributed across large areas and it is expected that the transmitter will be somewhere with the area formed by each receiver. The thesis will consider arrays where all sensors can be seen at one point but can have various arrangements, typically with each element

being spaced out less than a wavelength of the incoming signal.

According to [2.7], there are three main categories of direction finding methods: "Beamforming", "maximum likelihood" and "subspace". Each of these methods have the same main requirements needed of direction finding systems.

Each method has different performance characteristics that need to be carefully considered when developing a system [2.8] and their strengths and weaknesses will be summarised in the following sections.

2.2.1 Beamforming Methods

Conventional beam steering makes use of being able to steer a beam in a particular direction. A sweeping analysis of a signal can be performed by gradually changing the angle of the receive beam and then monitoring the power received.

The steering angle can be changed mechanically by rotating the whole array and correlating the maximum power received to the angle of rotation. Mechanical systems however depend on the speed of the antenna's rotation; conventional phased arrays are able to resolve this problem by changing the phases of individual received signals from each sensor to target a specific angle as described in Section 2.1.2.

2.2.2 Subspace Methods

Subspace methods are mathematical techniques used for dimension (such as spectral or direction) estimation, and are especially useful for making estimations in the presence of definable noise (usually Gaussian distributed noise). These methods work by reducing a set of samples down to a specific dimension, and in the case of direction finding, multiple DoAs can be scanned. Two of the most widely applied subspace methods used in the field are the MUSIC [2.9] and ESPRIT [2.10] algorithms.

MUSIC

The MUltiple SIgnal Classification algorithm was proposed by Schmidt in 1986 [2.9] as a method of detecting multiple signals from different directions in the presence of Gaussian distributed noise. Schmidt proposed that if each sensor of an N element array captured the data of D signals, then the matrix x can be modelled as:

$$
\begin{bmatrix} x_0 \\ x_1 \\ x_2 \\ \vdots \\ x_{N-1} \end{bmatrix} = \begin{bmatrix} a(\theta_1) & a(\theta_2) & \ldots & a(\theta_D) \end{bmatrix} \begin{bmatrix} s_1 \\ s_2 \\ \vdots \\ s_D \end{bmatrix} + \begin{bmatrix} g_0 \\ g_1 \\ g_2 \\ \vdots \\ g_{N-1} \end{bmatrix}
\tag{2.7}
$$

or

$$
x = As + g
\tag{2.8}
$$

In Equation (2.7), the A matrix can be described as a two-dimensional matrix of exponentials which describe the known $N \times D$ functions of element response and signal arrival directions (a matrix of steering vectors). For example, a linear array will have steering vectors similar to the individual elements in Equation (2.3) seen previously:

$$
a(\theta) = \begin{bmatrix} 1 \\ e^{-jkd\sin\theta} \\ e^{-jk2d\sin\theta} \\ \vdots \\ e^{-jk(N-1)d\sin\theta} \end{bmatrix}
\tag{2.9}
$$

where s is a matrix of D signals and g is a vector of N sets of noise samples. If the noise is evenly distributed (i.e. white noise) then the covariance matrix of x of L samples can be calculated as

$$
R_{xx} = \frac{xx^H}{L} = AR_{ss}A^H + \sigma^2 I
\tag{2.10}
$$
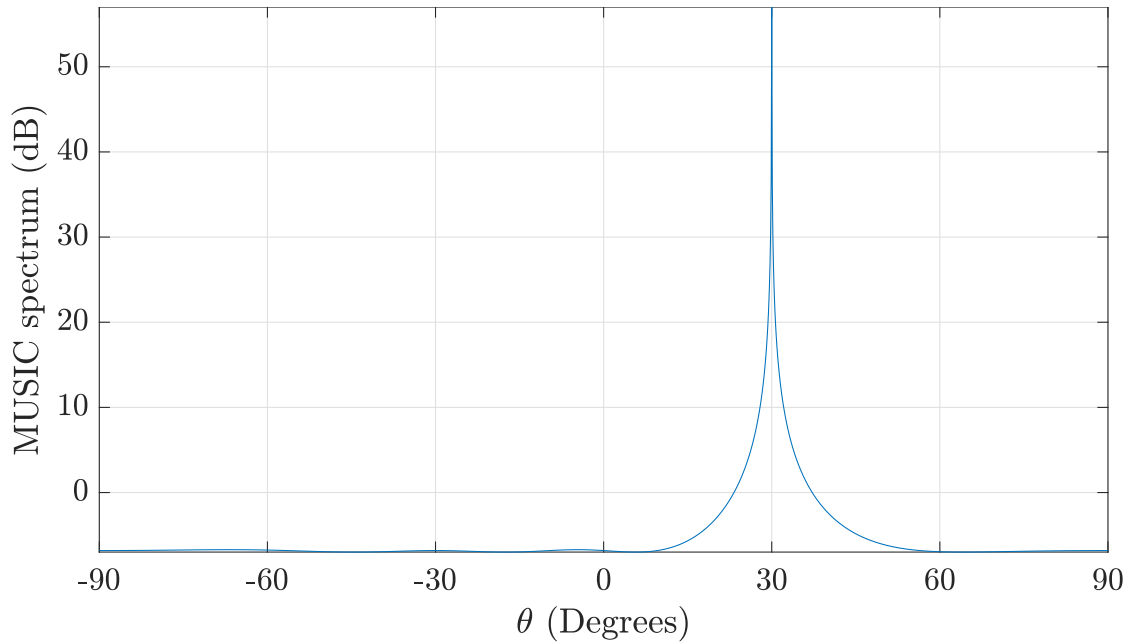
Figure 2.7: Example MUSIC spectrum calculated from a five element array and a signal propagating from $30°$.

where $\boldsymbol{I}$ is an $N \times N$ identity matrix, $\boldsymbol{R_{ss}}$ is the covariance matrix of $\boldsymbol{s}$ and $\boldsymbol{A}^H$ is the Hermitian transpose of $\boldsymbol{A}$.

Schmidt showed that if an ordered eigendecomposition of $\boldsymbol{R_{xx}}$ is made (eigenvalues ordered according to value and their corresponding eigenvectors arranged in the same order) then the smallest eigenvectors formed the noise subspace and the largest eigenvectors formed the signal subspace. The number of the vectors in the signal subspace should be the same as the number of signals, which should be known beforehand. If these subspaces are separated into their separate matrices then the noise subspace can be used to scan a particular direction for (the lack of) signals. A spectrum can be therefore obtained:

$$\boldsymbol{P_{music}}(\theta) = \frac{1}{\boldsymbol{a}^H(\boldsymbol{\theta})\boldsymbol{E_n}\boldsymbol{E_n^H}\boldsymbol{a}(\boldsymbol{\theta})} \tag{2.11}$$

By changing the value of θ iteratively until all relevant values are explored, it is possible to see peaks where the MUSIC algorithm is responsive to a signal in the chosen direction. Figure 2.7 shows a typical spectrum where a signal impinges on a five-element linear array at an angle of $30°$ in the presence of Gaussian distributed noise. It can be seen that the peaks occur at the exact position of the incoming signal.
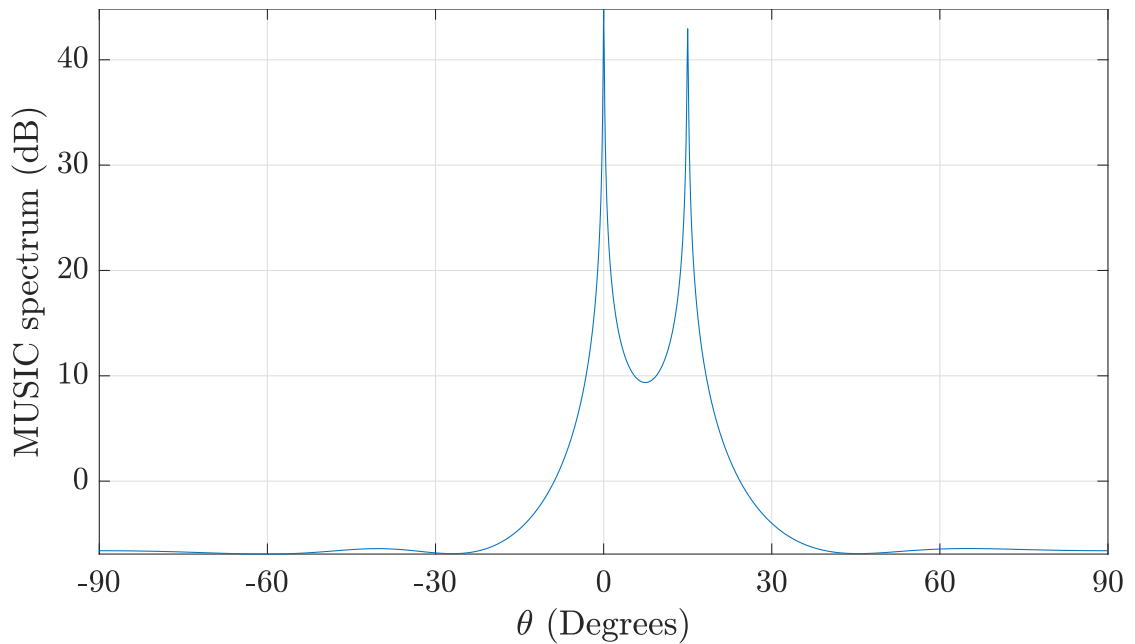
Figure 2.8: Example MUSIC spectrum calculated from a five element array and two non-coherent signals propagating from $0°$ and $15°$ respectively.

One major advantage of the MUSIC algorithm is that it can simultaneously scan for multiple signals, if two signals of a different frequency were transmitted towards the system described above at the same amplitude but from the direction of $0°$ and $15°$, then the MUSIC spectrum changes to represent the additional signal as shown in Figure 2.8. The general MUSIC algorithm described by Schmidt can detect up to $N-1$ incoherent signals.

It can be seen from Figure 2.8 that two sharp peaks correctly represent the signals and provides a good case for the use of MUSIC, however if an attempt was made to analyse two coherent signals, then the associated MUSIC spectrum would look more like Figure 2.9.

Here it can be seen that the information in the MUSIC spectrum is harder to interpret. This shows the disadvantage that current commonly used subspace algorithms have when trying to analyse coherent (same frequency/phase sources) and as a result, the MUSIC algorithm has been extended upon to deal with some short comings. For example, works by Li et al. [2.11] demonstrate that the MUSIC algorithm is effective even with coherent signals if the array samples are taken in a non-uniform manner.

Whilst accurate, the MUSIC algorithm is very computationally expensive due to the
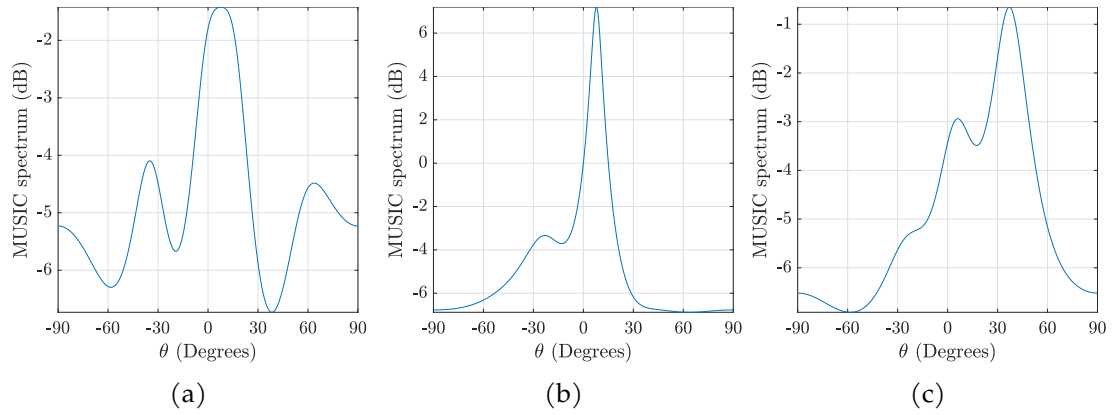
Figure 2.9: Example MUSIC spectrum calculated from a ten element array and two coherent signals propagating from $0°$ and $15°$ respectively, the simulation was run three times to display the effect of randomised noise on the estimation.

complexity of eigendecomposition as well as the need to scan each direction first; this becomes more difficult to process for larger numbers of elements used or the number of samples per element. It should also be highlighted that the process described can be followed only when there are fewer expected signals than there are sensors.

ESPRIT

Roy et al. developed the Estimation of Signal Parameters via Rotational Invariance Techniques (known as ESPRIT) in 1987, a few years after the MUSIC algorithm was developed and extended on the general theory onwards [2.10, 2.12]. Like MUSIC, ESPRIT provided high-resolution signal parameter estimation but depending on the situation can provide better performance and computational advantages. The key problems identified in MUSIC but mitigated in ESPRIT are the reduction in computational cost and the ability to use an arbitrary array geometry (under certain conditions outlined later) which reduces the calibration dependence of the algorithm.

If an arbitrary array of *doublets* (a pair of identical sensors with a set distance between them) of the same orientation was setup then two subarrays (each with N elements) $\boldsymbol{x}$ and $\boldsymbol{y}$ can be defined by selecting one of each sensor in the doublet. These subarrays will be spaced a distance d apart. The same signal model from Equation (2.7) can be used but the secondary array $\boldsymbol{y}$ will have its own distributed noise and a delay caused by the

position offset from x:

$$x = As + g_x$$
$$y = A\Phi s + g_y$$
(2.12)

where Φ represents a $D \times D$ diagonal matrix of exponents:

$$\Phi = \begin{bmatrix} e^{jkd\sin\theta_1} & 0 & 0 & 0 \\ 0 & e^{jkd\sin\theta_2} & 0 & 0 \\ 0 & 0 & \ddots & 0 \\ 0 & 0 & 0 & e^{jkd\sin\theta_D} \end{bmatrix}$$
(2.13)

If Φ can be estimated then each angle of the signal source can be derived also. Therefore the full system model in this case can be defined [2.10, 2.13]:

$$z(t) = \begin{bmatrix} x(t) \\ y(t) \end{bmatrix} = \begin{bmatrix} A \\ A\Phi \end{bmatrix} s(t) + \begin{bmatrix} g_x(t) \\ g_y(t) \end{bmatrix}$$
(2.14)

Just like the MUSIC algorithm, the correlation matrix of z needs to be computed and the eigenvectors of this correlation matrix can be sorted and separated into a noise and signal subspace U_s, each of which can be separated into submatrices x and y of same rank D

$$U_s = \begin{bmatrix} U_x \\ U_y \end{bmatrix}$$
(2.15)

and

$$U_x \Psi = U_y$$
(2.16)

By solving linear Equation (2.16) for Ψ, Roy et al. showed that the eigenvalues $\hat{\lambda}_\Psi$ for this matrix were equivalent to the diagonal elements of Φ, therefore a final expression

can be formed to calculate the DoAs of each of the signals [2.14]

$$\theta_D = \arcsin\left[\frac{-\arg(\log(\hat{\lambda}_{\Psi_D}))}{dk}\right] \tag{2.17}$$

Although ESPRIT requires more matrix manipulation and an extra eigendecomposition stage than a single MUSIC pass, overall this technique is computationally faster than the MUSIC algorithm because each signal direction can be solved in the expression above directly, without performing a scan of all possible angles. It does however require twice as many sensors to match the MUSIC criteria of $N > D$ and is therefore unusable by systems with a requirement of detecting as many signals as possible whilst using a minimal number of sensors.

Whilst MUSIC is favourable for systems that need to minimise the number of sensors used, ESPRIT is favourable for systems that have lower computational power. In either case the computations performed by either algorithm require manipulation and eigendecomposition of large matrices, which can be a difficult task for low-end processors.

Another caveat of subspace systems in general is that each element in the array has to be individually sampled which can be both computationally expensive and costly depending on the number of sensors used.

2.2.3 Maximum Likelihood

Maximum likelihood estimation uses statistical analysis using a mathematical model of a system to estimate which out of a set of signals travelling in different directions would most likely cause the occurrence of collected samples [2.15, 2.16]. Whilst the maximum likelihood methods use statistical modelling to estimate the most probable value for signal parameters, these methods are popular due to them being able to be used fairly consistently for a variation of configurations, provided that the likelihood equations are worked out beforehand. The theory has been applied to the array field [2.17].

A major concern for maximum likelihood estimators is their dependence on the number of samples taken [2.18], as high accuracy estimations are usually derived from large

sets of data; this means that if a source emitted a signal of short duration, the resultant maximum likelihood estimator may become inaccurate or biased towards noise in the readings. This is especially true for sources that are travelling, and when it is unknown when the signal source will start or finish, such as a sound emitted from an animal.

2.3   Frequency Diverse Arrays

While phased arrays provide the means for controlling the direction of a beam, there are other desirable features such as the ability to adjust range or the number of signals that are transmitted simultaneously [2.19]. As a result, array concepts with differing controllable properties per element have been developed.

Frequency Diverse Arrays (FDAs) were first introduced by Antonik et al. [2.20], who showed that by applying an additional frequency shift for each transmitter in an array, a scan angle that varies by range can be produced. From this concept, localisation methods using MUSIC have been produced [2.21] which can show some immunity to interference from targets that are in the same heading, but at a different range [2.22].

One of the major disadvantages of FDAs is the need produce multiple waveforms which may make them unsuitable if it is desirable to produce low cost systems with reduced complexity.

2.4   Time-Modulated Arrays

Whilst the control of each element's phase and amplitude provides a versatile way of being able to specify an exact direction to steer the main beam, the process of changing a signal's phase in real-time can be costly or computationally expensive and increasing the functionality of these systems requires complex designs. In addition, techniques which require multiple waveforms to be produced or scanned (such as in FDAs or subarray architectures) can become difficult or expensive to design.

In 1959 Shanks and Bickmore [2.23] proposed that the increase in demands of an-

tenna systems meant that a new fundamental technique using four-dimensions needed
to be described. This technique used elements in any array that were modulated in a
periodic manner. A periodic function applied to a signal generates Fourier components
that are time dependant, which means that multiple harmonic content with separate
spatial beam patterns can be produced. Shanks and Bickmore showed that the use of
time-domain techniques on an antenna had many desirable properties including finer
control on sidebands when compared with conventional arrays, as well as the intro-
duction of multiple steered beam paths [2.23, 2.24]. The equations for time-modulated
arrays can be likened to the conventional array Equation (2.3) but with the inclusion of
a time varying weighting function $U(t)$ instead of a static weighting function:

$$AF\left(\theta\right) = \sum_{n=0}^{N-1} U(t)e^{jknd\sin\theta} \tag{2.18}$$

The most simple case of implementing a time-varying function is to switch the ele-
ments of the array "on" or "off" in sequence as shown in Figure 2.10. In this case, the
function $U(t)$ can be defined as:

$$U_n(t) = \begin{cases} 1, & \tau_{n,on} \leq t < \tau_{n,off} \\ 0, & \text{otherwise} \end{cases} \tag{2.19}$$

where $\tau_{n,on}$ and $\tau_{n,off}$ are the switch on and off times respectively for the nth element
in the array.

2.4.1   Sidebands

There are many examples where multiple elements are switched on and off at the same
time [2.25, 2.26, 2.27]. Zhu et al. [2.27] demonstrated the time-domain output of a TMA
by using a switching pattern where six elements are on at any one time. This produces
the same effect as conventional arrays at any instance in time, but switching to a different
combination of elements produces a different directivity pattern. The work in [2.27] ex-
plains that whilst the instantaneous array factor has one frequency component, the peri-
odic switching to different combinations creates different frequency components overall.
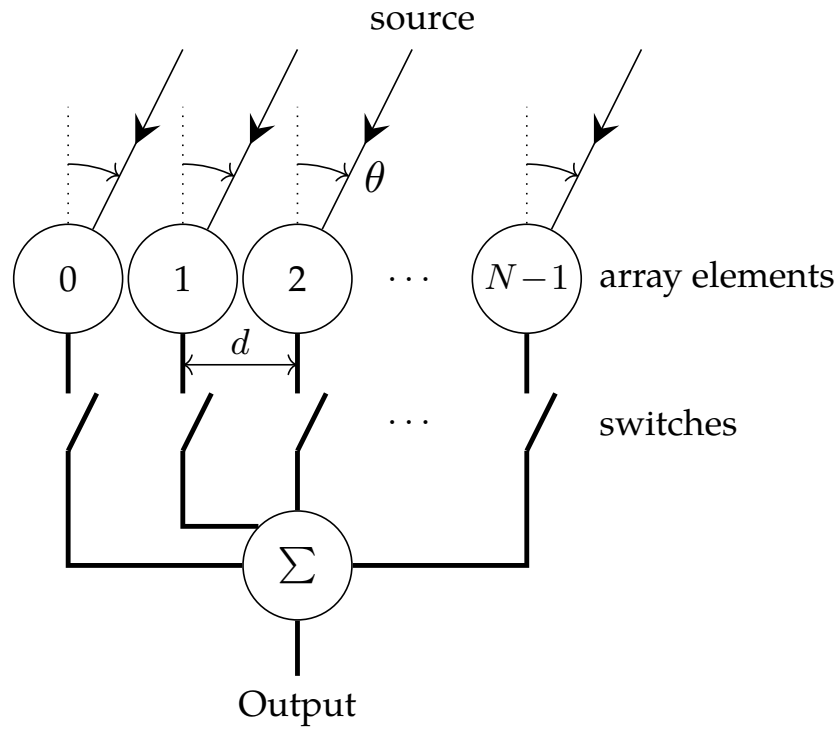
Figure 2.10: Example schematic of a time-modulated linear array with N elements spaced d distance apart.

These frequency components are known as sidebands.

Systems where many elements are on at the same time in different combinations can become difficult to describe numerically. In many of these cases, the systems were designed to suppress the production of sidebands. As mentioned in [2.25] and [2.27], the use of sidebands may be beneficial for systems that require directivity.

If each element is switched on then off uniformly in sequence (as shown in Figure 2.11), $U_n(t)$ becomes a periodic function and can be more easily formulated as an infinite sum of Fourier components indexed by h, each with coefficient $c_{h,n}$ [2.28]:

$$U_n(t) = \sum_{h=-\infty}^{\infty} c_{h,n} e^{-j2\pi h f_s t} \tag{2.20}$$

where the coefficients can be calculated as [2.24, 2.28]

$$\begin{aligned} c_{h,n} &= \frac{1}{T_s} \int_0^{T_s} U_n(t) e^{-jh2\pi f_0 t} dt \\ &= \frac{\sin \frac{\pi h}{N}}{\pi h} e^{\frac{-j2\pi h n}{N}} \end{aligned} \tag{2.21}$$
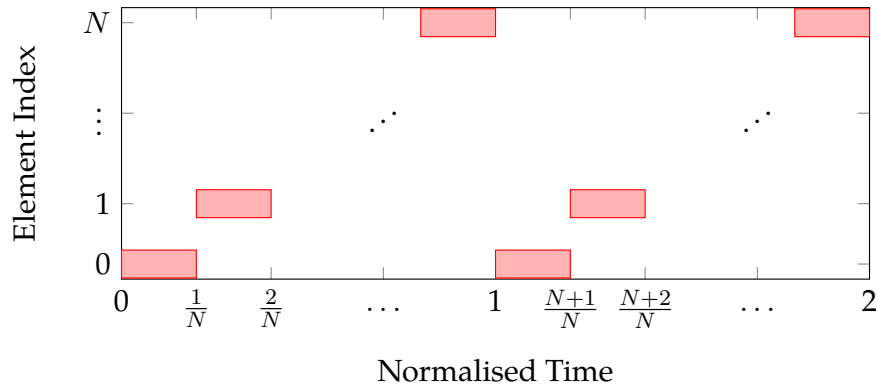
Figure 2.11: Example of an on/off time sequence for an array of N elements. A bar represents the time that an element is currently on.

The signal power is distributed among an infinite series of harmonics related to the switching pattern frequency $f_s = 1/T_s$, and centred on a main frequency f_0. Using the above equations, the array factor for a particular harmonic h can be calculated as:

$$AF(h, \theta) = \frac{\sin \frac{\pi h}{N}}{N \pi h} \sum_{n=0}^{N-1} e^{\frac{-2j\pi h n}{N}} e^{jknd \sin \theta} \tag{2.22}$$

In a two-element example where the elements are spaced out at half-wavelength this produces beam-patterns at the main frequency f_0 and $f_0 \pm f_s$ as shown in Figure 2.12. A three-element example is also shown in Figure 2.13, which has the same number of sidebands, but these are no-longer directed at the array's end-fire and point towards different directions.

2.4.2   Direction of Arrival Estimation with Time-Modulated Arrays

In the specific example described in Section 2.4.1 (where each element is switched uniformly in sequence), these sidebands are responsive in different directions and have their own array factors. This property of Time-Modulated arrays has only recently been exploited and appears to be a research area increasing with interest.

In this section, the two main direction-finding theories discussed in Wang et al.'s overview of time-modulated arrays [2.19] are discussed, both of which use two elements.
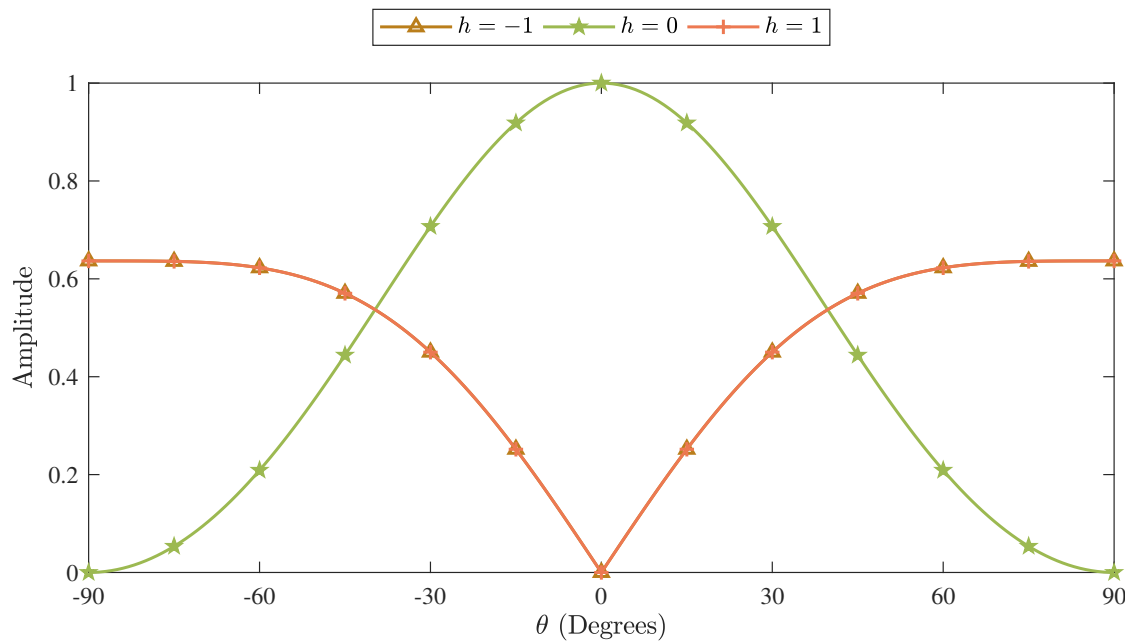
Figure 2.12: Array Factor of a two-element array with half-wavelength element spacing where the elements are switched between each other for the same period.
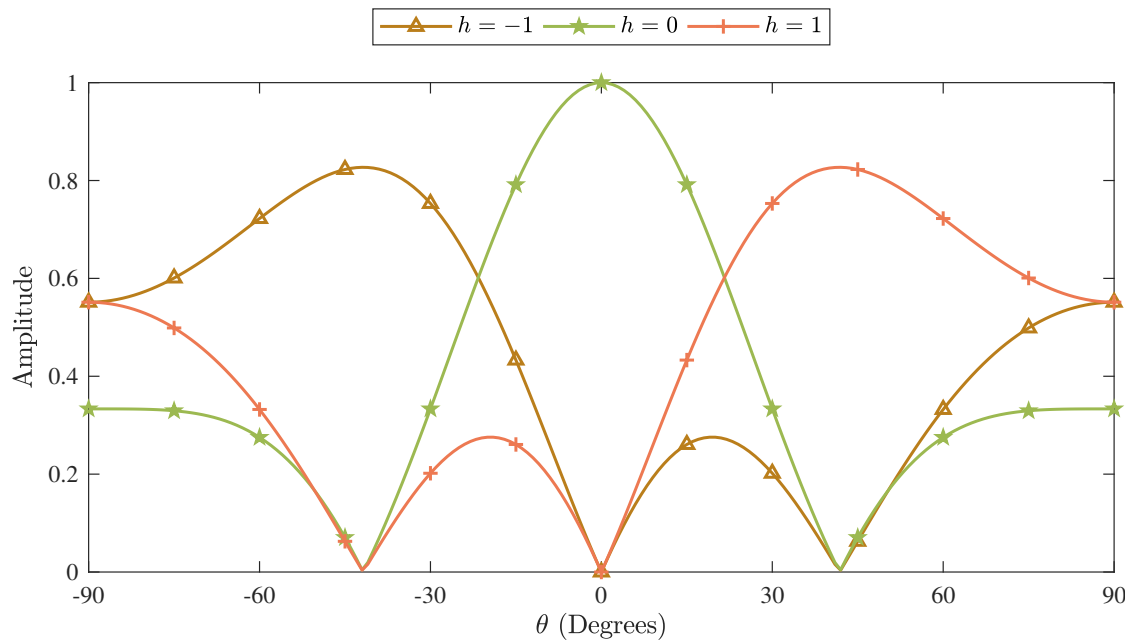
Figure 2.13: Array Factor of a three-element array with half-wavelength element spacing where the elements are switched between each other for the same period.

Beam Scanning Methods

Tennant and Chambers [2.29] showed that by changing the ratio of *on-times* between the two elements, the position of the sidebands as seen in Figure 2.12 could be adjusted. It was shown that the null of the sidebands move away from the broadside towards the end-fire and in the opposite direction depending on if the sideband of interest is negative or positive. Tennant and Chambers noted that this meant that the benefits of phase-steering could be obtained by simple time-switching, thus removing the need for phase-shifters or time-delay networks.

Harmonic Analysis

Later, Tennant [2.30] observed that comparisons of the power received in the fundamental frequency and the sidebands could indicate the DoA of the signal. This is especially true for a two element array that produces the sideband patterns as shown in Figure 2.12. As shown, the sidebands steer towards the end-fire, whilst the fundamental frequency steers towards the broadside. Tennant's work demonstrated the theory using antennas and showed that after correcting the phase of the elements, the directional response across all frequencies was in good agreement with the theory.

In 2015, He et al. [2.31] further demonstrated the direction finding capabilities of a two-element array by numerically deriving the relationship between the signal's DoA and the ratio of harmonic components. The theory was demonstrated experimentally using a pair of patch antennas, and an estimation of the DoA within $\pm5°$ was achieved.

In both of these methods, only two-elements were used. For a two element array, the power received in the sidebands is equal, regardless of the DoA. Therefore it may be difficult to differentiate between a positive or a negative angle relative to the broadside of the array unless phase information is obtained.

2.5   Properties of Real Arrays

The work described in this thesis makes certain assumptions when simulating TMLAs or deriving DoA algorithms. The two main assumptions are that the elements are switched on and off instantaneously, and that each of the elements receives power equally in each direction:

2.5.1   Non-ideal Switching

When deriving the Array Factors for TMLAs, Equation 2.4 and the work continued in this thesis assume that the on or off times are instantaneous. When such an array is sampled at this point, one sample is taken from one element and the next sample is taken from the next element without any attenuation [2.32] or additional delay. Real switches often have a non-linear response [2.33], and some delay before they are able to route signals. This delay is particularly important when considering very high frequency signals found in radio systems [2.34].

2.5.2   Directivity of Elements

An element which receives or transmits equally well in every direction is known as *omnidirectional* or as *isotropic* in the case of three-dimensional antenna [2.35]. The theories described in this thesis assume that each element is isotropic, however it is important to note that this is usually not the case. This assumption is common in DoA estimation theory, though there are examples where this has been taken into account [2.36]. Each element in an array can have its own directional response (directivity) which describes its relative receive or transmit power in any given direction. A response of an individual element can be easily represented in a polar graph as shown in Figure 2.14, which shows a typical cardioid response for DoA angles between $\pm 90°$. This directional response or *directivity* will vary depending on the specific element's aperture geometry [2.37].

If an array of three elements with directional response as shown in Figure 2.14 was used in a TMLA of three elements, then it would produce the Array Factor as seen in Fig-

(a) Polar Graph Representation

(b) Axis Graph Representation
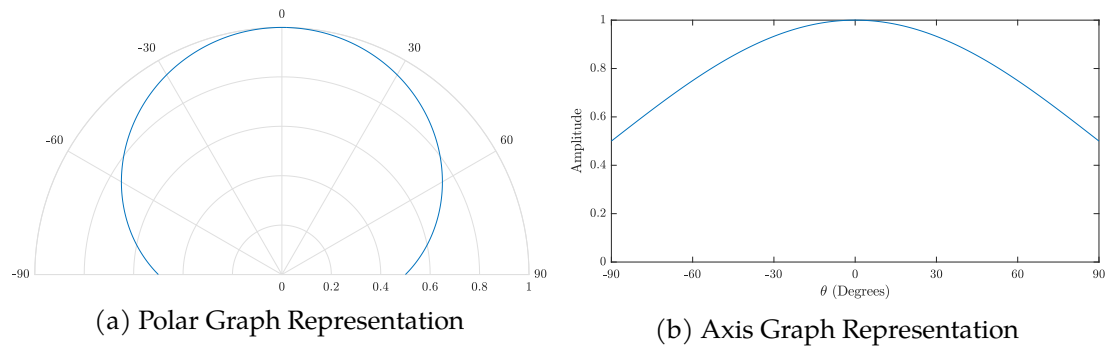
Figure 2.14: Two different representations of directivity, each showing the response of an element with a cardioid pattern for $-90° \leq \theta \leq 90°$.
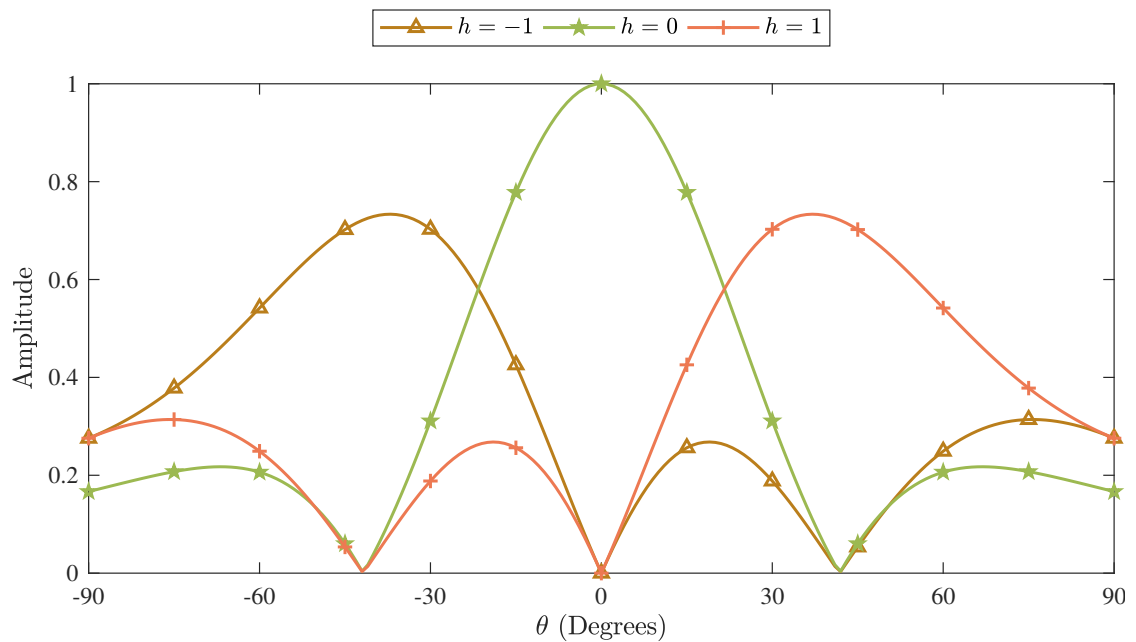
Figure 2.15: Array Factor of a three-element array with half-wavelength element spacing and each element having a cardioid response. The elements are switched sequentially and are active for the same period.

ure 2.15. When comparing this result with the array factor seen in Figure 2.13, it is clear that the main beam of the outer harmonics have been significantly affected and therefore DoA estimations that use these beams may be affected by non-isotropic element directivity.

2.6   Conclusions

Several different methods for obtaining a signal's DoA from a transducers array have been shown. The popular MUSIC and ESPRIT algorithms require multiple input stages

and often require large amounts of computational effort to work effectively.

Beam steering methods offer the benefit of only requiring one input stage. The computational effort is also reduced by using phase shifters or delay networks to sweep the beam and record where the maximum (or minimum) response is. However, since the power content needs to be analysed with each angle scanned, the time in obtaining a direction estimate may be increased.

It has been shown the TMAs offer further benefit by distributing the power of an incoming signal into multiple sidebands that are produced simultaneously. By analysis of this harmonic content, it is possible to obtain an estimate without scanning or using complicated algorithms. For a two-element array, a complex DFT may be needed to produce an estimate that is accurate within a full hemispherical range; this may be difficult to achieve using very simple processors.

A major theme of this thesis is the development of the theory in time-modulated arrays, and there is an interesting opportunity to further utilise them to obtain more accurate, or less computationally demanding direction of arrival estimates.

References

[2.1] C. Dolph, "A Current Distribution for Broadside Arrays Which Optimizes the Relationship between Beam Width and Side-Lobe Level," *Proc. IRE*, vol. 34, no. 6, pp. 335–348, June 1946.

[2.2] Y. Tong, "Time Modulated Linear Arrays," Doctoral Thesis, The University of Sheffield, 2013.

[2.3] K. Kishore, *Antenna and Propagation*. New Delhi: International Publishing House Pvt. Ltd., 2009.

[2.4] W. Stutzman and B. Davis, "Antennas for Wireless Communications – Basic Principles and System Applications." Virginia Tech, 2006.

[2.5] M. Mouhamadou, P. Vaudon, and M. Rammal, "Smart Antenna Array Patterns Synthesis: Null Steering and Multi-user Beamforming by Phase Control," *Prog. Electromagn. Res.*, vol. 60, pp. 95–106, 2006.

[2.6] H. Chaker, "Null steering and multi-beams design by complex weight of antennas array with the use of APSO-GA," *WSEAS Trans. Commun.*, vol. 13, pp. 99–108, 2014.

[2.7] Rohde & Schwarz, "Introduction into Theory of Direction Finding," *Radiomonitoring & Radiolocation*, pp. 26–49, 2010.

[2.8] L. Godara, "Application of antenna arrays to mobile communications. II. Beamforming and direction-of-arrival considerations," *Proc. IEEE*, vol. 85, no. 8, pp. 1195–1245, 1997.

[2.9] R. Schmidt, "Multiple emitter location and signal parameter estimation," *IEEE Trans. Antennas Propag.*, vol. 34, no. 3, pp. 276–280, Mar 1986.

[2.10] R. Roy and T. Kailath, "ESPRIT - Estimation of Signal Parameters Via Rotational Invariance Techniques," *IEEE Trans. Acoust.*, vol. 37, no. 7, pp. 984–995, July 1989.

[2.11] A. Li, S. Wang, and F.-p. Hu, "DOA Estimation of Coherent Signal Using MUSIC Algorithm with Nonuniform Sampling," in *2008 Congr. Image Signal Process.*, vol. 5. IEEE, 2008, pp. 431–435.

[2.12] A. Paulraj, R. Roy, and T. Kailath, "Estimation of Signal Parameters via Rotational Invariance Techniques - ESPRIT," in *Nineteeth Asilomar Conf. Circuits, Syst. Comput. 1985.* Pacific Grove, CA, USA: IEEE, 1985, pp. 83–89.

[2.13] GIRD Systems, Inc., "An Introduction to Music and Music Education as Social Praxis," Tutorial Presentation, Cincinnati, OH, USA. [Online]. Available: http:// www.girdsystems.com/pdf/GIRD{_}Systems{_}Intro{_}to{_}MUSIC{_}ESPRIT. pdfhttp://www.girdsystems.com/tutorials-pd.html

[2.14] J. Foutz, A. Spanias, and M. Banavar, *Narrowband Direction of Arrival Estimation for Antenna Arrays*, 1st ed. Arizona State University: Morgan & Claypool, 2008.

[2.15] U. Sandkuhler and J. Bohme, "Accuracy of maximum-likelihood estimates for array processing," in *ICASSP '87. IEEE Int. Conf. Acoust. Speech, Signal Process.*, vol. 12. IEEE, pp. 2015–2018.

[2.16] L. L. Cam, "Maximum Likelihood: An Introduction," *Int. Stat. Rev. / Rev. Int. Stat.*, vol. 58, no. 2, p. 153, August 1990.

[2.17] M. Li, Y. Lu, and B. He, "Array Signal Processing for Maximum Likelihood Direction-of-Arrival Estimation," *J. Electr. Electron. Syst.*, vol. 03, no. 01, 2013.

[2.18] H. Krim and M. Viberg, "Two decades of array signal processing research: the parametric approach," *IEEE Signal Process. Mag.*, vol. 13, no. 4, pp. 67–94, July 1996.

[2.19] W.-Q. Wang, H. C. So, and A. Farina, "An Overview on Time/Frequency Modulated Array Processing," *IEEE J. Sel. Top. Signal Process.*, vol. 11, no. 2, pp. 228–246, March 2017.

[2.20] P. Antonik, M. C. Wicks, H. D. Griffiths, and C. J. Baker, "Range-dependent beamforming using element level waveform diversity," in *2006 Int. Waveform Divers. Des. Conf.*   IEEE, January 2006, pp. 1–6.

[2.21] W.-Q. Wang and H. C. So, "Transmit Subaperturing for Range and Angle Estimation in Frequency Diverse Array Radar," *IEEE Trans. Signal Process.*, vol. 62, no. 8, pp. 2000–2011, April 2014.

[2.22] W.-Q. Wang, "Overview of frequency diverse array in radar and navigation applications," *IET Radar, Sonar Navig.*, vol. 10, no. 6, pp. 1001–1012, July 2016.

[2.23] H. E. Shanks and R. W. Bickmore, "Four-Dimensional Electromagnetic Radiators," *Can. J. Phys.*, vol. 37, no. 3, pp. 263–275, Mar 1959.

[2.24] H. Shanks, "A new technique for electronic scanning," *IRE Trans. Antennas Propag.*, vol. 9, no. 2, pp. 162–166, Mar 1961.

[2.25] G. Li, S. Yang, Y. Chen, and Z.-P. Nie, "A Novel Electronic Beam Steering Technique in Time Modulated Antenna Array," *Prog. Electromagn. Res.*, vol. 97, pp. 391–405, 2009.

[2.26] L. Poli, P. Rocca, L. Manica, and A. Massa, "Pattern synthesis in time-modulated linear arrays through pulse shifting," *IET Microwaves, Antennas Propag.*, vol. 4, no. 9, p. 1157, 2010.

[2.27] Q. Zhu, S. Yang, R. Yao, M. Huang, and Z. Nie, "Unified Time- and Frequency-Domain Study on Time-Modulated Arrays," *IEEE Trans. Antennas Propag.*, vol. 61, no. 6, pp. 3069–3076, June 2013.

[2.28] Y. Tong and A. Tennant, "A Two-Channel Time Modulated Linear Array With Adaptive Beamforming," *IEEE Trans. Antennas Propag.*, vol. 60, no. 1, pp. 141–147, January 2012.

[2.29] A. Tennant and B. Chambers, "A Two-Element Time-Modulated Array With Direction-Finding Properties," *Antennas Wirel. Propag. Lett.*, vol. 6, no. 11, pp. 64–65, 2007.

[2.30] A. Tennant, "Experimental Two-Element Time-Modulated Direction Finding Array," *IEEE Trans. Antennas Propag.*, vol. 58, no. 3, pp. 986–988, Mar 2010.

[2.31] C. He, X. Liang, Z. Li, J. Geng, and R. Jin, "Direction Finding by Time-Modulated Array With Harmonic Characteristic Analysis," *IEEE Antennas Wirel. Propag. Lett.*, vol. 14, pp. 642–645, 2015.

[2.32] G. Bogdan, Y. Yashchyshyn, and M. Jarzynka, "Time-Modulated Antenna Array With Lossless Switching Network," *IEEE Antennas Wirel. Propag. Lett.*, vol. 15, pp. 1827–1830, 2016.

[2.33] X.-j. He, B.-s. Jin, Q. Wu, and J.-h. Yin, "Time response and dynamic behavior of electrostatic driven RF MEMS capacitive switches for phase shifter applications," in *2006 IEEE Antennas Propag. Soc. Int. Symp.* IEEE, 2006, pp. 1965–1968.

[2.34] C. He, L. Wang, J. Chen, and R. Jin, "Time-Modulated Arrays: A Four-Dimensional Antenna Array Controlled by Switches," *J. Commun. Inf. Networks*, vol. 3, no. 1, pp. 1–14, Mar 2018.

[2.35] C. Coleman, *An Introduction to Radio Frequency Engineering*. Cambridge: Cambridge University Press, 2004.

[2.36] R. Sanudin, N. H. Noordin, A. O. El-Rayis, N. Haridas, A. T. Erdogan, and T. Arslan, "Analysis of DOA estimation for directional and isotropic antenna arrays," in *2011 Loughbrgh. Antennas Propag. Conf.* IEEE, November 2011, pp. 1–4.

[2.37] A. Manikas, *Differential Geometry in Array Processing*. Imperial College Press, 2004.

3 | Direction of Arrival Estimations with Time-Modulated Linear Arrays

PREVIOUSLY, it has been shown that as few as two elements are required to construct an array with direction finding properties. This chapter describes a technique that can be used for direction finding using the sidebands produced by time-modulated arrays and suggests methods of improving the accuracy of the technique. To show the relevance of the technique, it is compared with the latest DoA estimation methods that use TMAs.

3.1   Introduction

The MUSIC [3.1] and ESPRIT [3.2] algorithms described in Chapter 2 are well established, and a high level of precision can be obtained using them providing that the precise array characteristics are known beforehand. These algorithms make use of subspace methods where each element in the array usually needs to be recorded concurrently. These systems are expensive, and the necessary matrix manipulation requires a lot of computational power to achieve an accurate estimation of the target signal's DoA. It has been shown that TMAs are able to produce unique beams in sidebands simultaneously.

Finding the DoA of a signal is an interesting application in both RF and acoustic domains. Ultrasonic systems using an array of transducers exist, such as for robotic or vehicle guidance [3.3, 3.4] applications. In this domain, two popular techniques of acquiring positional information include Time Difference of Arrival (TDoA) [3.5] or phase steering [3.6] to obtain a DoA estimation. For TDoA techniques, each sensor needs to be
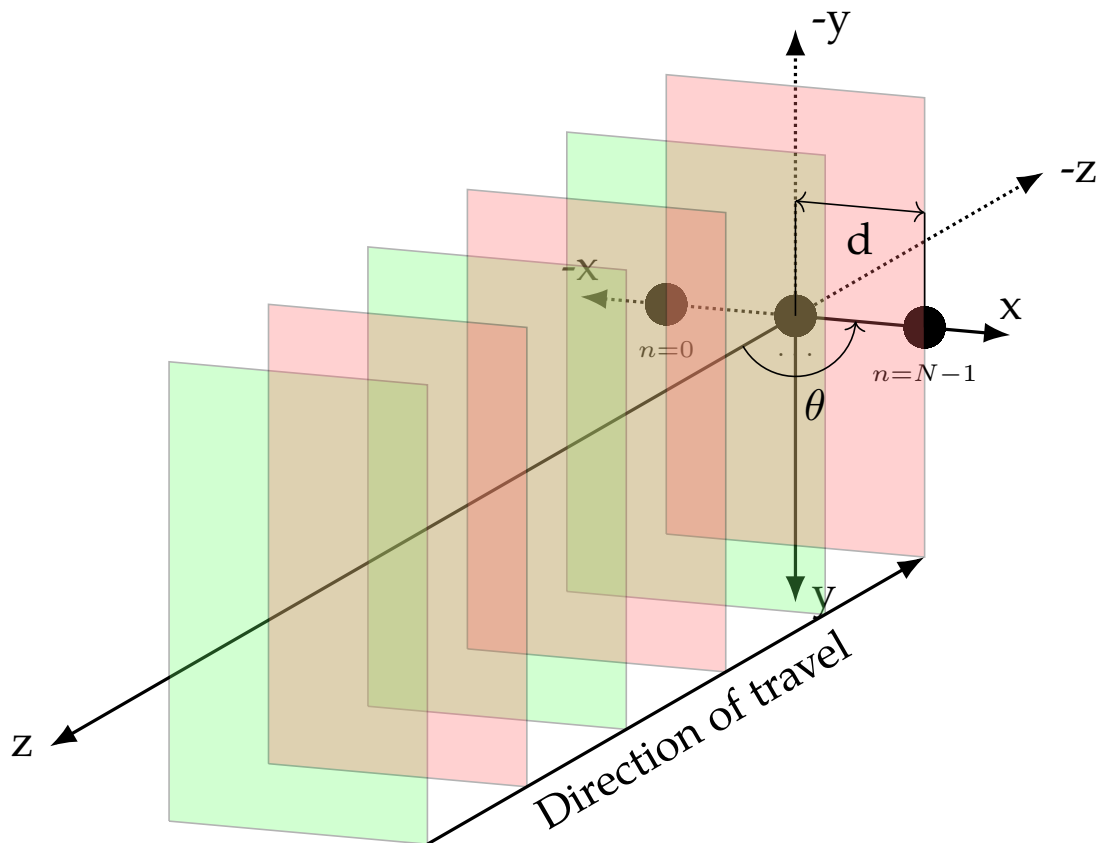
Figure 3.1: Model of an N element time-modulated array with d spacing. A plane wave is impinging on the array at the axis broadside ($\theta = 0$).

sampled simultaneously and then cross-correlated to find the DoA. For phase steered arrays, each element's phase needs to be controlled to produce a beam in a particular direction, which is usually swept across a range of directions.

Larger TMAs produce a greater number of sidebands and therefore it is possible to utilise TMLAs operating in the receive mode only to form beams in multiple locations simultaneously [3.7]. A TMA will benefit from only requiring a single analogue input stage with the sensors being switched on periodically to drive that input. In this chapter, an estimation for direction of arrival will be obtained using frequency analysis of the sidebands generated from an N element array as shown in 3.1.

As described in Chapter 2, algorithms that have low computational complexity have been developed [3.8, 3.9] for use with two-element TMLAs. He et al. [3.9] demonstrated that it is possible to extract an estimation for a signal's DoA using a two element time-modulated array by performing a two-point DFT. Whilst this method can significantly reduce the complexity of the algorithms, it may also be prone to errors when multipath

reflections and noise are introduced, especially in situations where a small number of samples are captured.

This chapter suggests an alternative computationally efficient method using TMLAs to estimate the DoA which demonstrates better noise-immunity than the method described in [3.9]. The use of this new method with a greater number of sensors shows that DoA estimations can be accurately produced even in the presence of noise and multi-path reflections.

3.2   Background Theory

It has been shown in Chapter 2 that the signal power is distributed among an infinite series of harmonics related to the switching pattern frequency $f_s = \frac{1}{T_s}$, and centred on a main frequency f_0. In this chapter, the case of a uniformly switched array (i.e., $(\tau_{n,off} - \tau_{n,on}) \times N = T_s$, and each element is switched on in sequence) is continued.

To make the following calculations simpler, Equation (2.22) can be generalised if R is defined as the ratio of element spacing to signal wavelength λ,

$$R = \frac{d}{\lambda} = \frac{kd}{2\pi} \tag{3.1}$$

Now, the normalized Array Factor for each harmonic can be written as

$$AF(h, \theta) = \frac{\sin \frac{\pi h}{N}}{N \pi h} \sum_{n=0}^{N-1} e^{2j\pi n R (\sin \theta - \frac{h}{RN})} \tag{3.2}$$

Figure 3.2 shows the normalized response of the dominant harmonics (i.e., $f_0 \pm 2f_s$, $f_0 \pm f_s$, f_0) in a five-element array with each harmonic having a maximum amplitude at a different angle (i.e., $\pm 53.1°$, $\pm 23.6°$, $0°$). From Equation (3.2), it can be shown that the direction in which the maximum response occurs for each harmonic can be calculated as:

$$\theta_h = \sin^{-1} \frac{h}{RN} \tag{3.3}$$
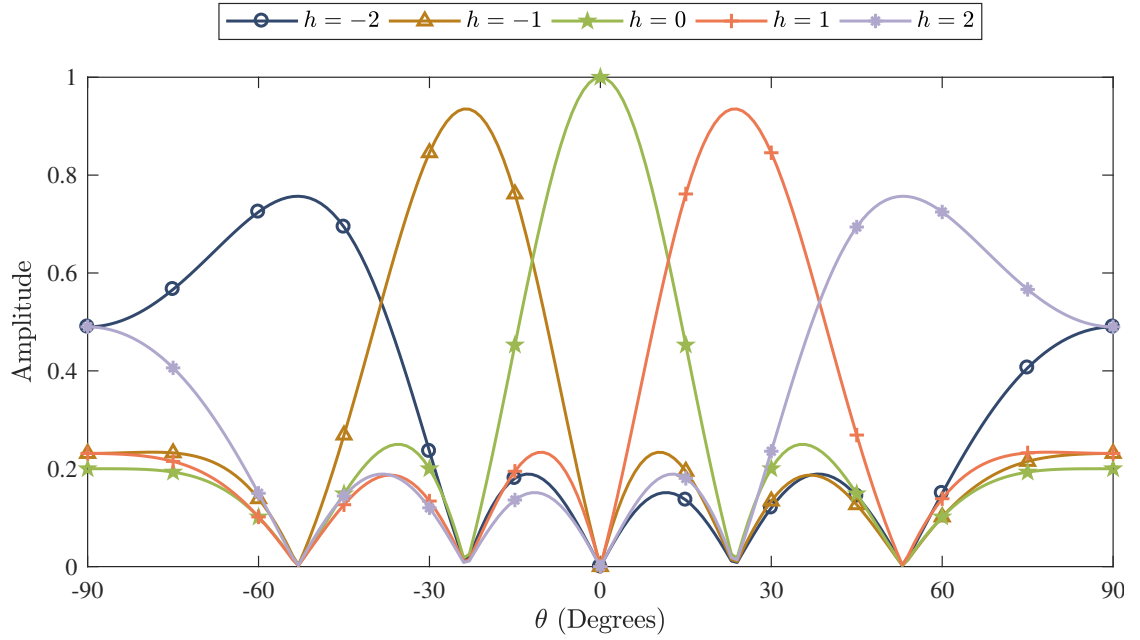
Figure 3.2: Simulated Array Factor of a five-element array with half-wavelength element spacing, showing five different harmonics when each element is switched on and off uniformly in sequence.

It can also be observed that the point at which each harmonic's maximum amplitude occurs also marks the point where all other harmonics are at a minimum. The signal power associated with each sideband X_h can be easily identified using a DFT. In practical terms this means that by analytical study of the magnitude of each sideband, a value for a given received signal's DoA can be derived [3.8].

The positions of each harmonic beam greatly depend on the value of R as defined in Equation (3.1). If the spacing of each element is reduced (R becomes smaller), the main beam angles of each harmonic as calculated in Equation (3.3) will be more widely spaced. As can be seen in Figure 3.3, if the value of R becomes greater than 0.5 (half-wavelength spacing), harmonics will obtain grating lobes due to the effect of spatial aliasing. As shown in the figure, using a spacing so that $R = 0.75$ means that each harmonic has two main beams where the amplitude is above 0.6. Throughout this chapter, spacing will be chosen so that $R = 0.5$ which ensures that each of the harmonics has a single main beam within the range of $\pm 90°$.
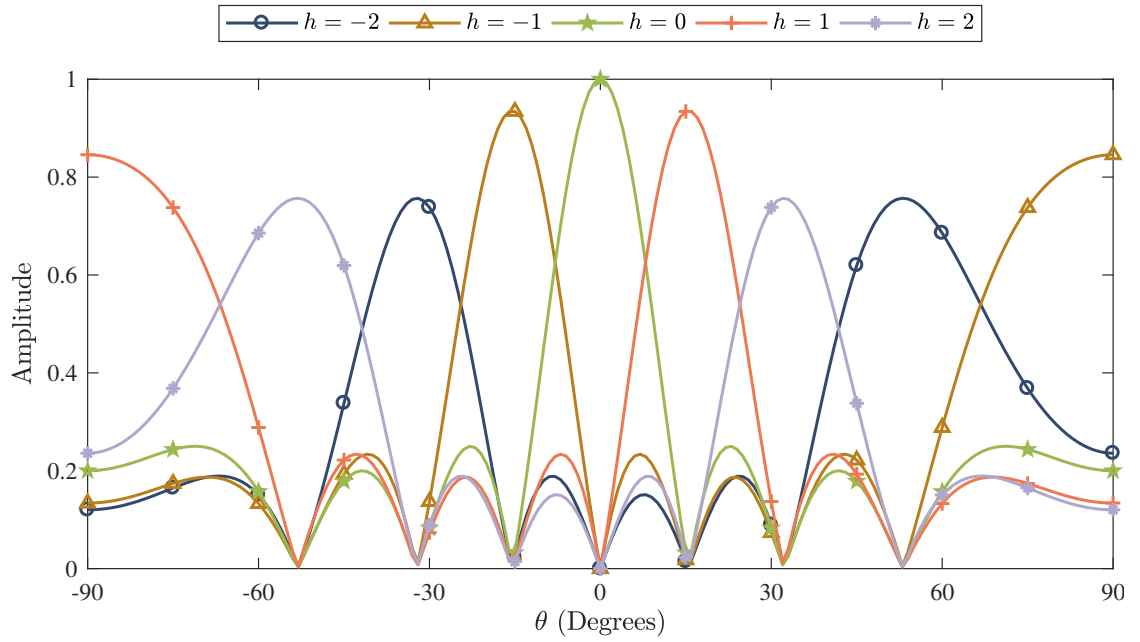
Figure 3.3: Simulated Array Factor of a five-element array with three quarter-wavelength element spacing. Showing five different harmonics when each element is switched on and off uniformly in sequence.

3.3   Proposed Method of Determining the DoA

The approach taken in this thesis is realised by finding the associated harmonic frequencies relating to both the signal frequency and the array switching frequency. For example, an array with five elements (i.e. $N = 5$) will distribute the power of an incoming signal into frequencies at $f_0 - 2f_s$, $f_0 - f_s$, f_0, $f_0 + f_s$ and $f_0 + 2f_s$. As shown in Equation (3.3), each of these harmonics has a known main beam angle θ_h (i.e., $-53.1°$, $-23.6°$, $0°$, $23.6°$ and $53.1°$).

If a single tone sinusoidal signal impinges on the example array at an angle θ (measured relative to the broadside direction). The combined signal at the output of the array will distribute power to one or more frequency bins each occuring at one of the harmonics described previously, and as shown in Figure 3.2. In the case where θ matches exactly one of the values of θ_h, only the associated harmonic frequency is expected to be present in the output. It can then be assumed that if the value of the largest DFT bin is dominant, while the adjacent bins are small, then the signal angle is close (but not equal to) to the main beam angle of that harmonic.

Conversely, if the amplitudes of the two largest adjacent bins are equivalent, then the signal is approximately half way between the two main beams. The DoA can be estimated by creating an average angle using the associated angles of the two harmonic beams. This average is weighted by the harmonic power level the array receives and an estimation of the DoA can therefore be expressed as:

$$\theta_{est} = \frac{X_\alpha \theta_\alpha + X_{\alpha+1}\theta_{\alpha+1}}{X_\alpha + X_{\alpha+1}} \qquad (3.4)$$

where X_α and $X_{\alpha+1}$ are the two largest DFT bins that are adjacent, and θ_α and $\theta_{\alpha+1}$ are the main beam angles associated with the corresponding harmonics.

The steps required to perform DoA estimation using the proposed method can be summarised as follows:

1. Collect a fixed number of samples from each sensor in turn. The harmonic frequency can be calculated as the reciprocal of the time taken to sample the set of all sensors.

2. Perform a single-tone DFT on each of the the fundamental and expected harmonics of the switching frequency.

3. Select the DFT bins with the two largest amplitudes and identify their main beam angles.

4. Create an estimated DoA using the values obtained in the previous steps, and in Equation (3.4)

For example, if an unknown signal source produces the frequency spectrum shown in Figure 3.4 when sampled with a five-element array, then the power levels of harmonics 1 and 2 are taken as X_α and $X_{\alpha+1}$ respectively and angles θ_α and $\theta_{\alpha+1}$ are found from Equation (3.3) as $23.6°$ and $53.1°$. Using Equation (3.4), the estimated signal DoA is $44.9°$.
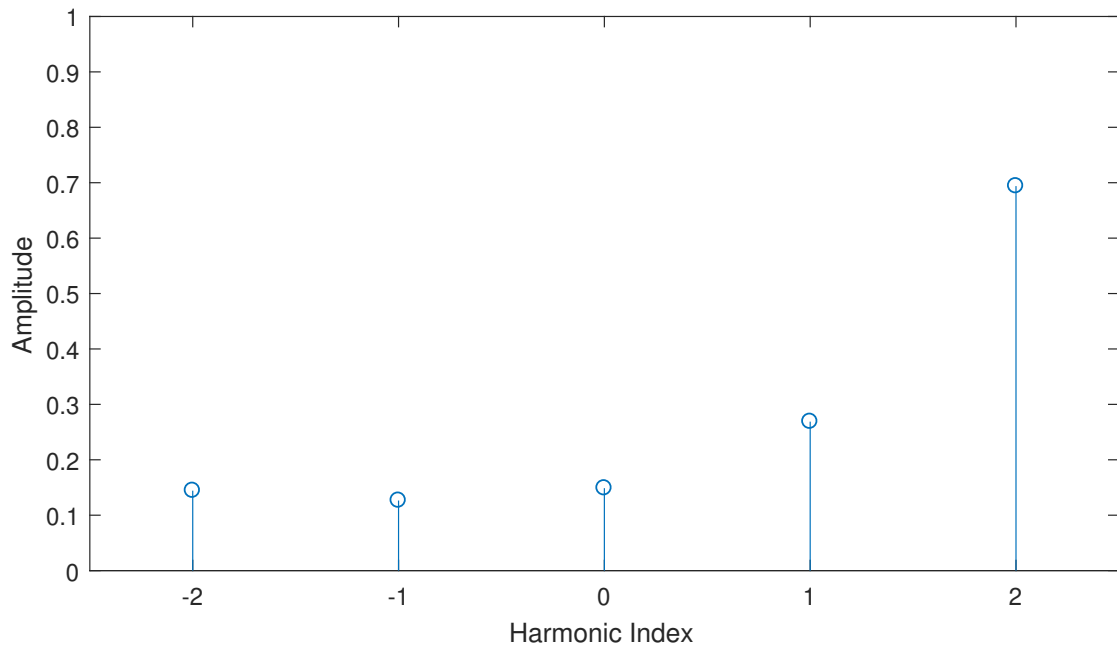
Figure 3.4: Power spectrum produced by a single sinusoidal source when sampled by a uniformly switched five-element time-modulated linear array. The signal is impinging on the array at an angle of $45°$.

3.3.1 Reducing Errors Near Null Regions

Figure 3.5 shows the amplitudes of each harmonic plotted against the associated main beam angles. The source in this example is located at $25.0°$ and the solid lines indicate the result for $(N = 5)$. In this situation, the choices of X_α and $X_{\alpha+1}$ are not clear. The first positive harmonic $(h = 1)$ is the dominant frequency, but the two adjacent harmonics $(h = 0, h = 2)$ are small and very similar in amplitude; both make possible candidates for the selection of X_α or $X_{\alpha+1}$. Using the method described, using the centre harmonic $(h = 0)$ in the estimation will produce an angle of $22.0°$ whereas using the second positive harmonic $(h = 2)$ in the estimation will produce an angle of $25.0°$.

Clearly, using the first and second harmonics for estimation would be the correct option, however determining which of the two small harmonics can be challenging especially in the presence of noise. It can be concluded following this argument that the largest errors occur when the incident angle of the signal is close to one of the harmonics' main beam or null regions.

This issue can be mitigated by processing the sampled data in a different way. If
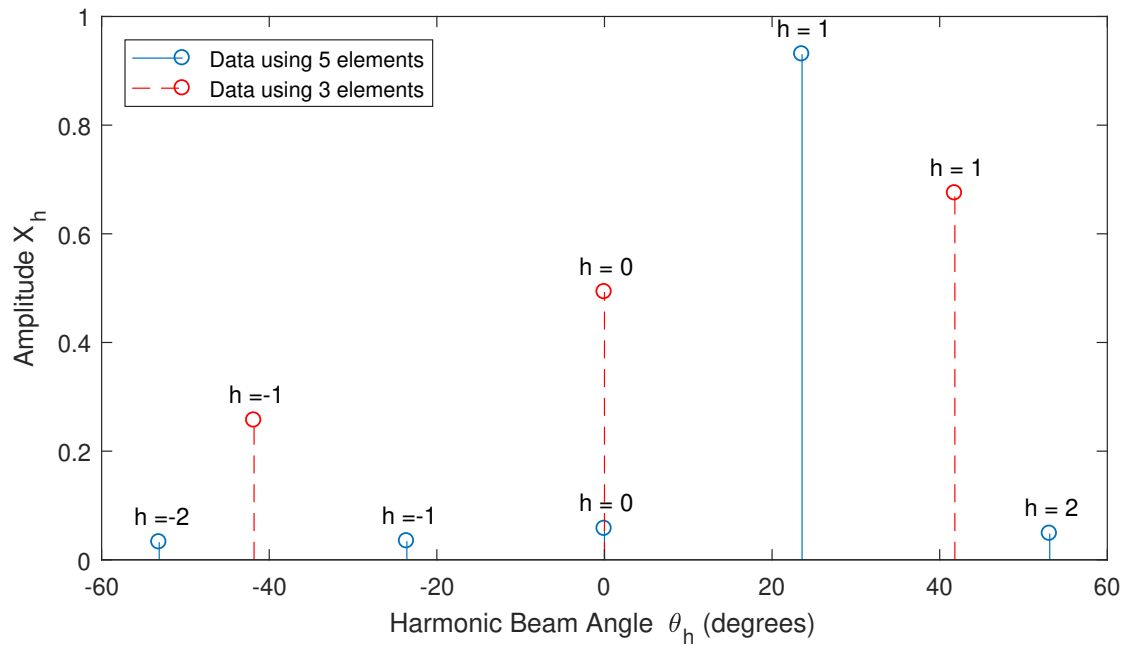
Figure 3.5: Power spectrum produced by a five-element array receiving a signal from a source at an angle of $25°$. When the samples from the outer elements are removed, then the array produces a new spectrum with different characteristics (shown as the dotted lines in the figure).

a number of samples has been taken from each element in turn but not repeated, it is possible to remove the samples recorded by the outer elements so that data from an $N-2$ element array is obtained. An example using five elements is given in Figure 3.6.

By removing the samples at each end of the full signal, a different frequency spectrum is produced, the modulation frequency becomes higher and the resultant harmonic beam directions change according to Equation (3.3). By selecting the number of elements used, errors caused by estimating the source direction using harmonic amplitudes
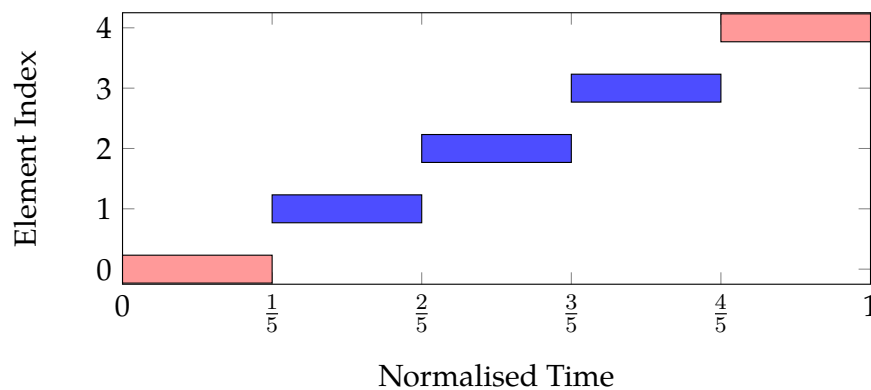
Figure 3.6: Time sequence showing how a three element array (shaded darker) can be obtained from a five element array.

close to the null regions can be avoided. Using the data provided, if harmonics 0 and 1 are taken as X_α and $X_{\alpha+1}$ in the three-element case then the method produces an estimation of $24.6°$.

3.4 Numerical Results

In this section, results of a simulation developed in MATLAB R2015a are provided to illustrate the use of the proposed technique. A source of 40 kHz was assumed, impinging on a five-element array, where each element was separated by $\lambda/2$. A sampling rate of 500 kHz was chosen and 200 samples were taken from each simulated isotropic receiver in succession, meaning that the expected harmonics are separated by 500 Hz. The results are shown Figure 3.7 (solid line) which gives the accuracy of the DoA estimation as a function of source angle.

The abrupt changes in estimation error observed at approximately $23°$ to $25°$ for the five-element array in Figure 3.7 are due to the algorithm selecting an incorrect smaller harmonic close to the null regions as explained in Section 3.3.1. In spite of there being no noise in this simulation, effects such as under-sampling and numerical errors still give rise to errors close to the null. If now the samples from the outer microphones are removed to consider the estimation error for $N = 3$ (shown as the dashed line in Figure 3.7) and then the results are re-analysed using the same method with new values of harmonic data, the inaccuracies can be mitigated by taking a composite of the two traces. Since the value of N has changed, the null regions located using Equation (3.3) for $N = 3$ and $N = 5$ are non-coincident. It is known at which angles the inaccuracies will occur and hence by selecting the result of either $N = 3$ or $N = 5$, the best case accuracy overall can be achieved as shown in Figure 3.8.
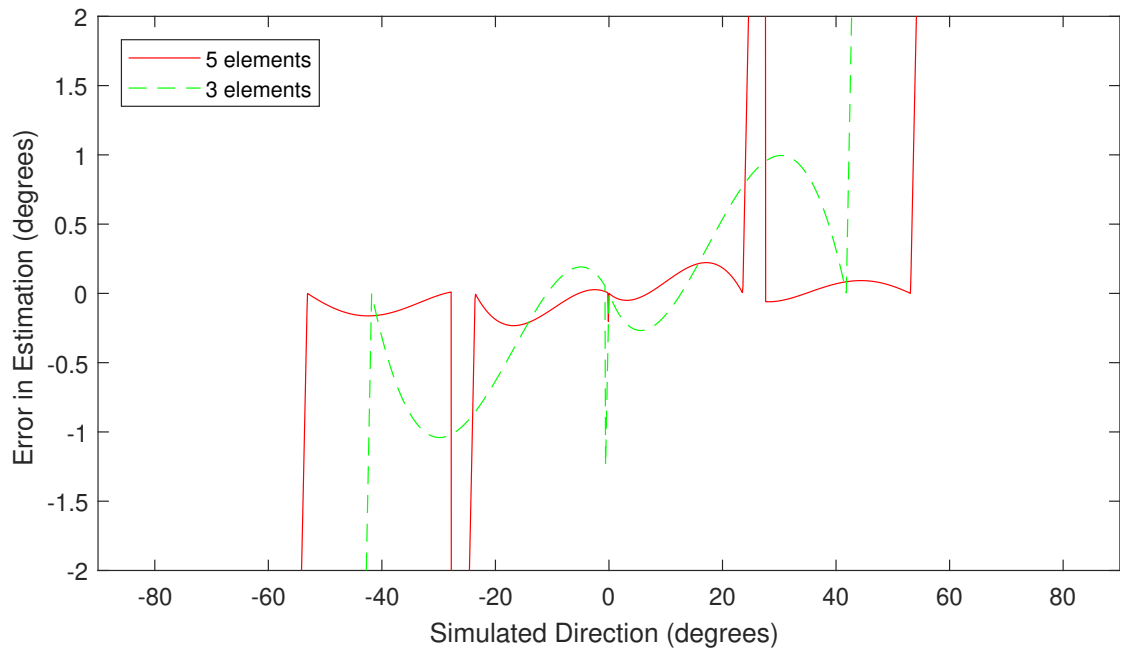
Figure 3.7: Simulated error in direction of arrival estimation of a linear array using five (solid) or three microphones (dashed).
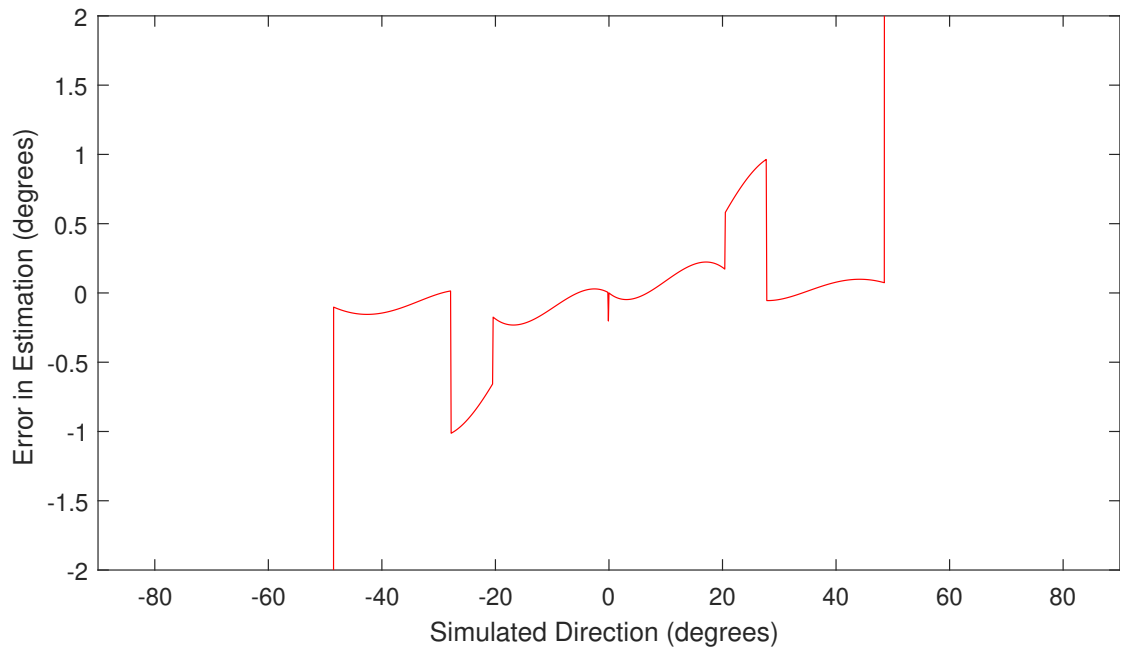
Figure 3.8: Simulated error in direction of arrival estimation when the best result is picked from a linear array using five or three of its elements.
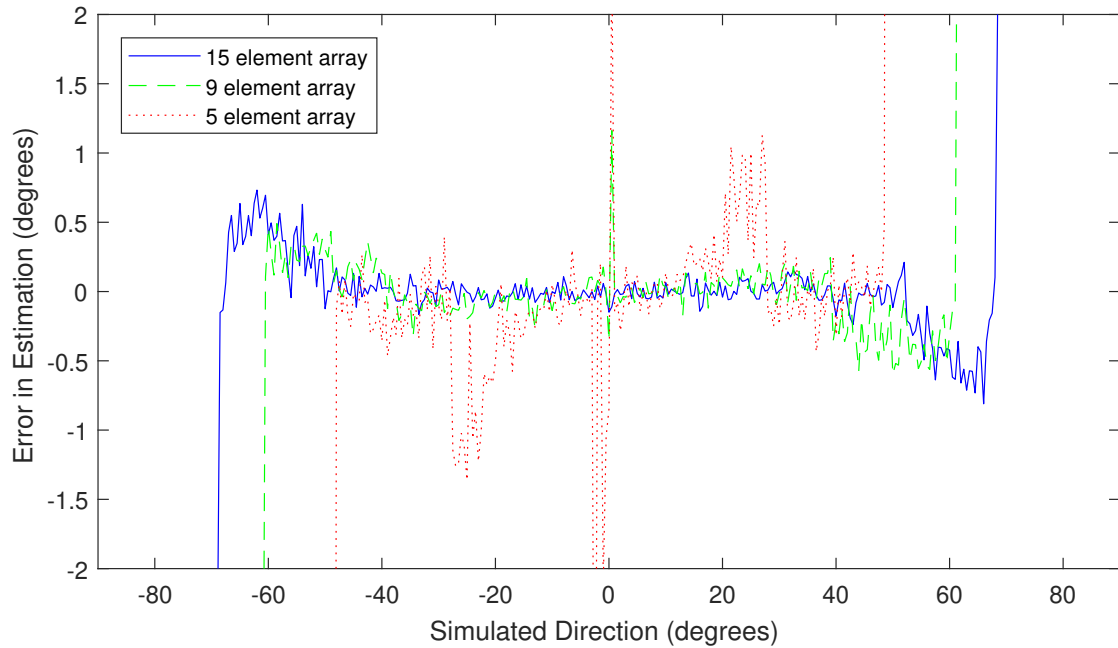
Figure 3.9: Simulated error in direction of arrival estimation with three different numbers of elements in the presence of noise. Each test had 1350 samples taken from an array with five (dotted), nine (dashed) or fifteen (solid) elements, where the source signal to noise ratio was 10 dB.

3.4.1 Added Noise

Multiple values of N were tested using a single source with additive white Gaussian distributed noise. The signal to noise ratio was fixed throughout all tests at 10 dB. Figure 3.9 shows that using a larger number of elements increases the accuracy of the method, as well as increasing the effective angular range of the system.

3.4.2 Multiple Incoherent Signals

Using this method, it is also possible to detect multiple incoherent signals simultaneously if the frequency of the second signal and its harmonics generated by switching do not interfere with the DFT approximations performed on the first signal and its harmonics. In this case, the frequency of each of the signals will have its own value of R and therefore the designer of the system must space the array elements at less than half a wavelength apart at the highest frequency to avoid spatial aliasing.

For example, to track two acoustic signals with frequencies 40 kHz and 44 kHz, the

maximum spacing between elements should be 0.0039 metres. In this case, R for the 44 kHz signal would be 0.5, but would be approximately 0.45 for the 40 kHz signal.

3.4.3 Multiple Coherent Signals

The theory so far has assumed that a signal is received from a singular path at the array. In reality, a signal with a wider transmit beam can also reflect off of surrounding surfaces and reach the array at a multiple angle. Whilst these multipath signals should have attenuated power, they can still affect the direction of arrival estimation. In Chapter 2, it was shown that the subspace algorithms such as MUSIC and ESPRIT can be affected by this environmental problem when signals are in close proximity.

The DoA algorithm proposed by He et al. [3.9] makes use of the complex content of two harmonics generated by the array, but each of these harmonics are used in the algorithm regardless of where the signal is positioned within the $\pm 90°$ range. This means that if a second coherent signal impinges on the array at a different angle, the signal will have a greater effect on the DoA estimation. The algorithm proposed in this chapter makes use of a larger number of elements, and chooses between a selection of harmonic data at different signal directions.

To show the difference between how each algorithm responds, another simulation was designed to emulate a two-element TMLA with half-wavelength spacing, receiving a 40 kHz sinusoidal acoustic signal. The array took 675 samples from one element before switching to the next and sampled at a rate of 500 kHz. Two complex DFTs were taken at the target frequency (40 kHz) and the positive harmonic frequency (40.37 kHz) and the direction finding algorithm proposed by He et al. [3.9] was used to obtain a DoA estimation.

Figure 3.10 shows the frequency response of the array in the full $\pm 90°$ range. The error in DoA estimation depending on the signal frequency can be seen in Figure 3.11 and shows that without interference, there is a very small amount of error in the direction finding resolution.
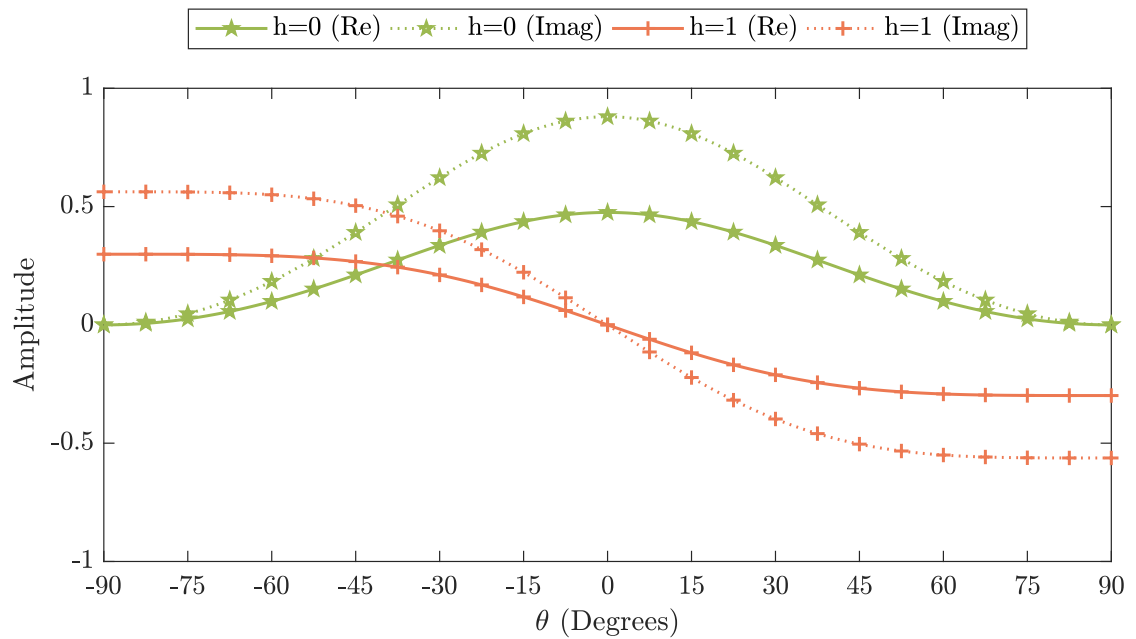
Figure 3.10: The complex frequency response of the centre and outer harmonics of a two-element TMLA receiving a single sinusoidal signal at various angles.
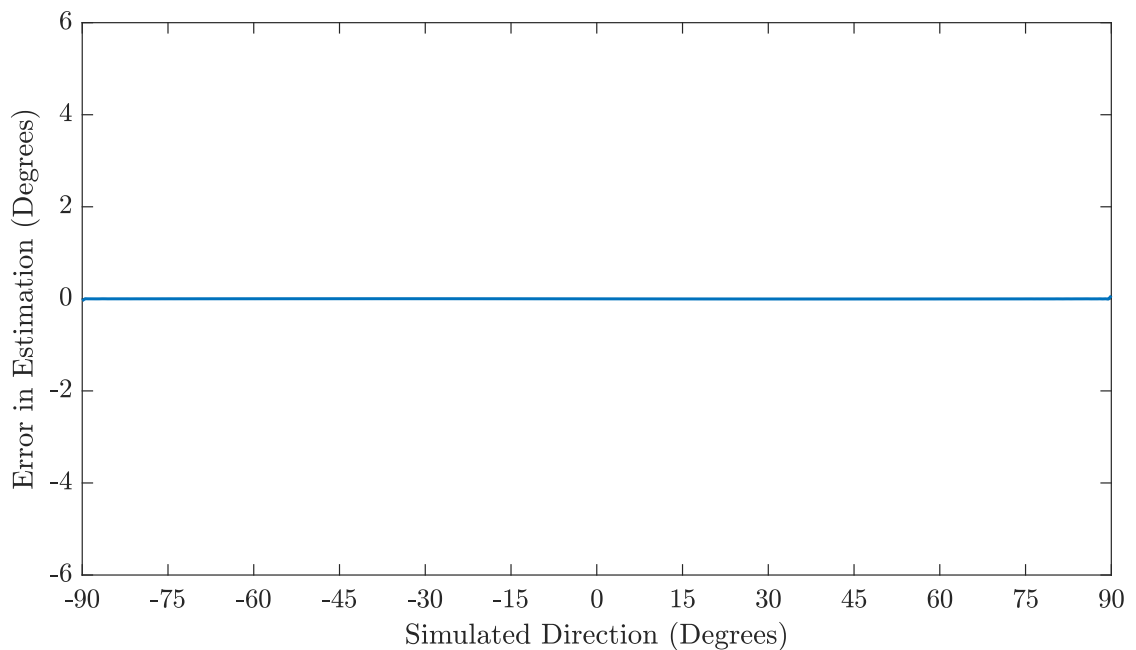
Figure 3.11: Simulated error in direction of arrival estimation using two elements and the algorithm proposed by He et al. [3.9] under ideal conditions.
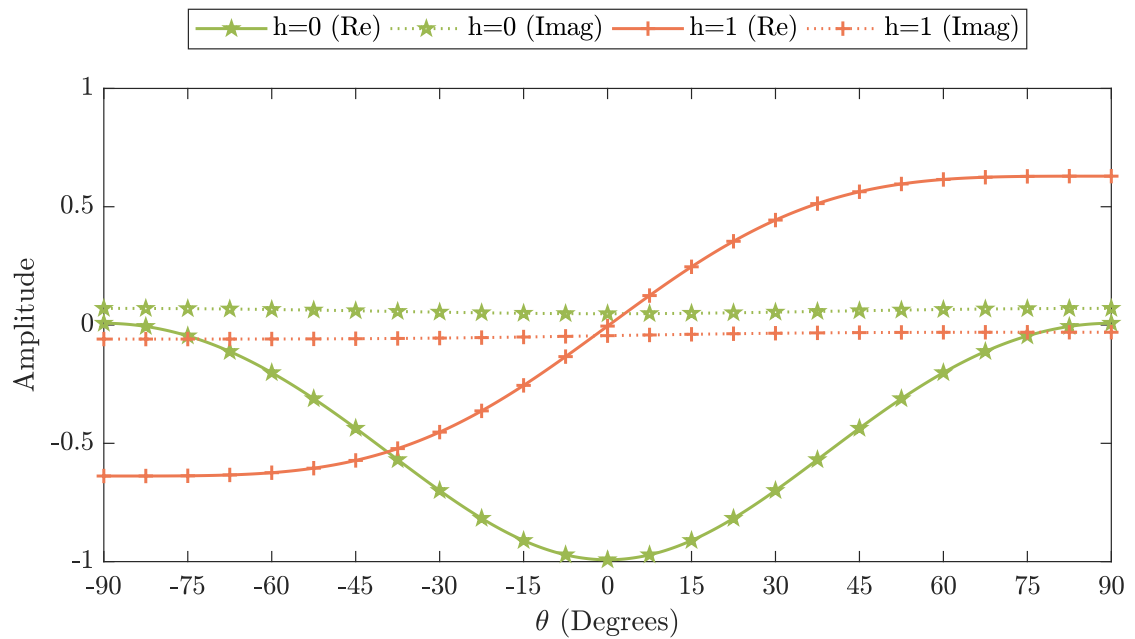
Figure 3.12: The best case complex frequency response of the centre and outer harmonic of a two-element TMLA receiving a primary sinusoidal signal at various angles, and a secondary signal propagating from a fixed position of 30°.

A second signal with the same 40 kHz frequency was added to the simulation, but at 10% of the amplitude as the primary signal. While the positions of the first signal change from ±90°, the secondary signal was kept at a fixed position of 30°. Since the phase of both the signal and interfering is usually unknown, the simulation was made to produce a random initial phase and the best and worst cases (in terms of estimation accuracy) out of 100 simulations were saved.

The simulated frequency domain responses and the DoA estimation errors were measured again and results can be seen in Figures 3.12 and 3.13 for the best case, and Figures 3.14 and 3.15 for the worst case. Clearly the results of this method vary depending on the phases of the two signals and in the worst-case, is no longer suitable for direction finding.
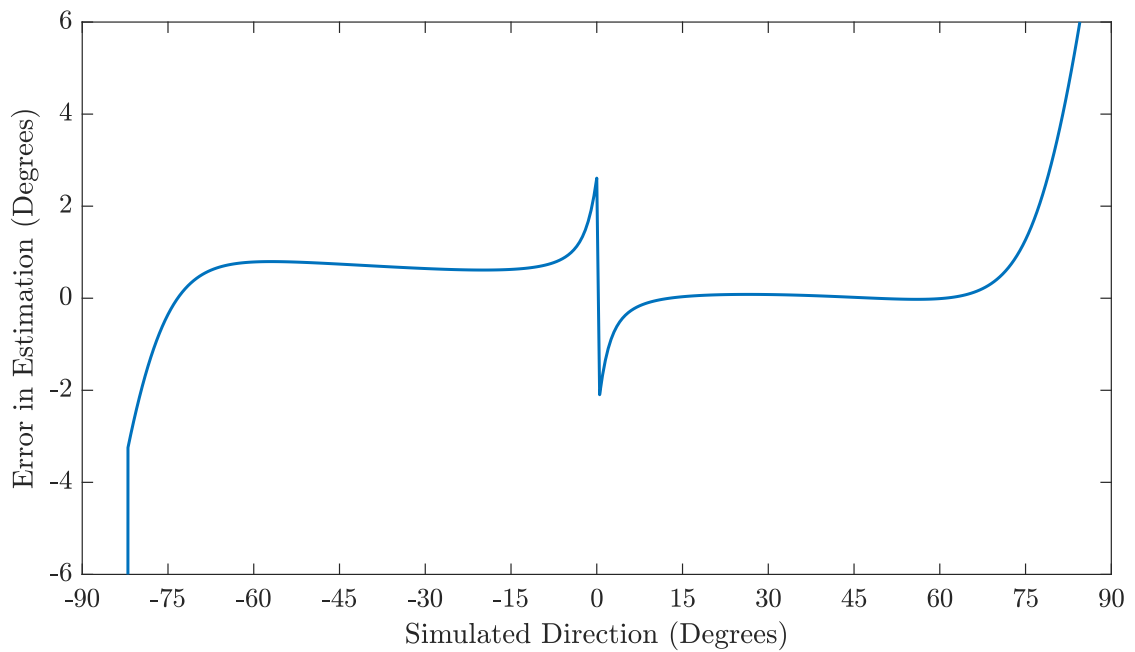
Figure 3.13: Best case simulated error in DoA estimation using two elements and the algorithm proposed by He et al. [3.9] when a second low-power signal with random initial phase is fixed at 30° is added.
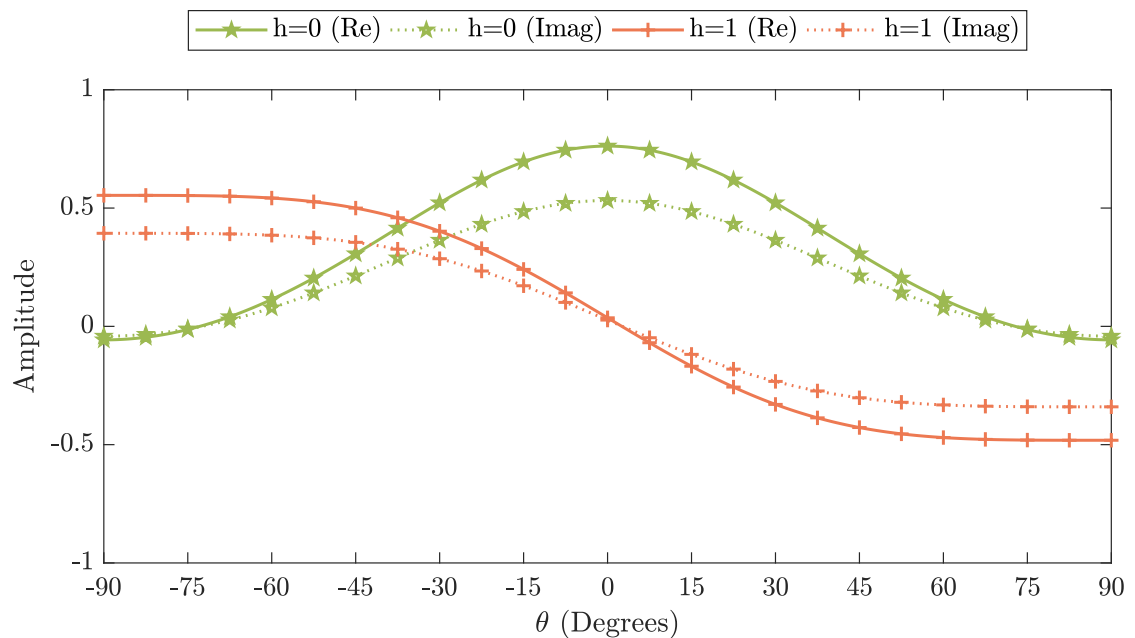
Figure 3.14: The worst case complex frequency response of the centre and outer harmonics of a two-element TMLA receiving a primary sinusoidal signal at various angles, and a secondary fixed signal propagating from a fixed position of 30°.
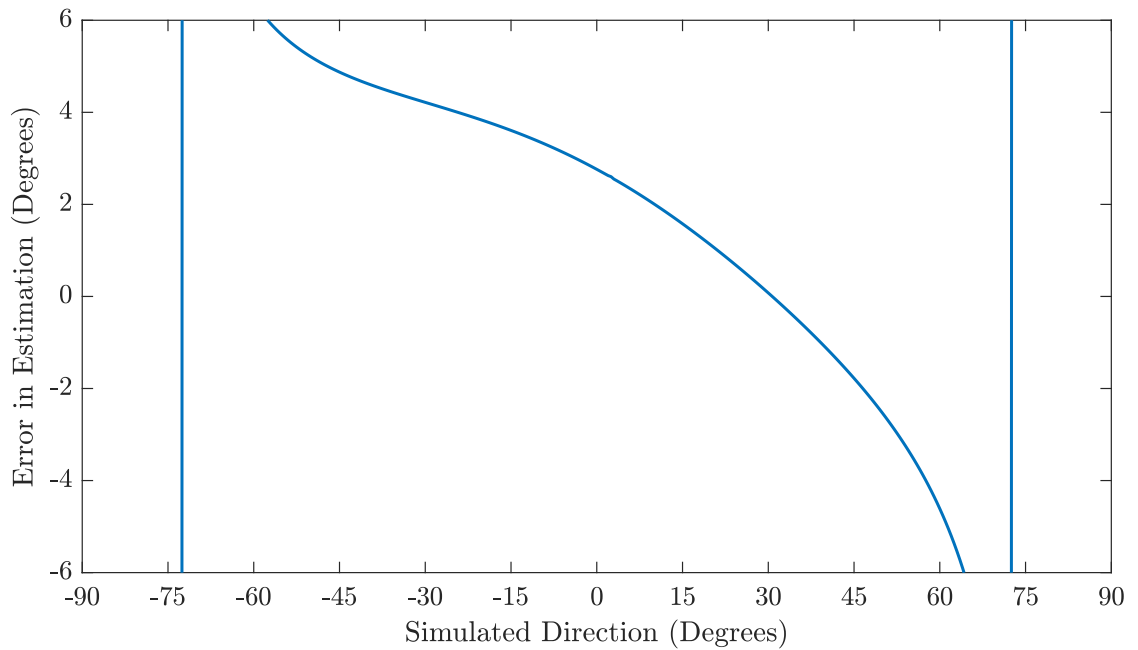
Figure 3.15: Worst case simulated error in DoA estimation using two elements and the algorithm proposed by He et al. [3.9] when a second low-power signal with random initial phase is fixed at $30°$ is added.

In contrast, the same scenario was performed on five, nine and fifteen-element arrays using the algorithm proposed in Equation (3.4), the total number of samples remained at 1350, but 5, 9 and 15 DFTs were performed to produce a real-valued magnitude. Figure 3.16 shows the frequency response at several harmonics for the 5-element array, which can be compared to Figure 3.2. It can be seen that the first positive harmonic has been amplified due to the extra power received at $30°$, the other harmonics have minimal effect on the DoA algorithm because only the two largest harmonics are selected. Figure 3.17 shows that the DoA resolution has been reduced overall, but generally received better results than that of the previous method. With additional elements, the adverse effect of the extra signal is reduced.

As shown in Section 3.3.1, the small regions of increased error that occur near the sideband nulls can be reduced by obtaining a secondary set of DFTs with reduced data.
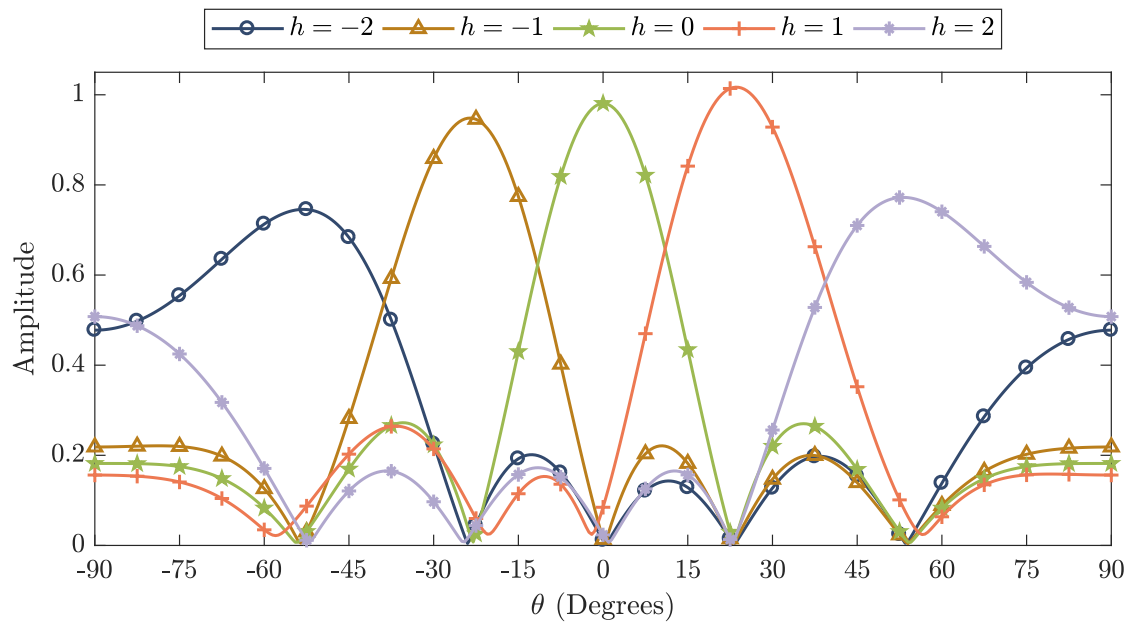
Figure 3.16: The magnitude of each harmonic generated by a five-element TMLA receiving a sinusoidal signal at various angles, and a second fixed low-power signal propagating from a fixed position of $30°$.
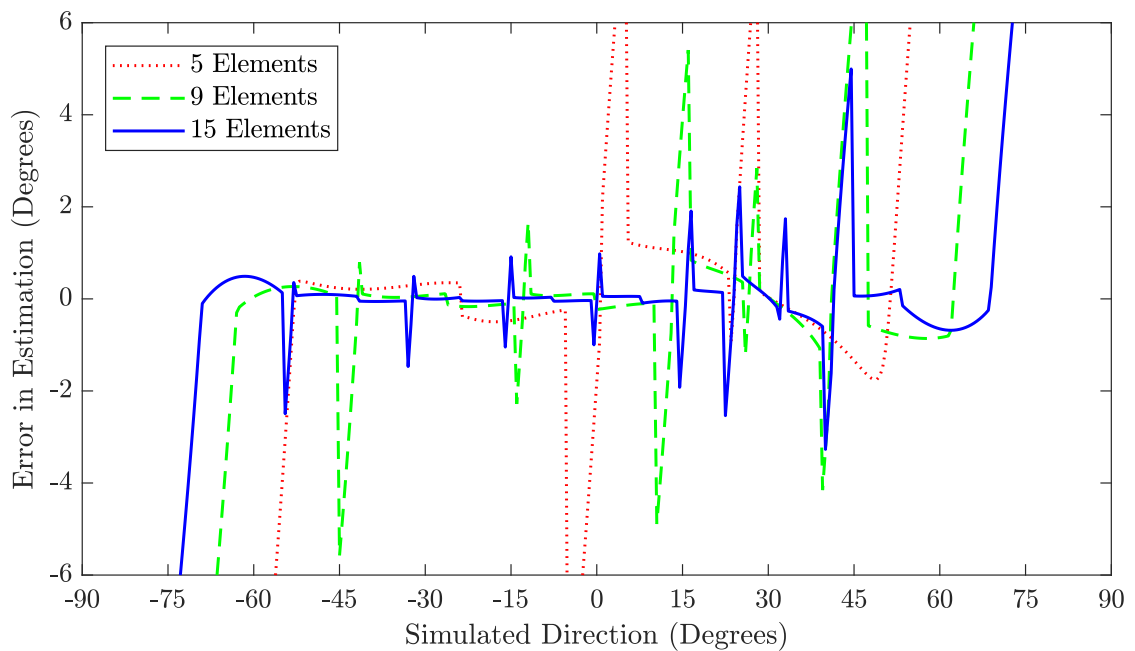
Figure 3.17: Simulated error in DoA estimation using five, nine, and fifteen elements and the algorithm proposed in this chapter when a second signal fixed at $30°$ is added.
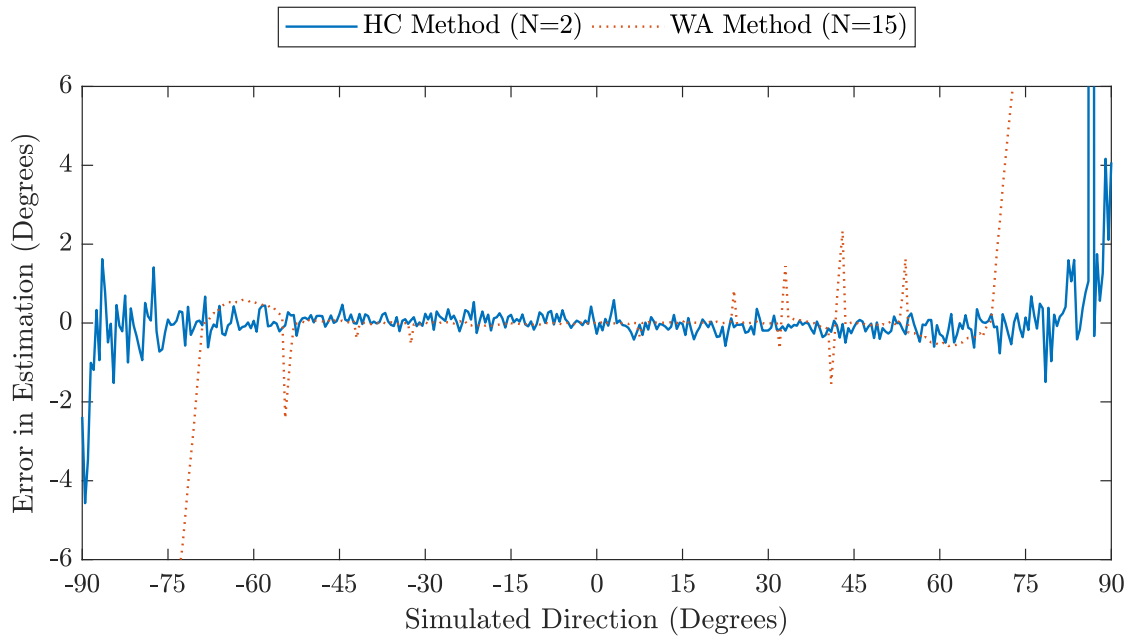
Figure 3.18: Simulated error in direction finding when using the harmonic characteristic method (HC) using 2 elements and the weighted average method (WA) for 15 elements, when the array is illuminated in the presence of noise at 20 dB SNR.

3.4.4 Immunity to Noise

To evaluate the proposed method's immunity to noise and to compare it to the harmonic characteristic method, varying levels of Gaussian-distributed noise were generated. Figures 3.18, 3.19 and 3.20 show the error in direction finding in the presence of noise at 20 dB, 10 dB and 0 dB signal-to-noise ratio (SNR) respectively. It can be seen that the weighted average method proposed in this chapter is generally more noise immune, however the harmonic characteristic method proposed in [3.9] maintains a greater angular range. It can also be seen that the error in estimation using the weighted average method is greatest at the angles calculated by Equation (3.3). Errors at these specific regions when using the weighted average method become similar to the errors at any position using the harmonic characteristic method at noise levels greater than 10 dB SNR.

With decreased SNR, the difference in noise immunity becomes apparent. It should be noted that this is the case for a small number of samples taken. The harmonic characteristic method has been shown to perform well with larger sample counts in [3.9].
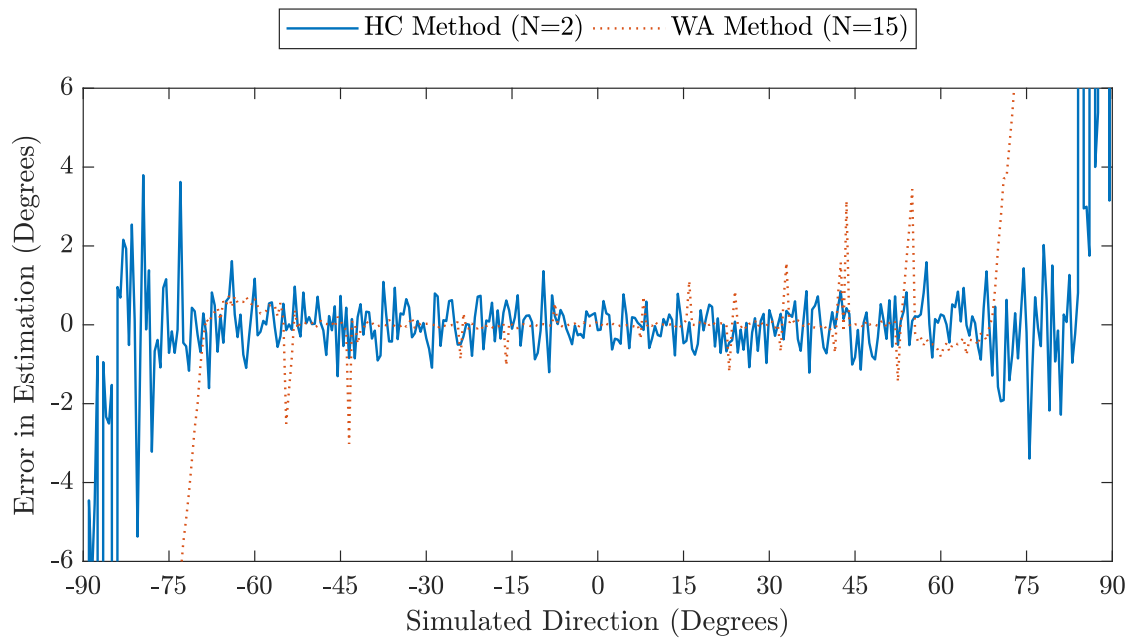
Figure 3.19: Simulated error in direction finding when using the harmonic characteristic method (HC) using 2 elements and the weighted average method (WA) for 15 elements, when the array is illuminated in the presence of noise at 10 dB SNR.
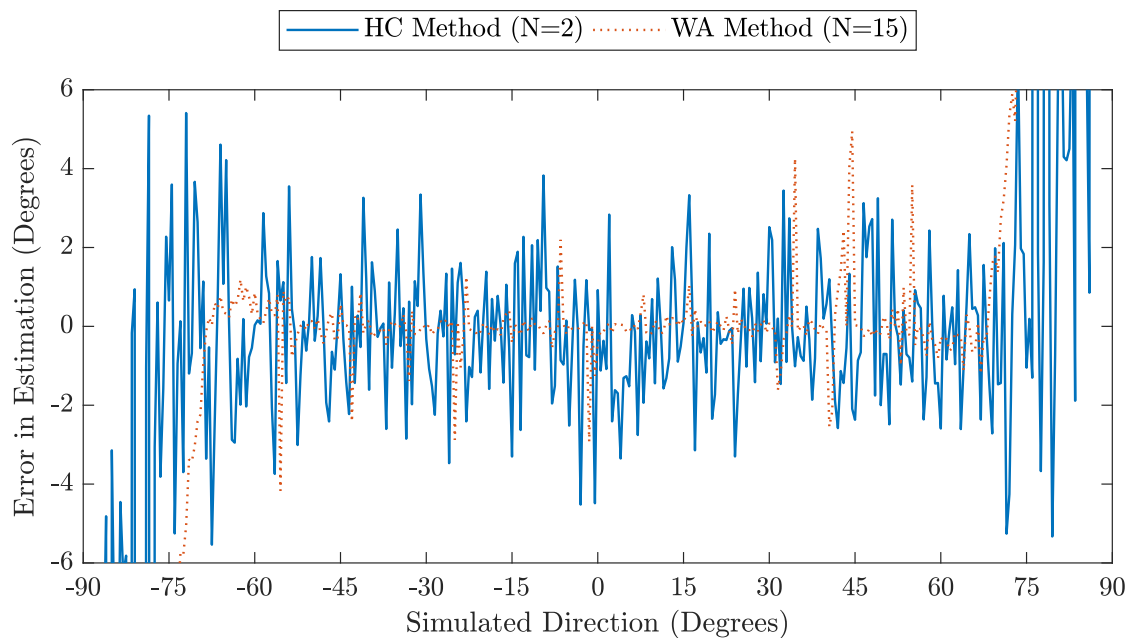
Figure 3.20: Simulated error in direction finding when using the harmonic characteristic method (HC) using 2 elements and the weighted average method (WA) for 15 elements, when the array is illuminated in the presence of noise at 0 dB SNR.
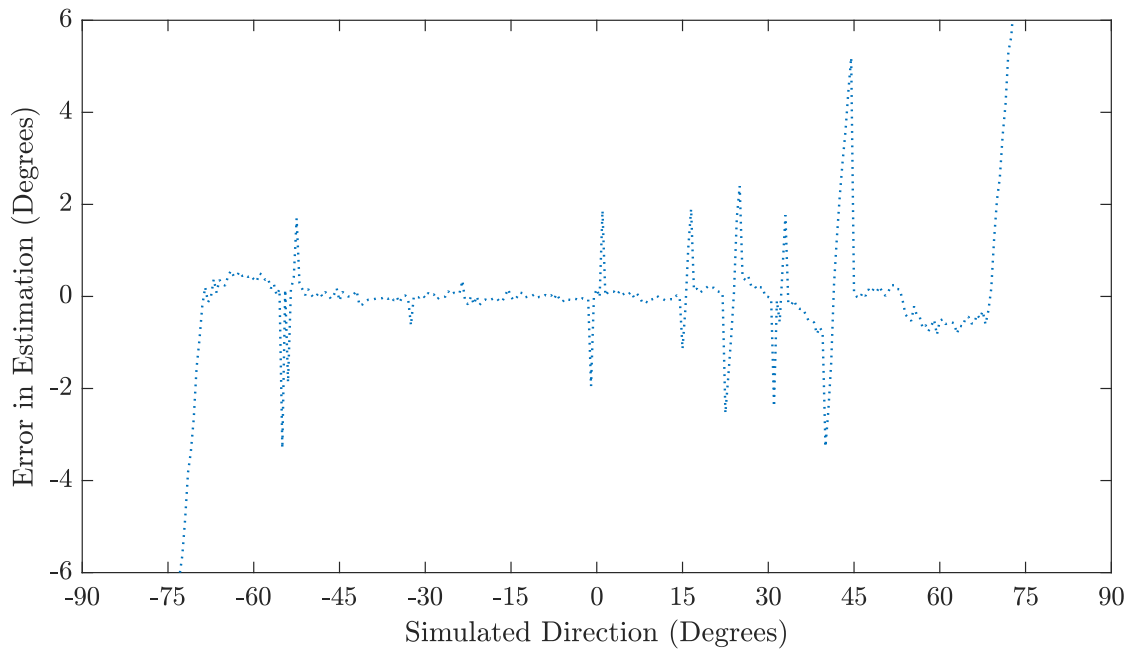
Figure 3.21: Simulated error in DoA estimation using 15 elements with 10dB SNR and the algorithm proposed in this chapter when a second signal fixed at $30°$ is added.

To combine results from sections 3.4.3 and 3.4.4, Figure 3.21 shows the typical direction finding accuracy when a 15 element array operates with 10dB SNR and a secondary signal with 10% amplitude fixed at $30°$. It can be seen that for the majority of the $\pm70°$ range, the method is able to provide a DoA estimation with $\pm1°$ accuracy, with decreased accuracy at the harmonic null regions and also near to the interfering signal.

3.5 Experimental Results

A linear five-element microphone array using MEMS microphones of type SPU0410LR5H-QB was constructed (Figure 3.22) with an inter-element spacing of 4.25 mm. This array spacing was chosen to be half the wavelength of a signal transmitted from a narrow-band 40 kHz piezoelectric acoustic source. This source was a generic device of type 400ST160 having a bandwidth of approximately 2 kHz and a transmit pressure of approximately 110 dB Sound Pressure Level (SPL). It was driven from the $50\,\Omega$ output of a function generator producing a 40 kHz sine wave. A National Instruments "myRIO" was used for the processing of the received signal. The Field-Programmable Gate Array (FPGA) on the myRIO was setup to produce a digital waveform to control a set of complementary metal-oxide-semiconductor (CMOS) analogue switches that select between
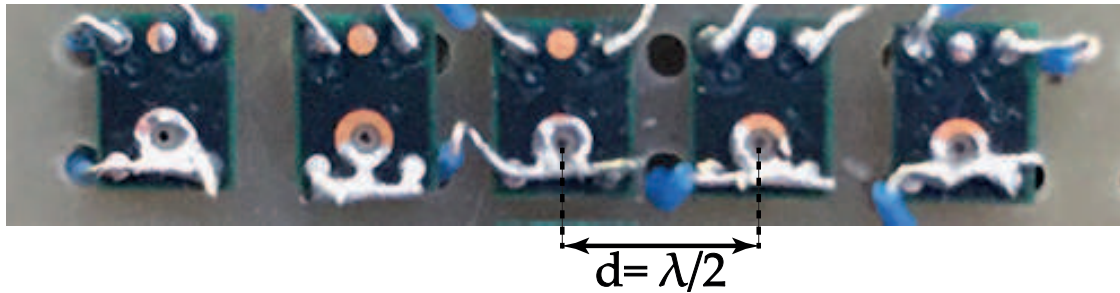
Figure 3.22: Setup of the experimental microphone array with an inter-element spacing (d) of approximately $\lambda/2$ where λ is the wavelength of a 40 kHz acoustic wave. Each microphone is a SPU0410LR5H-QB [3.11] Micro-Electromechanical Systems (MEMS) omnidirectional microphone.

the individual microphone elements. A single analogue signal was captured at a rate of 500 kHz. 200 samples were captured for each element before switching to the next element meaning that 1000 samples were taken overall. The real-time processor chip on the myRIO performed DFTs at 39 kHz, 39.5 kHz, 40 kHz, 40.5 kHz and 41 kHz during the acquisition stage. Where null regions were detected, the process switched to using data from the centre three microphones, and DFTs were performed at 39.17 kHz, 40 kHz, and 40.83 kHz. The method described in Section 3.3 was used in LabVIEW 2015 [3.10] to predict the source's one-dimensional heading.

The transmitter was securely mounted and fixed in position, 0.5 m from the array centre and carefully aligned so that the array was illuminated in the main beam. The microphone array was mounted on a positioner and rotated around its axis as shown in the example Figure 2.10. For each bearing angle measured, 1000 samples were taken and the DFT amplitudes were analysed to estimate the source direction θ_{est} and this estimation was compared with the known direction θ. In addition, performance data was produced using LabVIEW's Tick Count facilities.

Figure 3.23 shows that the beam patterns of the constructed unit are in good agreement with those predicted theoretically. It can also be seen that there are a few distortions in the patterns of the outer-harmonics, there are many possible explanations for this but the theory assumes omnidirectional receivers and does not account for the presence of a surface behind the array or the complexities of real transducers (e.g., intra-element coupling). Nonetheless, Table 3.1 shows that the results represent good DoA performance and agree with the overall trends that would be predicted. It is clear that

Table 3.1: The estimation results obtained from the system attempting to locate a source at various Direction of Arrivals (DoAs). The estimates marked in **bold** are the estimates chosen by the system as its solution.

θ	θ_{est} Using 5 Elements	θ_{est} Using 3 Elements	Absolute Error ($\lvert\theta_{est} - \theta\rvert$)
00	**−2.457**	−3.034	2.457
05	**05.519**	04.714	0.519
10	**09.523**	09.815	0.477
15	**14.390**	16.608	0.610
20	**21.048**	21.310	1.048
23.6	19.853	**24.331**	0.731
25	20.094	**26.542**	1.542
30	**31.533**	29.953	1.533
35	**34.440**	34.027	0.560
40	**42.142**	28.376	2.142
45	**42.777**	39.570	2.223
50	**44.499**	39.147	5.501
55	**47.483**	36.020	7.517

the system is generally more accurate when using the data from a larger number of elements, but the use of switching to using the data from three elements has proved beneficial in the cases where the signal direction was close to one of the harmonic's null regions ($23.6°$).

The mean average time taken to convert the set of eight DFTs to an angle estimation was 29 μs. The time to perform the method described in [3.9] was also measured to compare the proposed method's computational complexity. The mean average time taken to convert the two DFTs to an estimation in this case was 41 μs. This is expected as the handling of complex arithmetic is usually significantly slower in these systems.
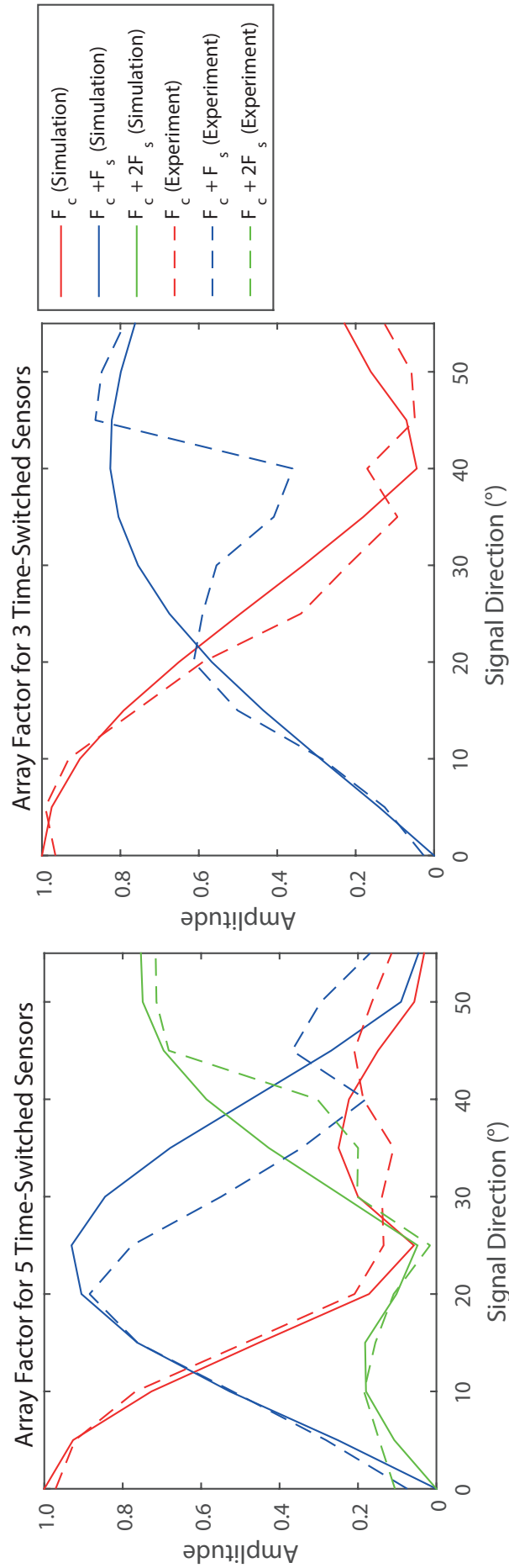
Figure 3.23: The received harmonic content of an experimental five-element linear microphone array compared to the expected numerical results.

3.6   Weighting by Harmonic Index

The method described in this chapter is a linear estimation, and therefore makes the assumption that each harmonic has equal maximum amplitude, and each beam has an equal angular separation. It was shown previously that in the case of sequentially switching through the array and for a given incoming signal, the maximum amplitude of each sideband is known. Therefore, the harmonics can be normalized in response to the main beam operating at the centre frequency, which produces the array factor as shown in Figure 3.24:

$$AF_{norm}(h, \theta) = \frac{AF(h, \theta)}{\text{sinc}\,\frac{h}{N}} \tag{3.5}$$

Instead of interpolating an angular heading based of of the known angles of the beam, an alternative approach would be to use a harmonic index number that is normalised, so that it becomes a non-integer between the same $\pm\frac{N}{2}$ limits. For example if power of the incoming main beam was distributed so that sidebands with indexes 1 and 2 were largest and equal to each other, then the interpolated harmonic index would set as 1.5. If the new index is used in place of h in Equation (3.3) then a single direction estimate can be obtained.

$$h_{est} = \frac{X_\alpha h_\alpha + X_{\alpha+1} h_{\alpha+1}}{X_\alpha + X_{\alpha+1}} \tag{3.6}$$

$$\theta_{est} = \sin^{-1} \frac{h_{est}}{RN} \tag{3.7}$$

Figure 3.25 shows how the modified technique (also including the error reduction technique as described in Section 3.3.1) performs with various numbers of elements in the array. As can be seen when comparing Figure 3.26 with Figure 3.9, the modified technique has improved accuracy when using different numbers of elements, and in ideal conditions the spikes of inaccuracies found in the previous version of the technique have been reduced.
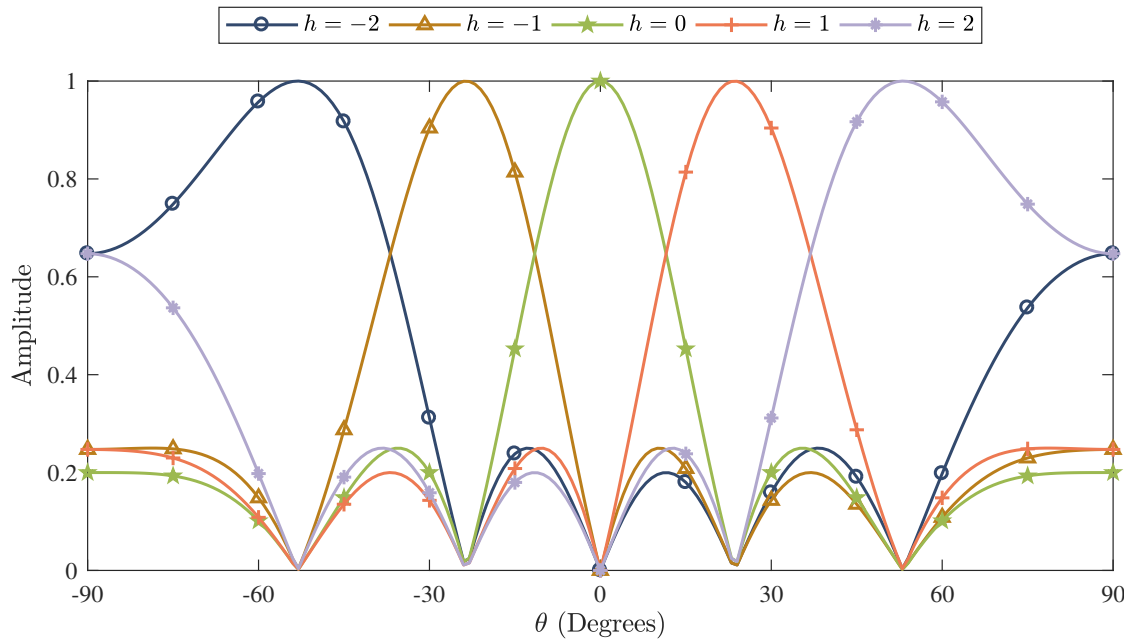
Figure 3.24: Array Factor of a five-element array (switched sequentially) with half-wavelength element spacing. Each sideband has been normalised in relation to the main beam.
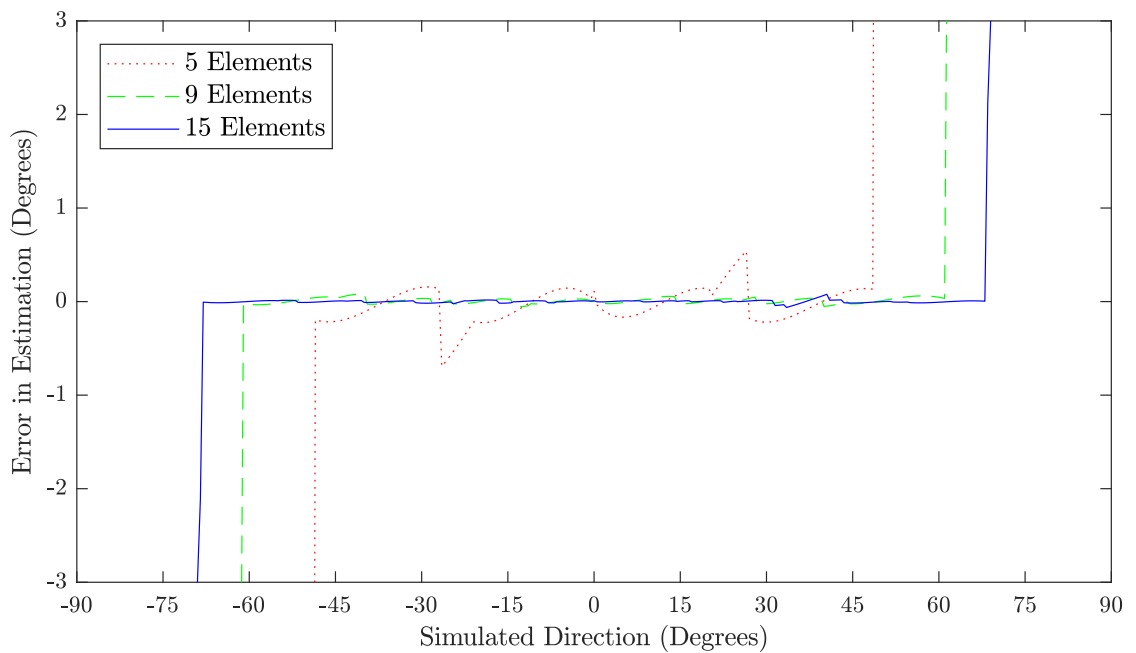
Figure 3.25: Simulated error in direction of arrival estimation of a linear array using fifteen (solid), nine (dashed) or five microphones (dotted) in ideal conditions.
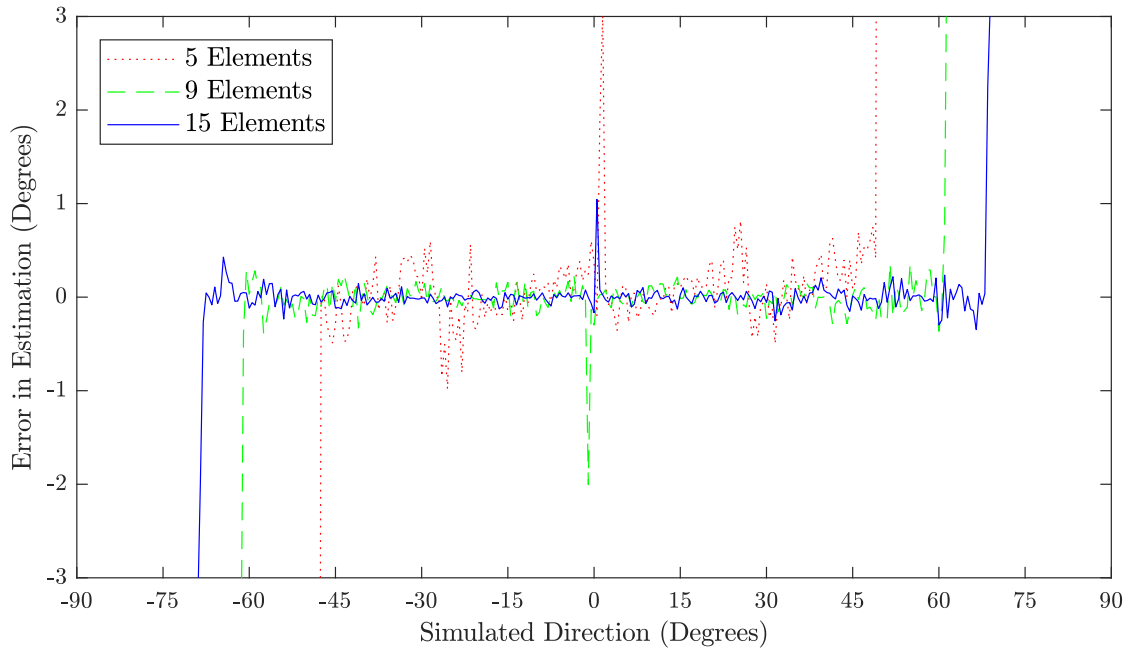
Figure 3.26: Simulated error in direction of arrival estimation (using the harmonic index weighting method) with three different numbers of elements in the presence of noise. Each test had 1350 samples taken from an array with five (dotted), nine (dashed) or fifteen (solid) elements, where the source SNR was set to 10 dB.

3.7   Conclusions

A direction-finding method with both low hardware and computational requirements has been introduced and evaluated for acoustic signals. Both numerical simulations and a full implementation of the algorithm using MEMS sensors to achieve fast direction-finding with ultrasonic frequencies has been presented. The use of small MEMS sensors makes practical implementations of ultrasonic acoustic arrays possible. The technique was demonstrated using a prototype system containing an FPGA and a real-time processor, but the method can be implemented using any single device with one analogue input and digital lines to switch between sensors in a circuit.

Furthermore, since the proposed method only requires real-valued magnitudes of the frequency content, it is possible to use optimised algorithms, such as the Goertzel algorithm [3.12], to compute the amplitudes of the harmonic content for the array, minimising the processing time and complexity needed to obtain a DoA estimation. For more accurate estimations using the harmonic powers, interpolating a harmonic index and using Equation (3.7) produces a more accurate estimation than if the known angles

in each harmonic are interpolated. This is especially true when more elements are used to distribute the power into a larger number of sidebands.

The technique demonstrated in this chapter has been compared with more computationally demanding estimators and in the case of [3.9], the use of sensitive functions or complex arithmetic is avoided by the use of real-valued powers. These existing estimators are highly accurate in ideal conditions, but the technique demonstrated in the present chapter has obtained good DoA resolution in comparison and can be performed using relatively simple systems that can be adapted to suit a variety of requirements. Furthermore, the method proposed in this chapter demonstrates a good level of immunity to noise and multipath reflections.

If the system to be implemented requires high angular accuracy in the presence of noise, then the use of a greater number of microphones is preferable. If the system is required to find positions of signals that are short in duration, then it is possible to reduce the number of samples per microphone whilst keeping consistency in the direction-finding resolution.

References

[3.1] R. Schmidt, "Multiple emitter location and signal parameter estimation," *IEEE Trans. Antennas Propag.*, vol. 34, no. 3, pp. 276–280, Mar 1986.

[3.2] R. Roy and T. Kailath, "ESPRIT - Estimation of Signal Parameters Via Rotational Invariance Techniques," *IEEE Trans. Acoust.*, vol. 37, no. 7, pp. 984–995, July 1989.

[3.3] P. Webb and C. Wykes, "High-resolution beam forming for ultrasonic arrays," *IEEE Trans. Robot. Autom.*, vol. 12, no. 1, pp. 138–146, 1996.

[3.4] W. Munro, S. Pomeroy, M. Rafiq, H. Williams, M. Wybrow, and C. Wykes, "Ultrasonic vehicle guidance transducer," *Ultrasonics*, vol. 28, no. 6, pp. 350–354, November 1990.

[3.5] V. Kunin, M. Turqueti, J. Saniie, and E. Oruklu, "Direction of Arrival Estimation and Localization Using Acoustic Sensor Arrays," *J. Sens. Technol.*, vol. 01, no. 03, pp. 71–80, 2011.

[3.6] S. Harput, A. Bozkurt, and F. Y. Yamaner, "Ultrasonic phased array device for real-time acoustic imaging in air," in *Proc. - IEEE Ultrason. Symp.*, vol. 8, no. 11.   IEEE, November 2008, pp. 619–622.

[3.7] H. Shanks, "A new technique for electronic scanning," *IRE Trans. Antennas Propag.*, vol. 9, no. 2, pp. 162–166, Mar 1961.

[3.8] A. Tennant, "Experimental Two-Element Time-Modulated Direction Finding Array," *IEEE Trans. Antennas Propag.*, vol. 58, no. 3, pp. 986–988, Mar 2010.

[3.9] C. He, X. Liang, Z. Li, J. Geng, and R. Jin, "Direction Finding by Time-Modulated Array With Harmonic Characteristic Analysis," *IEEE Antennas Wirel. Propag. Lett.*, vol. 14, pp. 642–645, 2015.

[3.10] National Instruments, "LabVIEW," 2015.

[3.11] Knowles Accoustics, "SPU0410LR5H-QB Product Datasheet," 2013. [Online]. Available: http://www.knowles.com/eng/content/download/5755/91802/version/3/file/SPU0410LR5H-QB+revH.PDF

[3.12] G. Goertzel, "An Algorithm for the Evaluation of Finite Trigonometric Series," *Am. Math. Mon.*, vol. 65, no. 1, pp. 34–35, January 1958.

4 | Producing Unique Beams in Time-Modulated Planar Arrays

T‍HE situation often arises where a signal propagating through three-dimensional space needs to be localised. A heading in these cases is usually two-dimensional. In this chapter, the use of time modulation is explored to create two-dimensional estimations, and the techniques seen previously in this work are extended and analysed numerically.

4.1 Introduction

In Chapter 3, DoA estimation was achieved in one dimension, but it could in theory be extended to two dimensions by using a second orthogonal linear array. In this case, a separate input stage for each axis would be needed to obtain an estimation. If there is a strict requirement on having a single input stage (e.g. in order to minimise complexity), then each array would have to be sampled consecutively. If a target was moving across the two axes at speed, the two obtained values would be slightly desynchronised. Therefore, there is a need to see if unique beams can be created in two-dimensions.

A known solution to the problem of two-dimensional beam steering is the planar array. By controlling the individual amplitudes and phases of each element aligned in a grid, another dimension of control is obtained [4.1] and the main beam produced by the array can be controlled in terms of an azimuth (ϕ), and elevation (θ) response. As with the conventional linear arrays, each element of a conventional planar array needs individual analogue control and input stages. The time-modulated alternative to the

conventional method is to use a Time-Modulated Planar Array (TMPA).

Much of the recent literature has focused on producing specific patterns for the centre frequency, or on reducing the sidebands that occur during the switching process [4.2, 4.3, 4.4]. The methods and benefits of multiple simultaneous sidebands steering in two dimensions have been studied less frequently in the literature.

Poli et al. [4.5] showed that the calculations and design of TMPAs can be simplified by modelling the array as a multiplication of two TMLAs on orthogonal axes, referring to the signal's position in terms of azimuth and elevation angles. The work described in this chapter uses such a simplification, in order to produce a number of harmonic beams equal to the number of array elements. Each of these beams are steered in a unique direction and operate on different harmonic frequencies. To make the results obtained from the planar array more easily comparable to the theories described in Chapter 3, the angular position of the signal is given in terms of broadside angles along orthogonal axes.

Whilst conventional arrays use amplitude weightings per element as described in Chapter 2, a time-modulated alternative was demonstrated by Tong and Tennant [4.6], who showed that by changing the switch-on times of each element across in a specific pattern and by adjusting the length of time that individual elements are turned on so that they match the ratio of amplitudes used in a conventional amplitude weighting, similar array factors at the centre harmonic could be achieved. This technique was demonstrated for a TMLA using well-known weighting distributions such as the Dolph-Chebyshev distribution [4.7].

Applying weighting distributions using time switching is now being commonly used in planar arrays. However, most of these works focus on reducing sidebands, and elements are usually switched on simultaneously in order to receive a higher response at the centre frequencies. The work described in this chapter uses the above concepts for TMPAs and describes a method of switching that allows the array to form multiple sidebands with a main beam pointing towards a unique two-dimensional location.

The chapter provides a brief overview of the theory behind TMPAs. A basic switch-

ing order needed for distributing multiple simultaneous beams is described and a set of equations for determining the steering angles of each harmonic in broadside angles and their equivalent in azimuthal and elevation angles are provided. The theory is extended by demonstrating how these harmonic patterns can be controlled whilst keeping the positions of the main beams in each harmonic. Section 4.3 provides results obtained from a numerical simulation of a TMPA in both the time and the frequency domain. Finally, the generation of beams from an array with equal time weighting is used to see how the DoA estimation methods derived in Chapter 3 can be extended for use with planar arrays, and therefore have a two-dimensional DoA estimation using only one input stage.

4.2 Theory

In this section, the equations that describe TMPAs are given and then rearranged to provide a definition of an array factor in terms of two broadside angles representing orthogonal axes. The theory is then extended on by using specific switching patterns to create unique harmonic beams.

4.2.1 Background

A planar array of $M \times N$ elements array equally spaced with distances d_x and d_y on the x and y axes respectively can be modelled as seen in Figure 4.1. The Array Factor for such an array can be derived from first principles and written as [4.2]:

$$AF(\theta, \phi, t) = e^{j\omega_0 t} \sum_{m=0}^{M-1} \sum_{n=0}^{N-1} U_{mn}(t) e^{jk \sin \theta (md_x \cos \phi + nd_y \sin \phi)} \tag{4.1}$$

where ω_0 is the angular frequency of the primary signal, k is its wave number, ϕ and θ are the signal azimuth and elevation angles respectively. $U_{mn}(t)$ is the switching function that turns each element either on or off in time which can be mathematically defined by:

$$U_{mn}(t) = \begin{cases} 1, & \tau_{mn,on} \le t < \tau_{mn,off} \\ 0, & \text{otherwise} \end{cases} \tag{4.2}$$
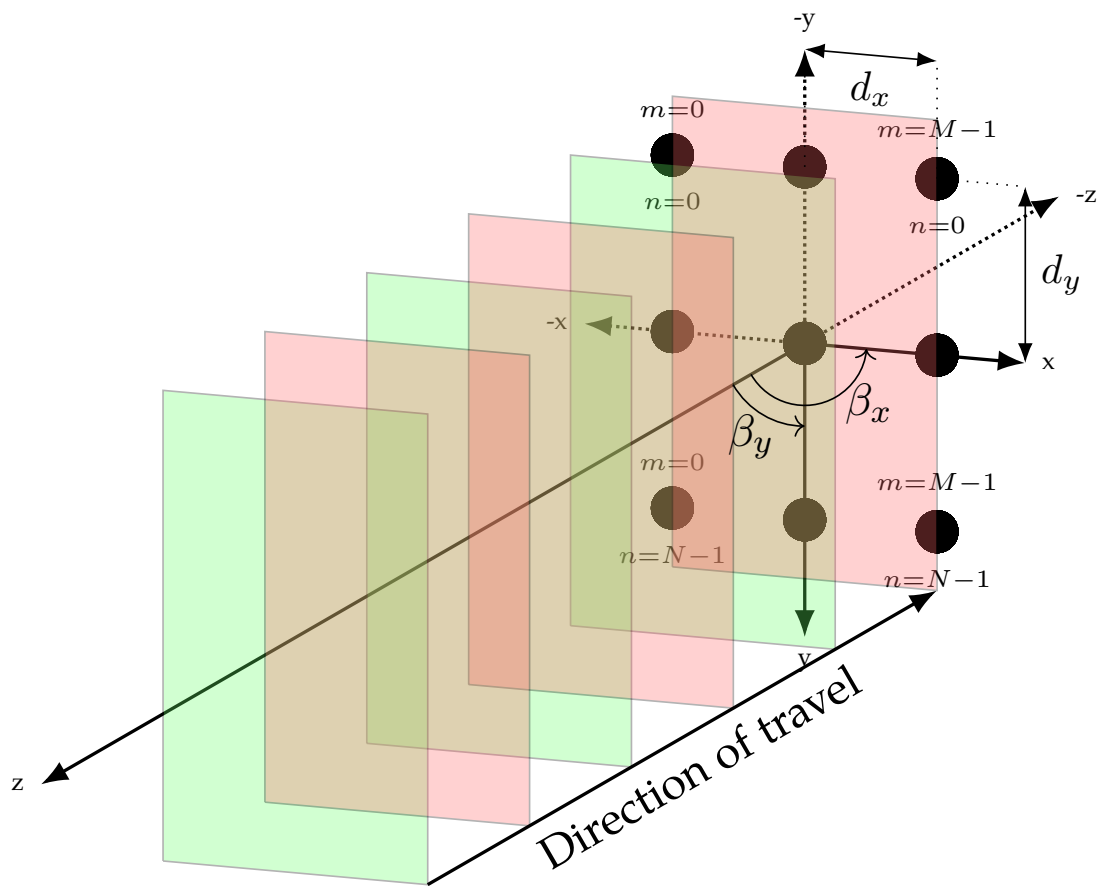
Figure 4.1: Model of an $M \times N$ element time-modulated array with $d_x \times d_y$ spacing. A plane wave is impinging on the array at both of the axes' broadsides ($\beta_x = \beta_y = 0$).

where $\tau_{mn,on}$ and $\tau_{mn,off}$ represent the switch on and off times for an element indexed by (m, n). This function can be periodic with angular frequency $\omega_s = 2\pi/T_s$ where T_s is the time taken to complete the switching sequence. This can be expressed as the sum of its Fourier coefficients with harmonic numbers indexed by h:

$$U_{mn}(t) = \sum_{h=-\infty}^{\infty} C_{mn}e^{jh\omega_s t} \tag{4.3}$$

The coefficients C_{mn} can be calculated as:

$$C_{mn} = \frac{1}{T_s}\int_0^{T_s} U_{mn}(t)e^{-jh\omega_s t}dt \tag{4.4}$$

In this chapter, it is assumed that the array is illuminated in the far field from the two broadside angles β_x and β_y which are related to ϕ and θ by:

$$\beta_x = \sin^{-1}\left(\sin\theta\cos\phi\right) \tag{4.5}$$

$$\beta_y = \sin^{-1}\left(\sin\theta\sin\phi\right) \tag{4.6}$$

Therefore, it can be shown that Equation (4.1) can be expressed as:

$$AF(\beta_x, \beta_y, t) = e^{j\omega_0 t}\sum_{m=0}^{M-1}\sum_{n=0}^{N-1} U_{mn}(t)e^{jk(md_x\sin\beta_x + nd_y\sin\beta_y)} \tag{4.7}$$

To obtain a two dimensional position that can be easily related to the methods outlined in Chapter 3, the array can also be modelled as the multiplication of two equations representing the array factors of orthogonal linear axes which have the switching functions $U_m(t)$ and $U_n(t)$ [4.5], which means that $U_{mn} = U_m \cdot U_n$. Using this simplification, it can be further shown that

$$
\begin{aligned}
AF(\beta_x, \beta_y, t) =& e^{j\omega_0 t}\sum_{m=0}^{M-1} U_m(t)e^{jkmd_x\sin(\beta_x)} \\
& \times \sum_{n=0}^{N-1} U_n(t)e^{jknd_y\sin(\beta_y)}
\end{aligned}
\tag{4.8}
$$

which will form the basis of predicting the main beam angle of each sideband produced

by the single output of the planar array. The following sections make use of this form to generate unique beam patterns across the range of harmonics.

4.2.2 Switching Pattern Used to Generate Distributed Harmonic Beams

As described by Tong and Tennant [4.6], the sequential switching of a linear array with periodic on times causes the beams of sidebands to form in unique directions across a single broadside axis. In order to extend on theories shown in Chapter 3, Equations (2.22) and (2.20) an be expressed in terms of M elements laying on the x-axis:

$$
\begin{aligned}
AF(\beta_x, t) =& \frac{1}{M} \sum_{h=-\infty}^{\infty} e^{j(\omega_0 + h\omega_s)t} \operatorname{sinc}\left(\frac{\pi h}{M}\right) \\
& \times \sum_{m=0}^{M-1} e^{2\pi j m R_x \left[\sin(\beta_x) - \frac{h}{M R_x}\right]}
\end{aligned}
\tag{4.9}
$$

where R_x is the ratio of element spacing d_x to the wavelength λ.

Each of the elements in a TMPA can be switched in any order. This chapter utilizes a pattern where the elements are switched on then off in sequence in the order $i = 0, 1, 2\ldots$, first by switching left to right on the top row of elements, then continuing to the next row until all elements have been switched once. This sequence is shown in Figure 4.2 and can be repeated continuously.

A definition of C_{mn} can be obtained using Equations (4.2) and (4.4). In these equations the individual positions of each element do not change the value of C_{mn}, and therefore its definition for a two-dimensional array with specific on times is the same as a linear array having the same number of elements and equivalent on times. In order to produce a definition of C_{mn} for a planar array, a single element index can be obtained by using the separate axes idexes m and n. For the specific pattern mentioned in this section, this single element index can be calculated as

$$
i = (Mn) + m
\tag{4.10}
$$

$$
\begin{array}{cccccc}
 & m=0 & m=1 & m=2 & \cdots & m=M-1 \\
n=0 & 0 & 1 & 2 & \cdots & M-1 \\
n=1 & M & M+1 & M+2 & \cdots & 2M-1 \\
n=2 & 2M & 2M+2 & 2M+2 & \cdots & 3M-1 \\
 & \vdots & \vdots & \vdots & \vdots & \ddots & \vdots \\
n=N-1 & (N-1)M & (N-1)M+1 & (N-1)M+2 & \cdots & NM-1
\end{array}
$$
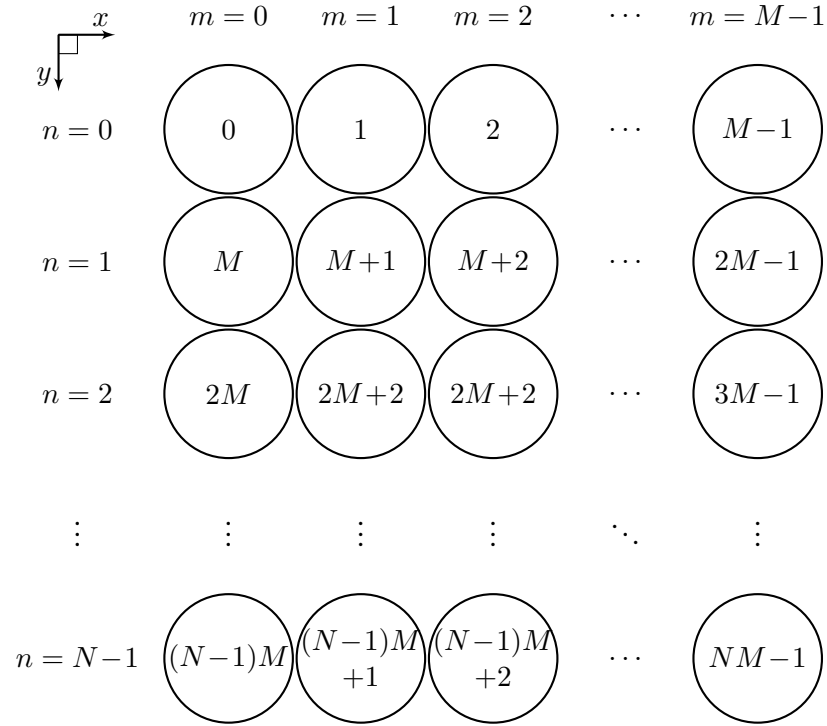
Figure 4.2: The normalised switched on times and order of an $M \times N$ element array in the proposed sequence.

therefore, C_{mn} can be calculated as:

$$
C_{mn}(t) = \operatorname{sinc}\left(\frac{\pi h}{MN}\right) e^{-\frac{j2\pi h[(Mn)+m]}{MN}} \tag{4.11}
$$

The normalised array factor for a planar array switched in the manner described is obtained by combining Equations (4.3) and (4.7) to obtain the switching function in terms of the sum of its Fourier components:

$$
U_{mn}(t) = \sum_{h=-\infty}^{\infty} \operatorname{sinc}\left(\frac{\pi h}{MN}\right) e^{-\frac{2jπh[(Mn)+m]}{MN}} e^{jh\omega_s t} \tag{4.12}
$$

and then substituting this expression for $U_{mn}(t)$ into Equation (4.11) to produce:

$$
\begin{aligned}
AF(\beta_x, \beta_y, t) = &\frac{1}{MN} \sum_{h=-\infty}^{\infty} e^{j(\omega_0+h\omega_s)t} \operatorname{sinc}\left(\frac{\pi h}{MN}\right) \\
&\times \sum_{m=0}^{M-1}\sum_{n=0}^{N-1} e^{-\frac{2\pi jh[(Mn)+m]}{NM}} \\
&\times e^{jk(md_x \sin\beta_x + nd_y \sin\beta_y)}
\end{aligned} \tag{4.13}
$$

In an array of $M \times N$ elements, it is expected that there will be $M \times N$ different sidebands numbered in the range of $\pm\frac{M \times N}{2}$. The switching of elements along the x-axis is M times faster than the switching of elements along the y-axis. As a consequence, changes in signal position along the x-axis broadside will cause changes in power across a larger frequency range than if the signal position were to change across the y-axis broadside. When modelling these harmonics to represent different axes h_x will be in the range of $\pm\frac{M}{2}$ and h_y will be in the range of $\pm\frac{N}{2}$. Assuming that h_x and h_y are both integers within the ranges described, their relationship with the actual sideband number h can be written as:

$$h = Nh_x + h_y \tag{4.14}$$

For example, in a 5×5 element array, measuring the power in the sideband $h = 2$ is the equivalent to measuring the separated sidebands $h_x = 0$ and $h_y = 2$, however measuring at $h = 3$ is equivalent of measuring the separated sidebands $h_x = 1$ and $h_y = -2$. A normalised array factor using these separated sidebands can be obtained and simplified to:

$$
\begin{aligned}
AF(\beta_x, \beta_y, t) = &\frac{1}{MN} \sum_{h=-\infty}^{\infty} e^{j(\omega_0 + h\omega_s)t} \operatorname{sinc}\left(\frac{\pi h}{NM}\right) \\
&\times \sum_{m=0}^{M-1} e^{2\pi jmR_x\left[\sin(\beta_x) - \frac{h_x + \frac{h_y}{N}}{MR_x}\right]} \\
&\times \sum_{n=0}^{N-1} e^{2\pi jnR_y\left[\sin(\beta_y) - \frac{h_y}{NR_y}\right]}
\end{aligned}
\tag{4.15}
$$

where R_y is the ratio of the element spacing on the y-axis d_y to the wavelength λ of the signal.

Figure 4.3 shows the main beam steering angles for each of the sidebands originating from a 5×5 element array. It is important to note that when using the above equations, $|\beta_x| + |\beta_y| \leq 90°$ (the boundary of which is shown as a dotted line) and these co-ordinates map to a single point on a hemisphere. The circled points on the figure that lie beyond the dotted line indicate beams that do not have a mappable point.
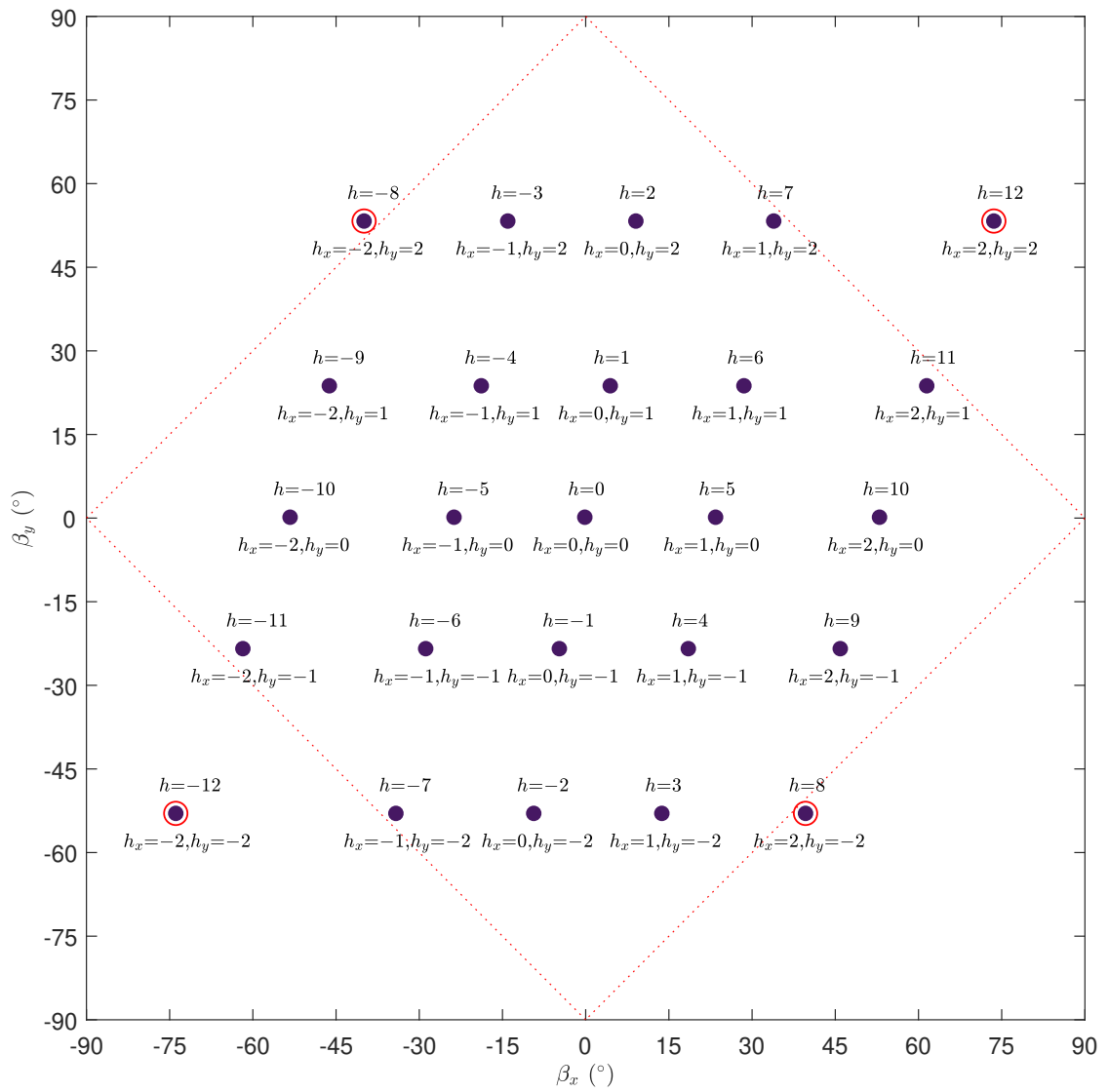
Figure 4.3: Harmonic beam steering angles of a 5×5 element array under the proposed switching scheme

It can be seen that each sideband has a unique two dimensional steering angle, but sets of beams may share the same y-axis broadside angle. This is contrary to using the beams of two independent TMLAs, where it is expected that the β_x and β_y combinations would form a square grid with linear spacing. Switching along two different axes using the sequence described has the effect of skewing the positions of the faster switching axis (i.e. the x-axis in the examples given in this chapter). Figure 4.4 shows the differences in beam position and amplitude along the x and y axes when looking at different h values.

Whilst these beams are different in amplitude and position, they share some of the same traits as would be found in a pair of orthogonal TMLAs. At the locations where each sideband is maximised, all other sidebands are minimised. From Equation (4.15) it can be shown that for each sideband, these locations map to unique combinations of β_x and β_y and these will occur at:

$$\beta_{y,\max}(h_y) = \sin^{-1}\left(\frac{h_y}{R_y N}\right) \tag{4.16}$$

$$\beta_{x,\max}(h_x, h_y) = \sin^{-1}\left(\frac{\frac{h_y}{N} + h_x}{R_x M}\right) = \sin^{-1}\left(\frac{h}{R_x M N}\right) \tag{4.17}$$

The maximum amplitude of these beams normalised to the main beam at the centre harmonic is:

$$\max(AF_h) = \mathrm{sinc}\left(\frac{\pi(Nh_x + h_y)}{MN}\right) = \mathrm{sinc}\left(\frac{\pi h}{MN}\right) \tag{4.18}$$

Since the relative amplitude of each beam is known, then each harmonic can be normalised during a post-processing stage to have the same amplitude response across each sideband. The two important features of the sidebands exploited in Chapter 3 can now be exploited here.
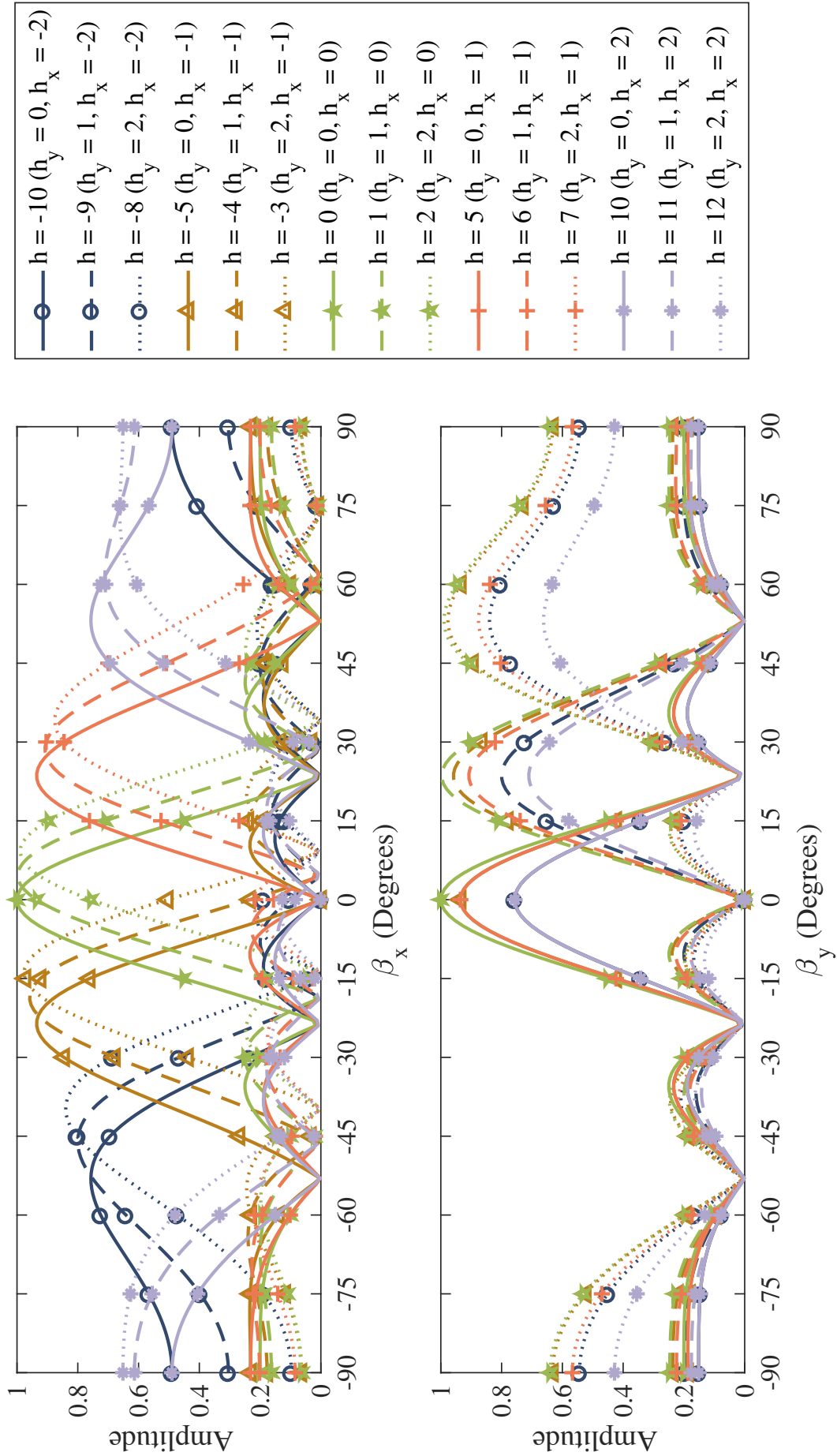
Figure 4.4: The maximum possible response of selected sidebands when analysing different broadside axes. Negative h_y values are not shown for clarity.

It is sometimes appropriate to make to use of a spherical co-ordinate system in DoA applications. The conversion back to azimuth ϕ and elevation θ angles is straight forward:

$$\phi = 2\tan^{-1}\left(\operatorname{cosec}\beta_y\left(\sin\beta_x - \sqrt{\sin^2\beta_x + \sin^2\beta_y}\right)\right) \qquad (4.19)$$

$$\theta = \sin^{-1}\left(\sqrt{\sin^2\beta_x + \sin^2\beta_y}\right) \qquad (4.20)$$

4.2.3 Creating Additional Beams

It was shown in Section 3.3.1 that if only one switching cycle was performed, the samples acquired by the end sensors of a linear array could be removed and DFT analysis could be performed as if it were a $N-2$ element array; this concept is also true for TMPAs. By removing the data from the elements on the first and last row, and performing the DFT analysis as if it were an $M \times (N-2)$ array then additional beams are formed. Some of these beams will have have different steering positions in both x and y axes, since the switching period of the y-axis has decreased, the harmonics formed along the x-axis will be less skewed. Figure 4.5 shows the maximum beam points for a 5×3 array which can be generated by removing the first and last row of data from the time series and recalculating the DFTs.

With the exception of the centre harmonic, which occurs at the target frequency, each of these beams occur at different frequencies. It is also important to note that the sideband beams along the centre of the y-axis have not differed in position. Such a feature could be useful in checking to see if the response of a signal at a particular beam is not related to an unexpected gain at a specific frequency (e.g. from noise or circuit gains and losses).
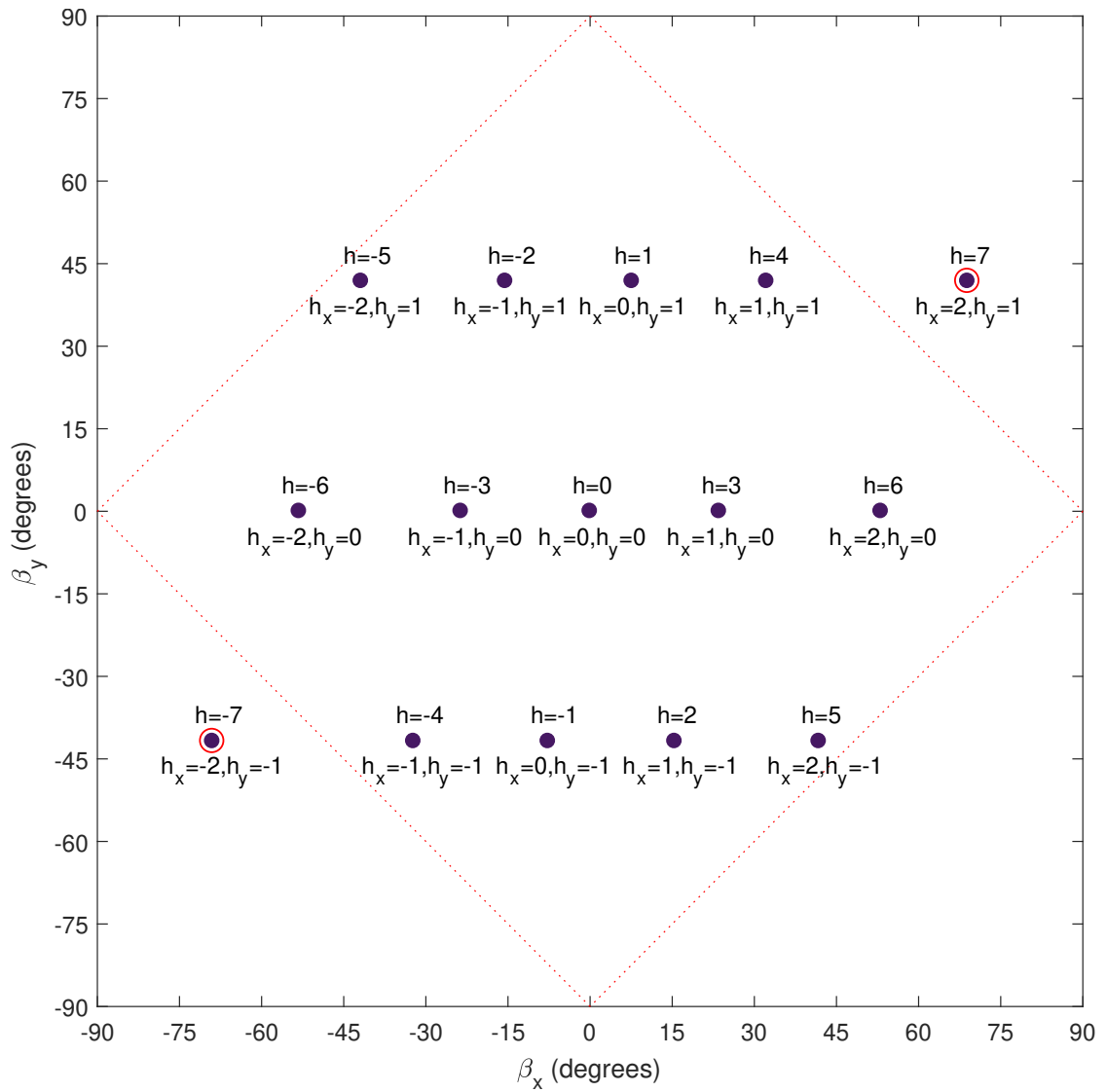
Figure 4.5: Harmonic beam steering angles of a 5×3 element array under the proposed switching scheme.
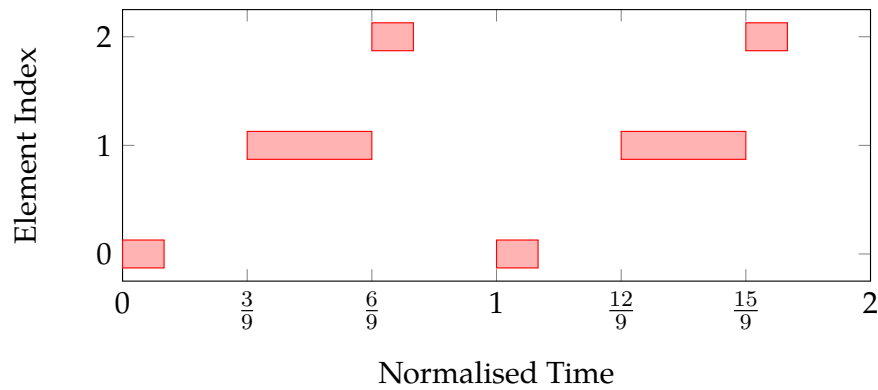
Figure 4.6: Example of an on/off time sequence for a three-element array with a $\{1, 3, 1\}$ time weighting.

4.2.4   Simultaneous Control of Sidelobes on Each Sideband

As shown by Tong and Tennant [4.6], so long as the on times for each element are distributed evenly across the switching sequence, the weighting for each element can be adjusted by decreasing the total length of time that it is switched on. Each element is on for a fraction of its allocated time depending on the weighting needed.

In an example, if three elements with equally distributed on times required the weighting $\{1, 3, 1\}$ as shown in Figure 4.6, the switching period would take place over nine quantised periods of time. The first element would switch on for one period, switch off and then wait two periods before switching to the next element, where it is on for three more periods. After this, it is switched off and the third element is switched on at the same time for a single period. The pattern can then be repeated after waiting an additional two periods. This switching pattern can be in practice controlled by using RF or analogue switches.

In conventional planar arrays, the weighting of well known distributions such as the binomial or Dolph-Chebyshev distributions can be calculated as a multiplication of two linear array weighting distributions [4.8]. Just as in linear arrays, weighting distributions for TMPAs may be realised by changing the length of time that each element is on for [4.5, 4.9]. If a function $W(i)$ stipulates the length of on time needed for element i in the sequence of a TMLA, then the weighting for each element in a planar array with the

(a) Binomial Distribution   (b) Dolph-Chebyshev Distribution
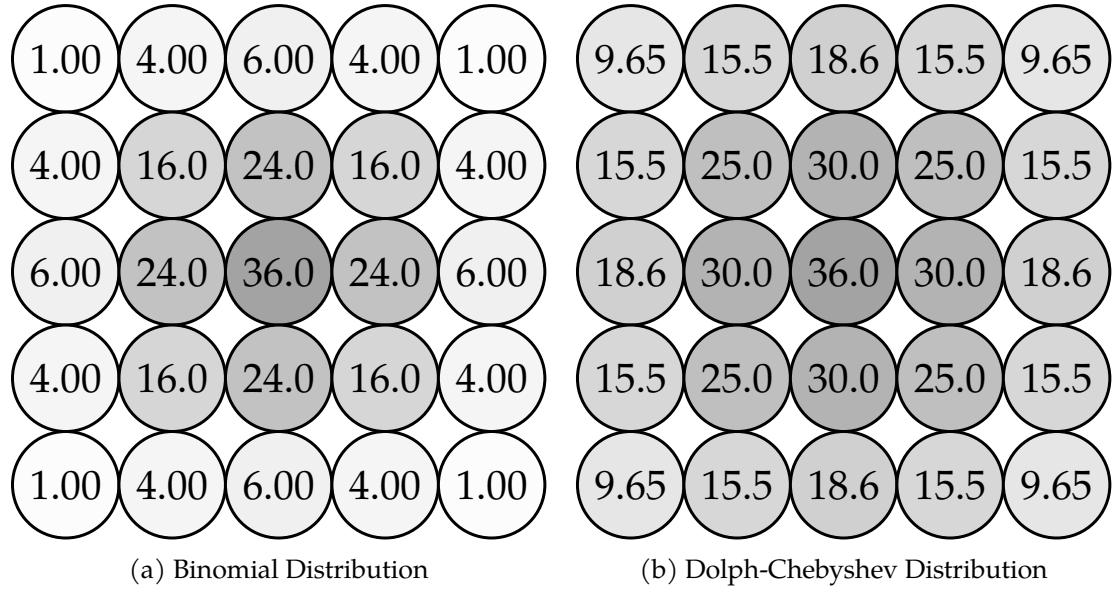
Figure 4.7: Weighting distributions needed to achieve a 5×5 element (a) binomial and (b) -20dB Dolph-Chebyshev array. Each element has been shaded according to its respective weighting.

switch sequence described in Section 4.2.2 is simply:

$$W(Mn + m) = W(m) \times W(n) \tag{4.21}$$

Figure 4.7 shows the weighting needed to achieve either a binomial, where the sidelobes are eliminated, or a Dolph-Chebyshev array, where the sidelobes are set to a specific level relative to the main beam. The binomial distribution for each element i on a single axis with I elements can be calculated as:

$$W(i) = \frac{I - 1!}{[(I - 1) - i]! i!} \tag{4.22}$$

Bresler's method [4.10] has been used to calculate the individual Dolph-Chebyshev distribution weights. The shading in the figure represents its weighting, which makes it clearer to see the difference in variations between the two distributions.

4.3   Numerical Results

In this section a 5×5 element array has been simulated and results including array weighting techniques are discussed.

A source producing a single sinusoidal frequency of 1 GHz was simulated numerically, impinging on a 5×5 isotropic element array with inter-element spacing set as $\lambda/2$. Each element was sampled for a specific duration in time before switching to the next element in the sequence as shown in Figure 4.2. The switching of elements occurred at 250 MHz, creating a harmonic frequency of 10 MHz. Although the switching on times of elements remained fixed, three patterns were tested, where the length of time that each element is sampled varies depending on the following weighting distributions:

(a) Flat Array — Each element is sampled for the full length of time it is switched on, sampling of the next element in the sequence occurs immediately after.

(b) Binomial Array — Each element is sampled for a fraction of the allocated time as shown in Figure 4.7 (a).

(c) Dolph-Chebyshev Array — Each element is sampled for a fraction of the allocated time as shown in Figure 4.7 (b).

4.3.1 Time Domain

Figure 4.8 shows the array output in the time domain when the signal is directed towards the array at an angle of $\beta_x = 30°, \beta_y = 30°$ (this corresponds to $\phi = \theta = 45°$). In the binomial and Dolph-Chebyshev distributions it is straightforward to observe where switching occurs.

It can also be seen that in the Binomial distribution case, the array spends more time switched off than on. The ratio of on time to off time is 28.4%, which yields a relatively low amount of received power. This ratio is significantly better in the Dolph-Chebyshev distributed array, at 54.8%.

4.3.2 Frequency Domain

A set of 25 DFT Amplitudes were collected in the range of 0.88–1.12 GHz (corresponding to each combination of x and y axis harmonics) for each angular position of the source. Figure 4.9 shows the array response after performing a DFT at two different harmonics.
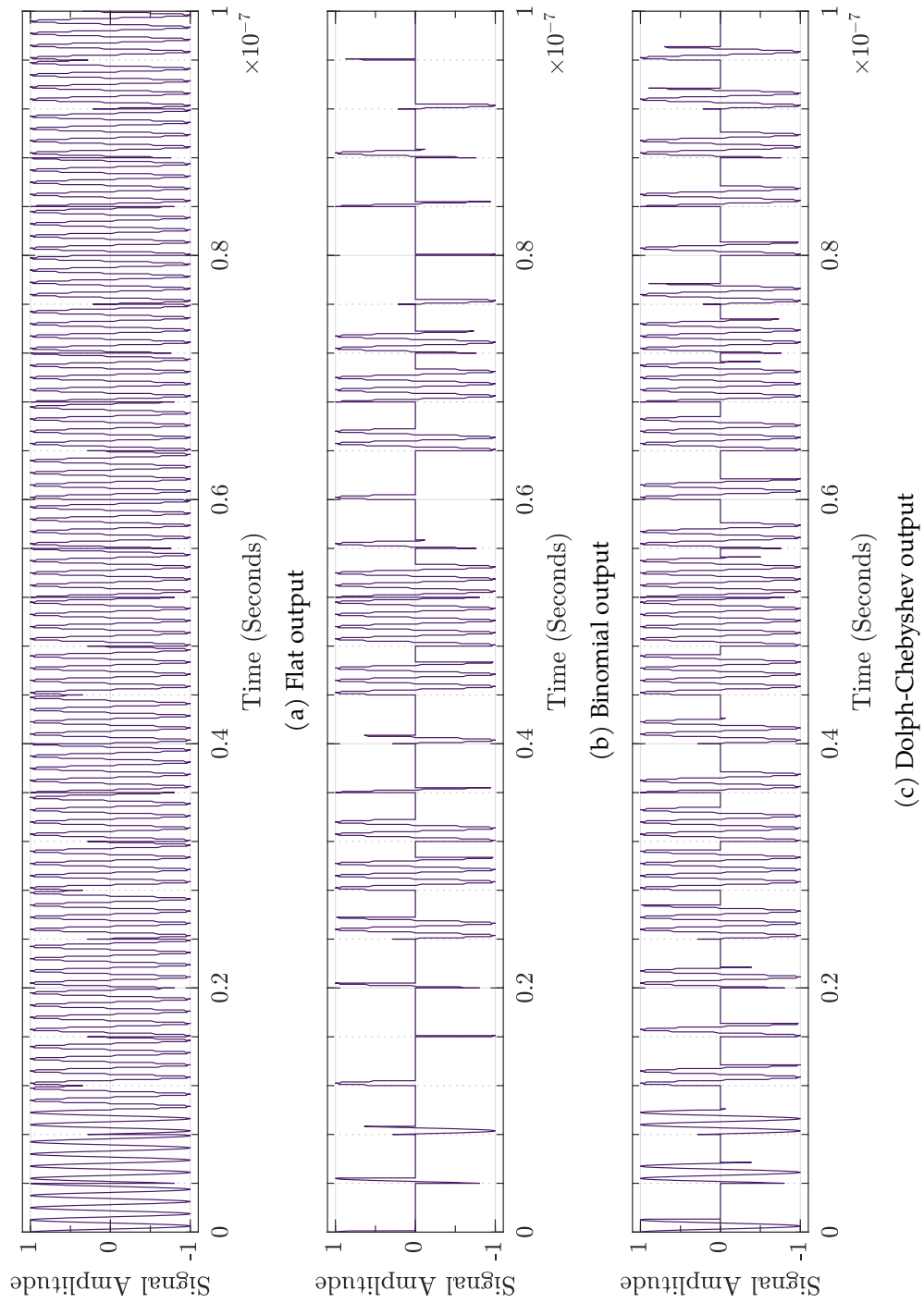
Figure 4.8: Time domain output of a 5×5 time-modulated array with different weighting distributions.

(a) Flat (h=0)

(b) Flat (h=6)

(c) Binomial (h=0)

(d) Binomial (h=6)

(e) Dolph-Chebyshev (h=0)

(f) Dolph-Chebyshev (h=6)
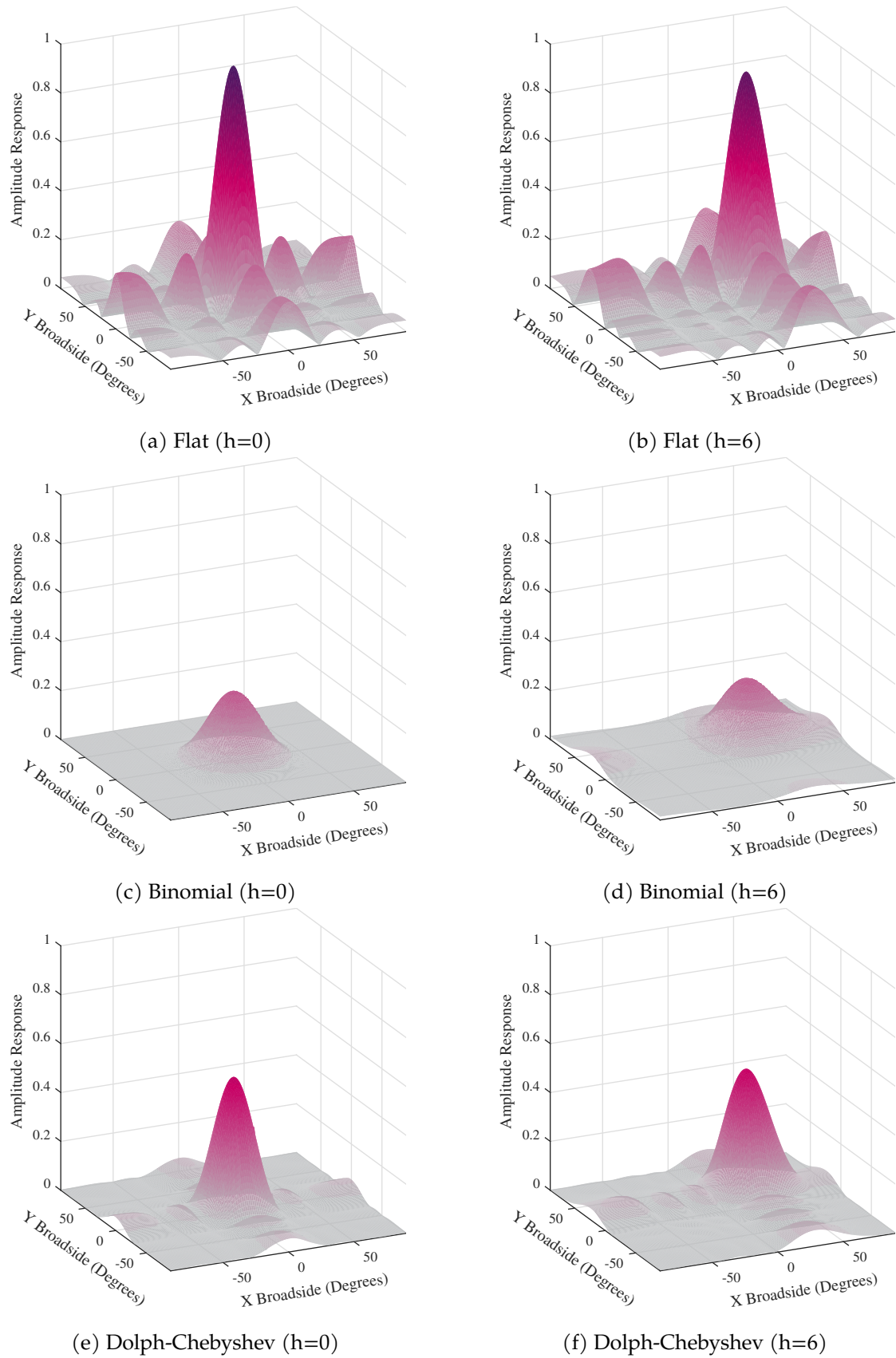
Figure 4.9: Beam patterns of a 5×5 element array with three different time-weighting distributions and two different scanning frequencies.

(a) Binomial (h=0) (b) Dolph-Chebyshev (h=0)
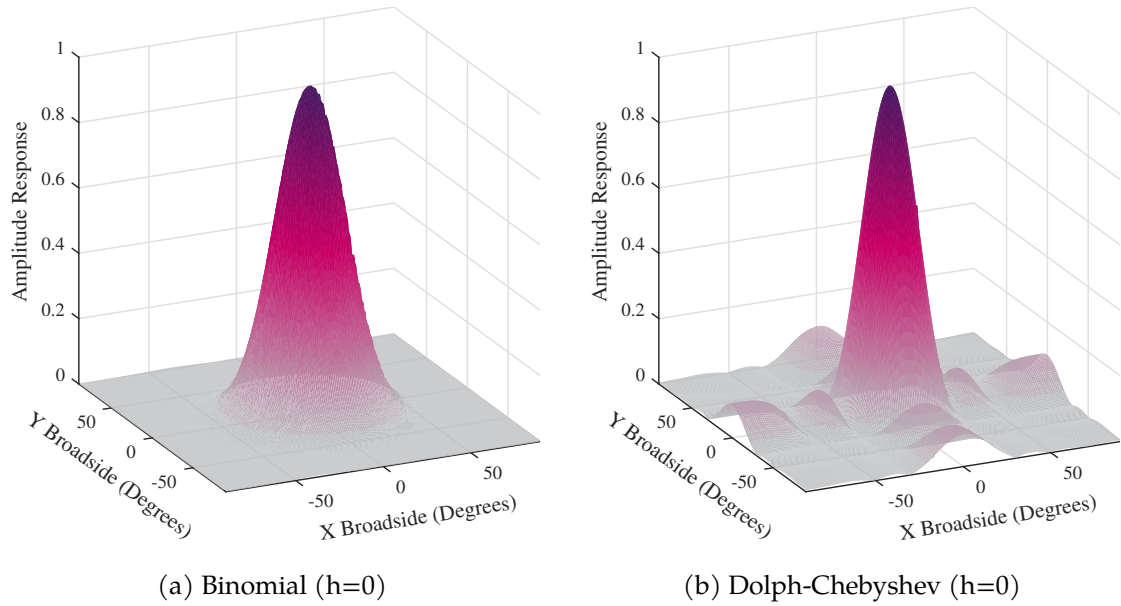
Figure 4.10: Normalised Beam patterns of a 5×5 element array at h=0 for two different time-weighting distributions

At $h_x = 0$, $h_y = 0$ ($h = 0$), it is clear that the array is most responsive at $\beta_x = 0°$, $\beta_y = 0°$, whereas at $h_x = 1$, $h_y = 1$ ($h = 6$), the point where the array is most responsive is at $\beta_x = 28.69°$, $\beta_y = 23.58°$. The effects of the time weighting are also in good agreement with the theory; in the binomial distribution, the sidelobes have been completely eliminated in every harmonic sideband, at the expense of producing a larger beam-width.

Table 4.1 shows the amplitudes relative to the maximum possible power received by the array (i.e. at $h_x = h_y = \beta_x = \beta_y = 0$). Since the maximum amplitude at $h = 0$ should be equal to the ratio of elements being on to elements being off (as mentioned in Section 4.3.1) the binomial distribution significantly reduces the response of the array. The slight discrepancies between the maximum amplitude of the beams at $h = 0$ and the ratios calculated in Section 4.3.1 are mainly due to the effects of sampling in the simulation. Figure 4.10 shows the response of the central frequency when the incoming signal is amplified to counteract this ratio (i.e. by 1.818 for Dolph-Chebyshev, and 3.496 for binomial), and highlights the useful properties of each distribution when compared to the flat distribution.

From Table 4.2 it can be seen that the target sidelobe level specified for the Dolph-Chebyshev array is only achieved at the centre harmonic, the levels of each sidelobe have

Table 4.1: The maximum power received by the array at each harmonic relative to flat distribution.

Weighting Distrbution	Maximum Amplitude	
	$h = 0$	$h = 6$
Flat	1.0000	0.9075
Binomial	0.2845	0.2687
Dolph-Chebyshev (-20dB)	0.5502	0.5169

Table 4.2: The maximum sidelobe level relative to the maximum amplitude of that harmonic using the same weighting distribution.

Weighting Distribution	Maximum Sidelobe Amplitude	
	$h = 0$	$h = 6$
Flat	0.2648 (-11.54 dB)	0.2354 (-11.72 dB)
Binomial	0.0000	0.0000
Dolph-Chebyshev (-20 dB)	0.0562 (-19.82 dB)	0.0663 (-17.84 dB)

still been greatly reduced, and only vary by small quantities. Where only one unique beam per harmonic is desired, the Dolph-Chebyshev distribution makes a good alternative to the binomial distrbution since the power received in the main beam direction is significantly greater compared to the power at its sidelobes or at the main beam of the binomial array in the same sideband.

4.4   Extending DoA Algorithms with Planar Arrays

In Chapter 3 it was shown that the DFT bins from a sequentially switched TMLA can be used for fast estimation of the signal broadside angle. The same estimation methods are also available in TMPAs with some small changes. In this section, the index weighted variant of the algorithm as described in Section 3.6 is used.

The following assumes the same switching order given in the previous sections of the chapter, where the elements on the x-axis are iterated through before the switching to the next row indexed on the y-axis. For y-axis estimations, the main and adjacent harmonics and their relevant harmonic index numbers can be used in the weighted average algorithm in Equation (3.7).

$$h_{y,est} = \frac{X_\alpha h_{\alpha,y} + X_{\alpha+1} h_{\alpha+1,y}}{X_\alpha + X_{\alpha+1}} \qquad (4.23)$$

$$\beta_{y,est} = \sin^{-1} \frac{h_{y,est}}{R_y N} \tag{4.24}$$

where X_α and $X_{\alpha+1}$ are the powers in the largest harmonics that are adjacent to each other. $h_{\alpha,y}$ and $h_{\alpha+1,y}$ are the integer indexes associated with these harmonics. The sideband chosen for X_α will also be used in the estimation of β_x

For x-axis estimations, the two selected harmonics should have the same value for h_y, therefore the largest harmonics selected will no longer be adjacent to each other but will be N bins away.

$$h_{x,est} = \frac{X_\alpha h_{\alpha,x} + X_{\alpha+N} h_{\alpha+N,x}}{X_\alpha + X_{\alpha+N}} \tag{4.25}$$

$$\beta_{x,est} = \sin^{-1} \left(\frac{\frac{h_{y,est}}{N} + h_{x,est}}{R_x M} \right) = \sin^{-1} \left(\frac{h_{est}}{R_x MN} \right) \tag{4.26}$$

In this form, X_α and $X_{\alpha+N}$ are the powers in the largest harmonics, and h_x and $h_{\alpha+N,x}$ mark the integer indexes associated with these harmonics.

4.4.1   Accuracy of the 2D Estimation Method

Since the power in each sideband vary when the target signal moves in any direction, the estimation algorithm's accuracy of one axis may depend on the signal's position in the other axis.

To evaluate the proposed method's accuracy, a numerical simulation was designed to emulate a single frequency signal impinging on a planar array with a configurable number of elements in each axis. The simulation iterated through combinations of x and y broadside angles in $0.5°$ increments and the difference between the estimated and actual signal position for each axis was recorded. Figure 4.11 shows the DoA accuracy of (a) the x-axis and (b) the y-axis for a 5×5 element array when switched in the sequence shown in Figure 4.2.

The results show that the estimation method suffers from the same limitations as detailed in Chapter 3, but also show that the y-axis estimations have larger areas of

(a) x-Axis Error

(b) y-Axis Error
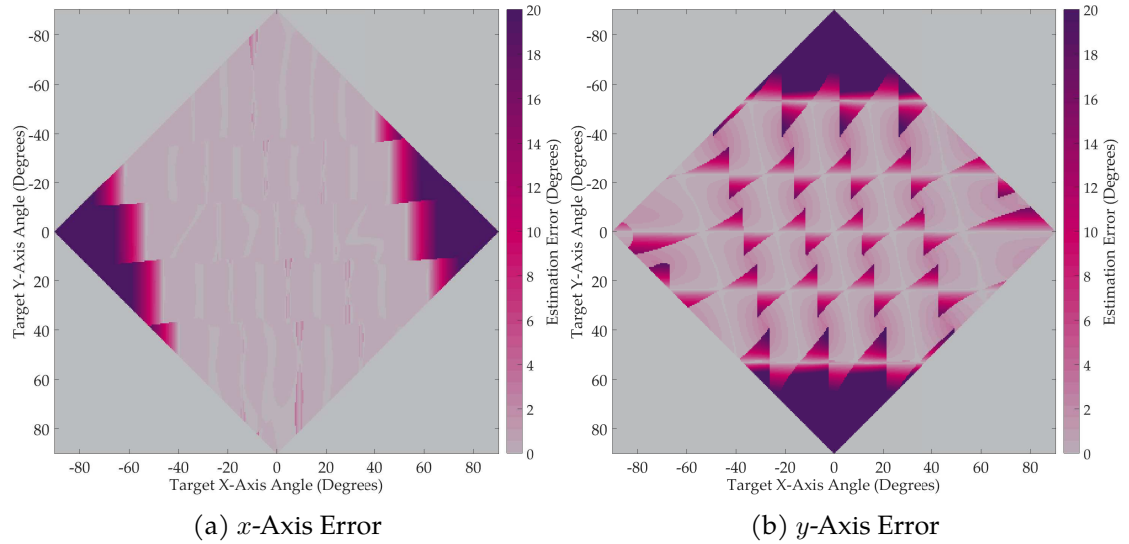
Figure 4.11: Errors in direction of arrival estimation when using a 5×5 time-modulated array switched sequentially. (a) shows the error in DoA estimation for the x-axis broadside angle, whilst (b) shows the error in DoA estimation for the y-axis broadside angle

inaccuracy than the x-axis estimations. The local maxima on the x-axis occur at the angles calculated using Equation (4.17), however, the local maxima on the y-axis occurs between them.

To get an overall impression of the performance of the weighted-average method using TMPAs, the Euclidean metric of the error in both estimated broadside angles (ϵ_x and ϵ_y) were used to form ϵ_{xy} i.e.

$$\epsilon_{xy} = \sqrt{\epsilon_y{}^2 + \epsilon_x{}^2} \qquad (4.27)$$

and this calculation was used to give a single value of accuracy in any given 2D position. Figure 4.12 shows the results of a 5×5 array, and Figure 4.13 shows the result of a 9×9 array.

The results show that in the 5×5 array, there are a number of regions with large areas of in-accuracies, where the error in the centre regions exceeds $15°$. As could be expected, a 9×9 element array greatly out-performs the 5×5 element array in terms of accuracy. Whilst the larger array exhibits a larger number of regions with inaccurate spikes, these regions are significantly smaller in area and magnitude (at approximately $7°$ at $\beta_x = \beta_y = 45°$).
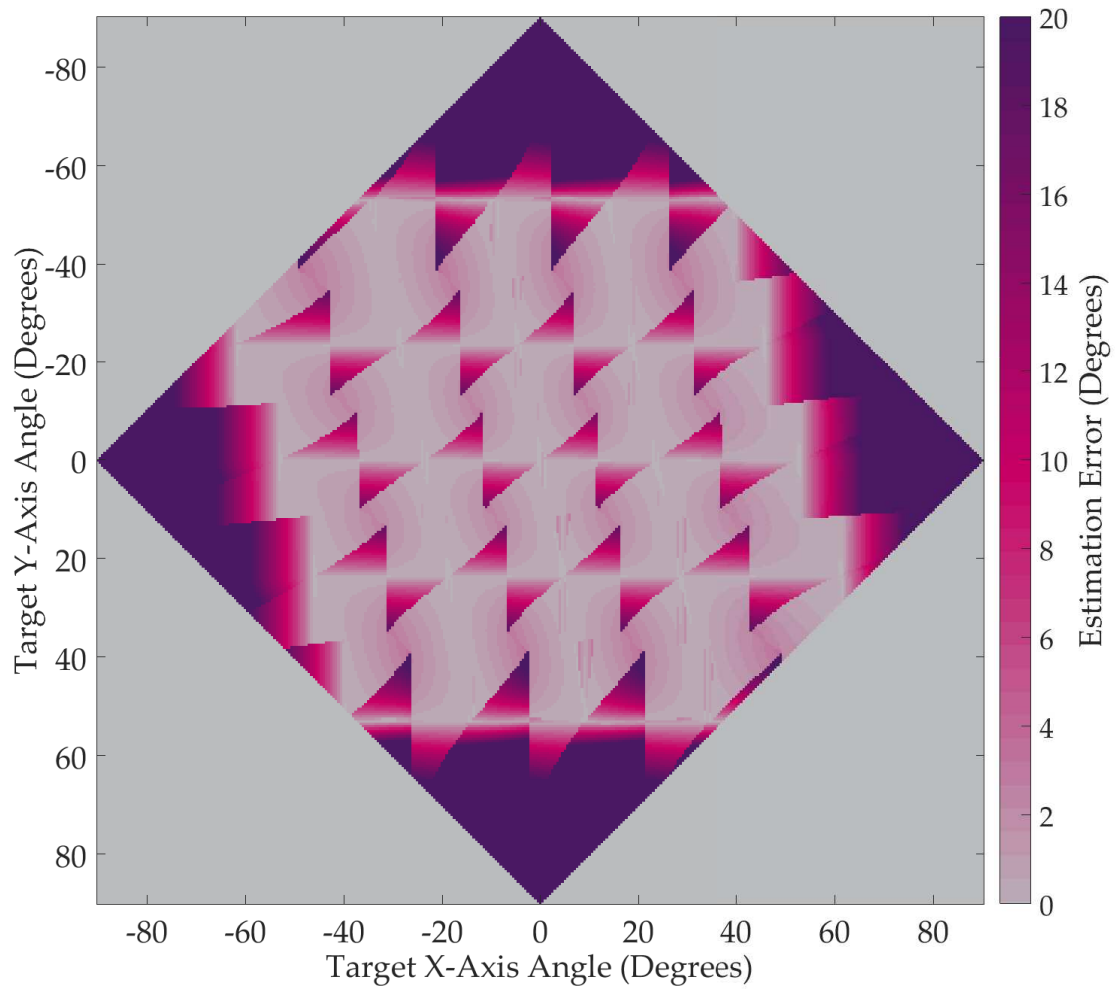
Figure 4.12: The combined error of the individual errors on the x and y broadside angles as seen in Figure 4.11 when using a 5×5 array switched sequentially. The value is calculated by forming a Euclidean metric using the error on both axes.
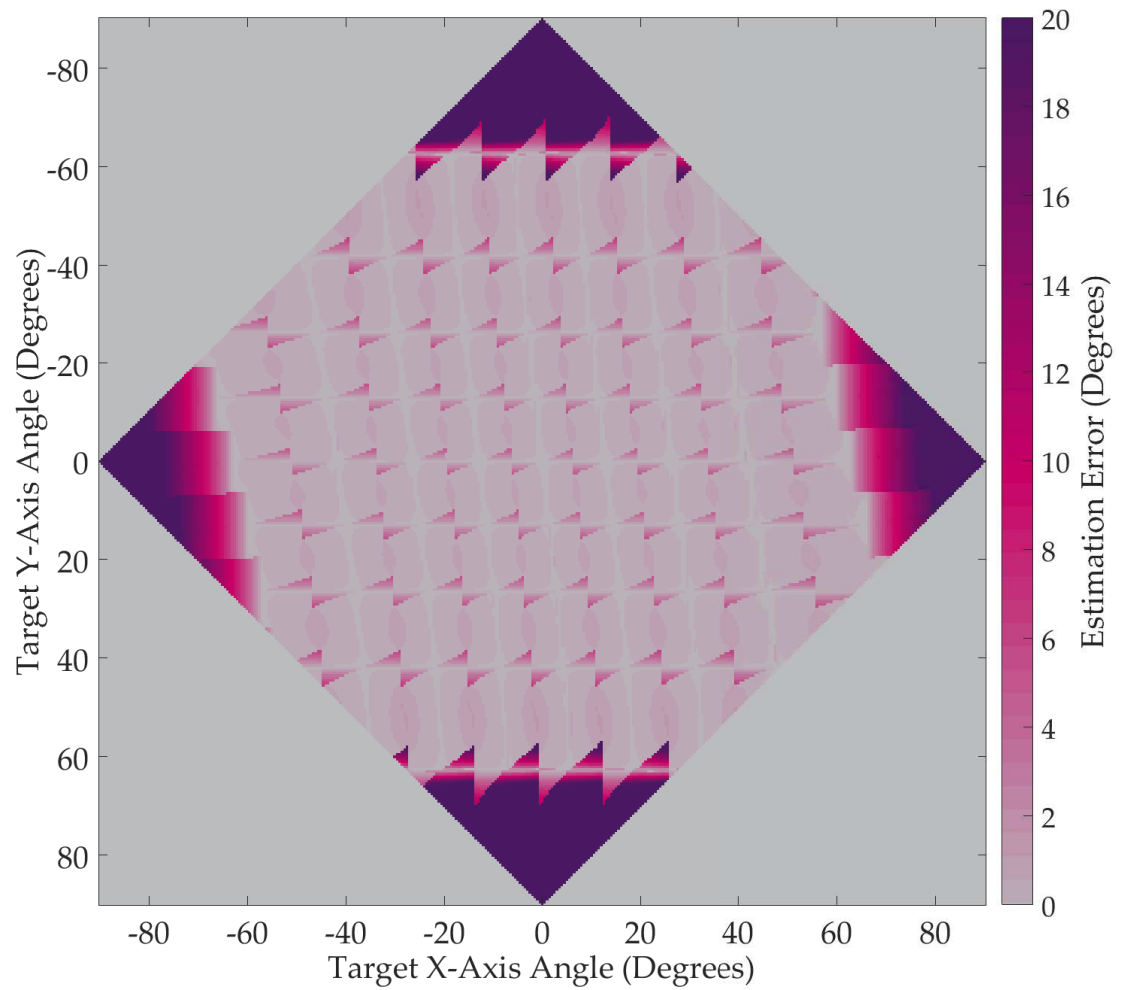
Figure 4.13: The combined error in DoA estimation of both x and y broadside angles when using a 9×9 array switched sequentially.

(a) Standard Switching Order

(b) Standard Steering Vectors (9×9)

(c) Reversed Switching Order

(d) Reversed Steering Vectors (9×9)
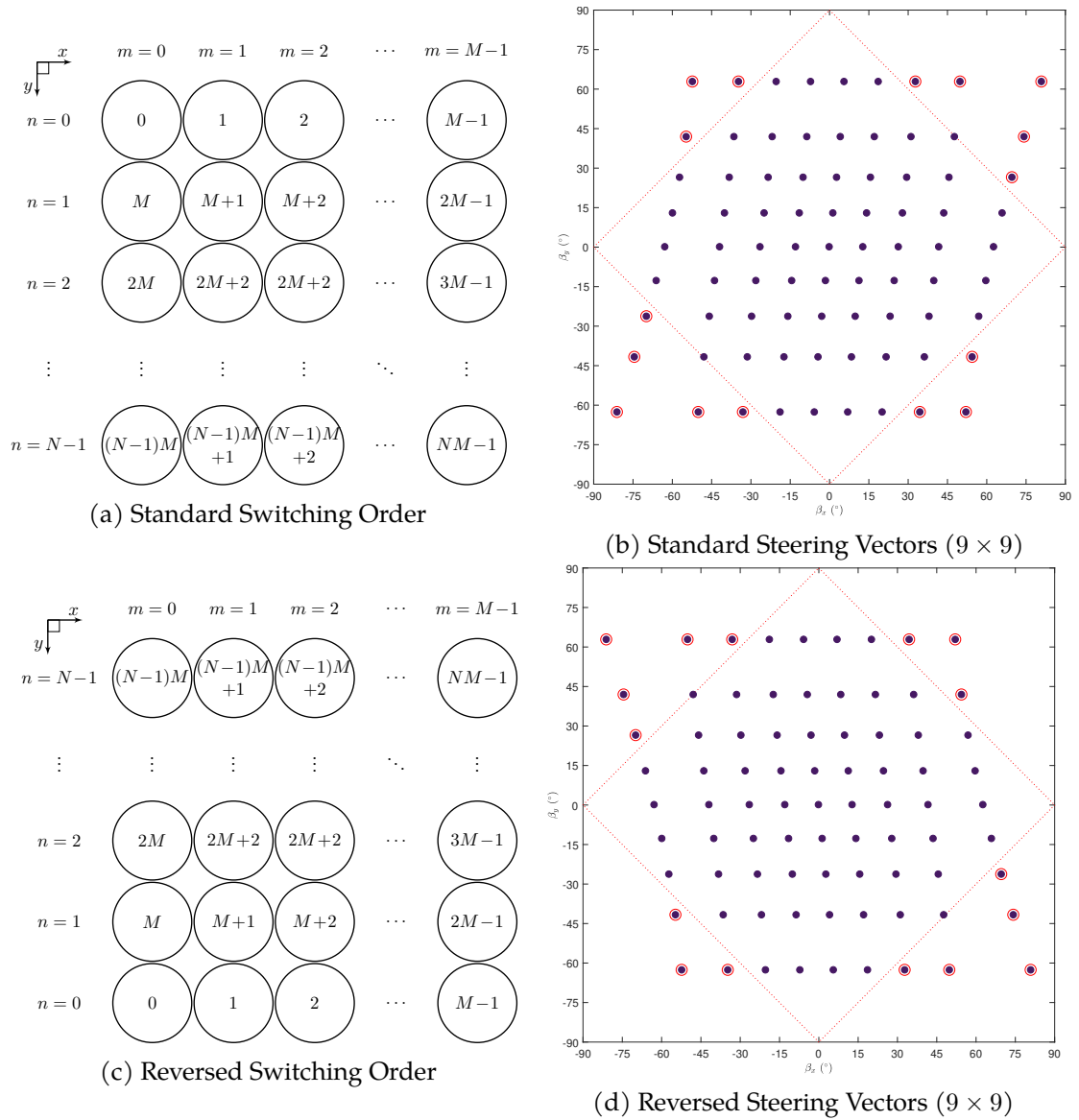
Figure 4.14: The switching patterns and their resultant harmonic beam directions for a 9×9 array. (a) and (b) show the results of an array switched from top to bottom, (c) and (d) show the results of an array switched from bottom to top.

4.4.2   Reversing the y-axis Switching Order

The theory so far has assumed the switching order is started from the top-left of the array, and finishes on the bottom-right as shown in Figure 4.2. However, the harmonic beam locations can change depending on the direction of switching in the y-axis, as shown in Figure 4.14. This means that the DoA error pattern will also change for the same size array, as shown in Figure 4.16.

For clarity, Figure 4.15 shows the beam directions of both switching directions shown
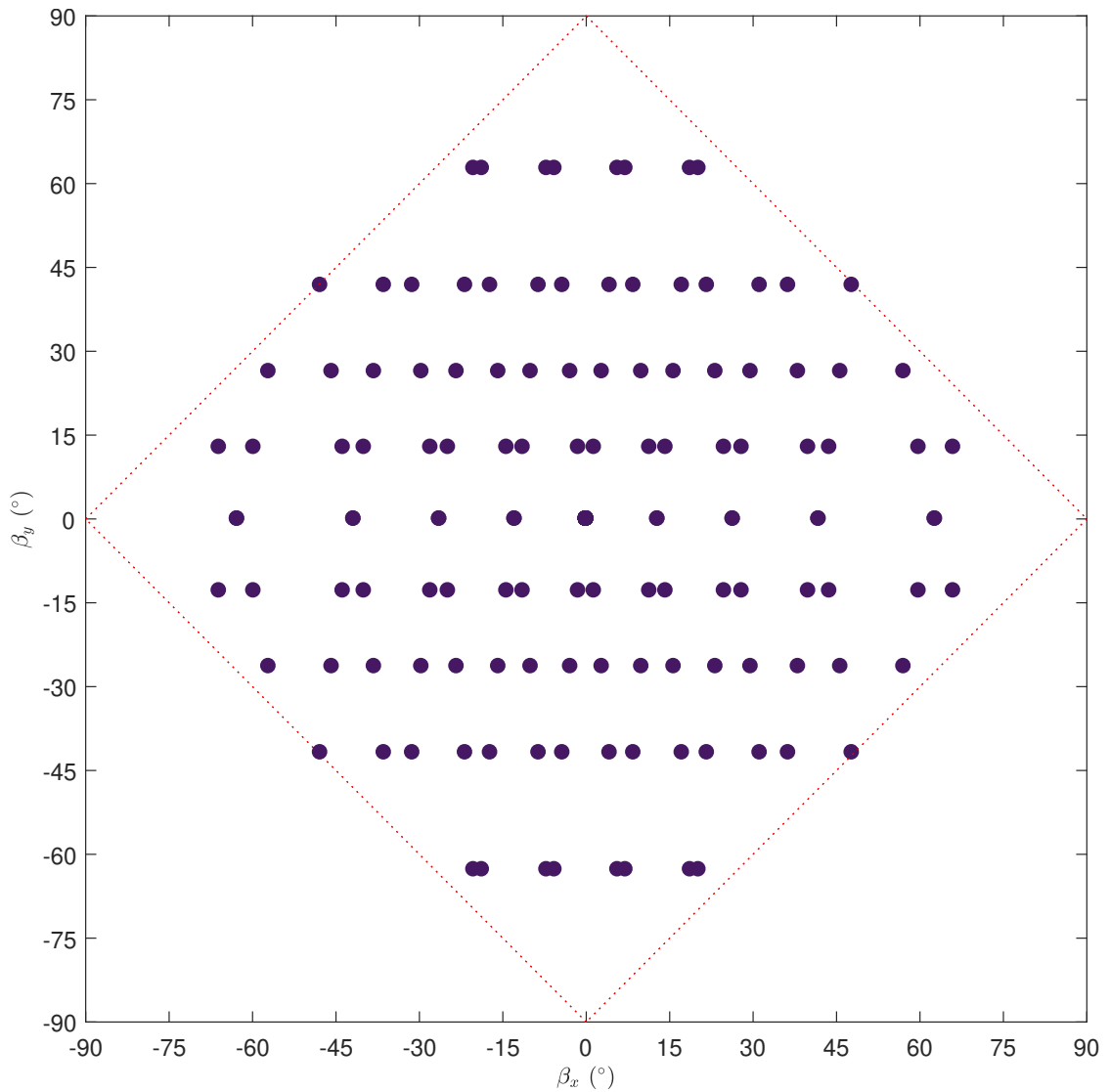
Figure 4.15: Both sets of steering positions for the harmonics from both switching directions seen in Figure 4.14 printed on the same graph. To show how the variation is in the fastest switching axis only.

in Figure 4.14. It can be seen that the variation is only in the fastest switching axis and away from the centre harmonics related to the y-axis. Since the null regions of other harmonics are located at each of these points, it may be beneficial to swap to a second switching direction when near the null region from the first.

By performing both switching patterns, and averaging the result of the DoA estimation, a final estimation can be obtained. Figure 4.17 shows that the average error is now symmetrical in the x-axis, and the spikes of inaccuracies found in the individual cases have been reduced (at approximately 3° at $\beta_x = \beta_y = 45°$).
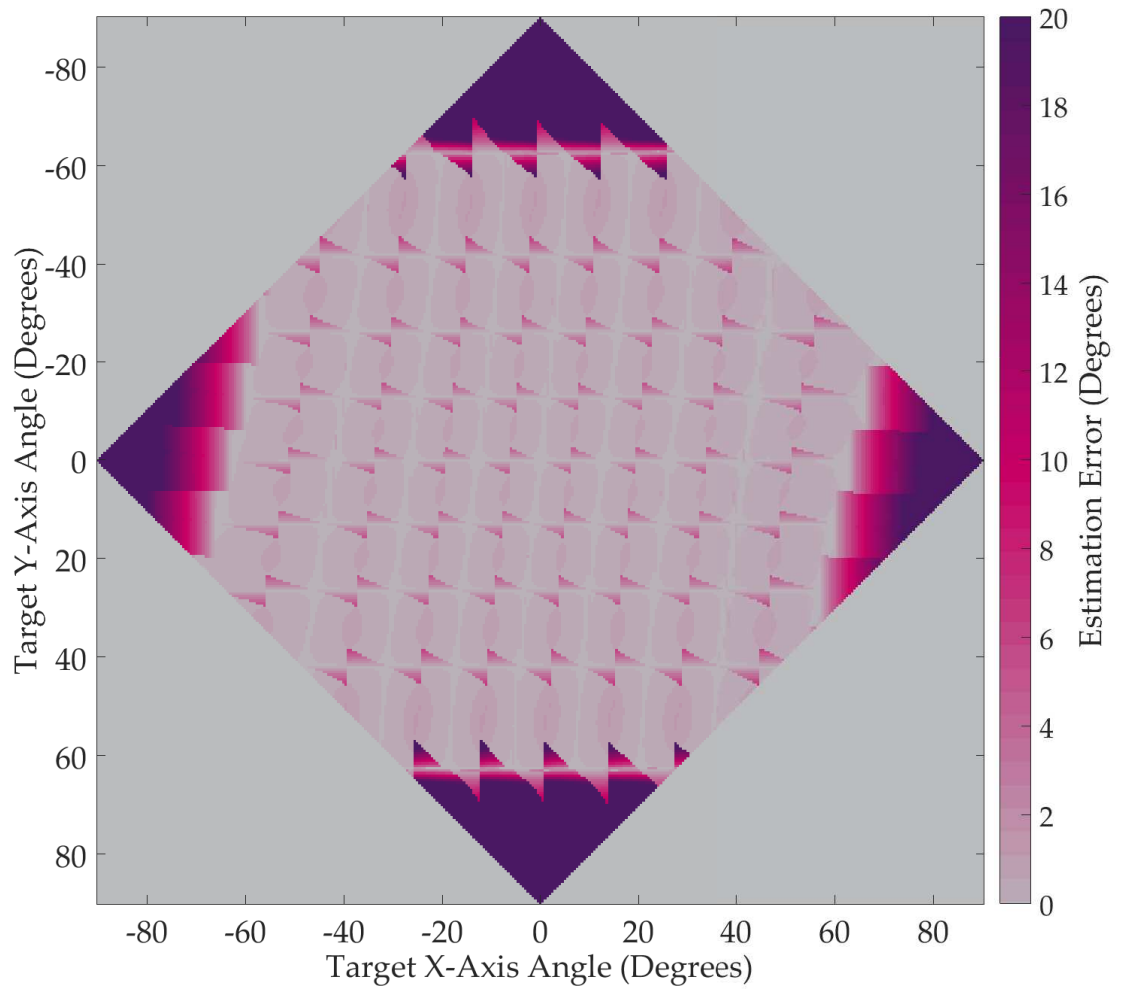
Figure 4.16: The average error in DoA estimation of both x and y broadside angles when using the same array as in 4.13 but when reversing the switching order in the y-axis only. i.e, when switching from bottom to top instead of top to bottom.
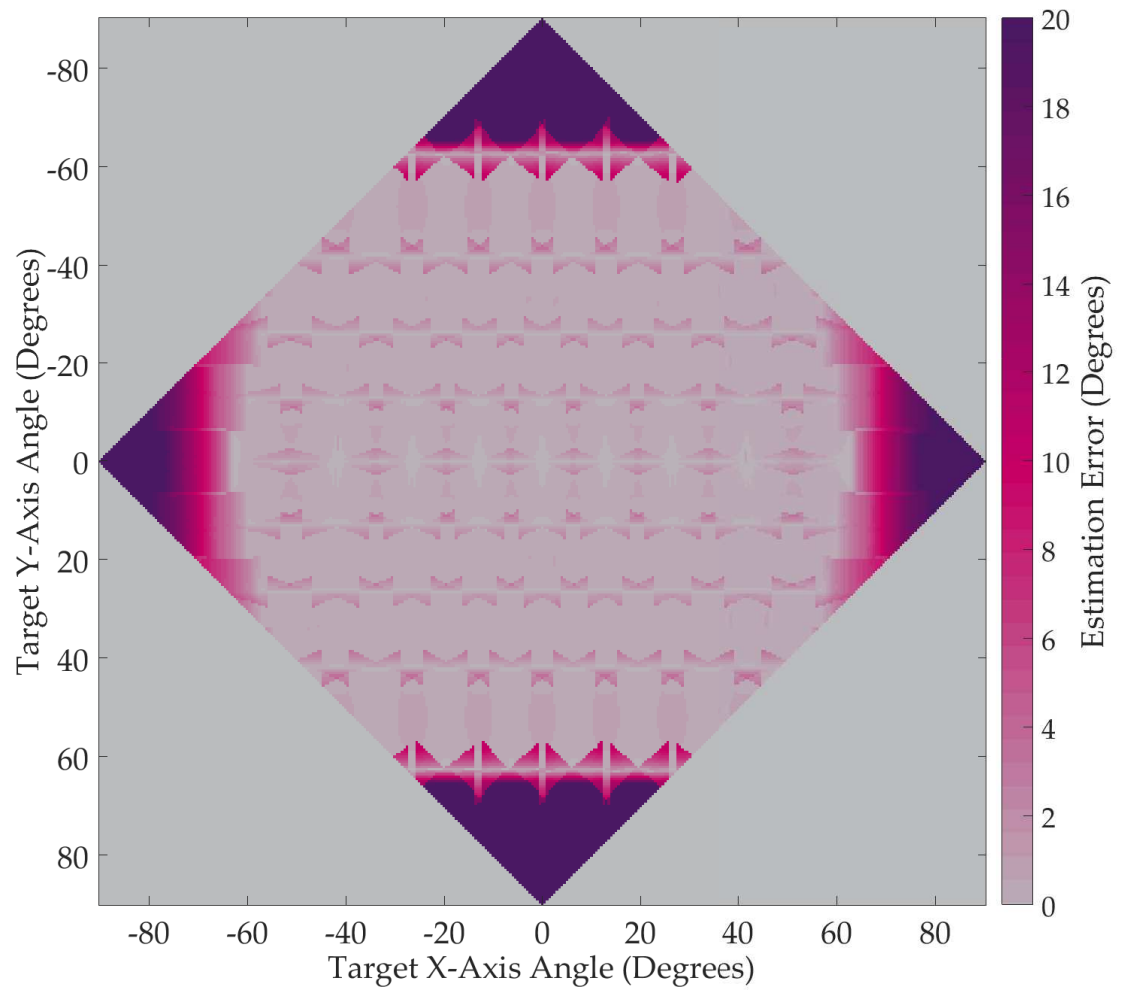
Figure 4.17: The combined 2D DoA error in estimation when using the average of the two individual errors gained from switching from top-to-bottom and bottom-to-top.

4.5   Conclusions

A method of producing predictable simultaneous beam patterns has been proposed and results of numerical simulations have been given which show good agreement with the theory. It has been demonstrated that switching a planar array sequentially is a simple way of obtaining unique beams for each sideband.

Applying a binomial weighting to this switching pattern gives a solution for when no sidelobes are desired. Due to the ratios of on times between the corner and central elements, much of the signal capturing time is spent receiving no power at all, and thus the array captures a relatively small amount of power. The Dolph-Chebyshev distribution offers a compromise between obtaining low sidelobes and maximising power in the main beam, just as it does with conventional arrays but for each sideband.

An extension to Chapter 3 in the context of planar arrays has been suggested, where a computationally simple method of 2D direction arrival as been derived and numerically tested for a single tone signal. As with the 1D estimation method, multiple signals can be can be tracked simultaneously by calculating the separate power spectrums of each signal, and using Equations (4.16) and (4.17). Each signal will have a different values for R_x and R_y, both of which should be less than or equal to 0.5.

It has also been demonstrated that mirroring the switching pattern (i.e. starting from the bottom of the array instead of the top) may also be beneficial for creating additional beams. It is possible to perform these different patterns on the same array simultaneously and route the signals to a secondary output. Not only will this increase the time efficiency of the array as described by Tong and Tennant [4.11] but it has been shown that the collection of harmonic beams in this secondary output is mirrored compared to the first, allowing a processor to compare between closely situated beams, or to tune into a signal's position more precisely.

References

[4.1] L. Dudás, P. Kovács, and R. Seller, "Digital Beamforming - Linear and Planar Array," in *2008 14th Conf. Microw. Tech.* Prague: IEEE, April 2008, pp. 1–5.

[4.2] L. Poli, P. Rocca, L. Manica, and A. Massa, "Time modulated planar arrays - Analysis and optimisation of the sideband radiations," *IET Microwaves, Antennas Propag.*, vol. 4, no. 9, p. 1165, 2010.

[4.3] E. Afacan, "Sidelobe Level and Sideband Optimization for Thinned Planar Antenna Arrays Using Time Modulation," in *2013 7th Eur. Conf. Antennas Propag.* IEEE, 2013, pp. 328–330.

[4.4] D. Ni, S. Yang, J. Li, J. Guo, and Z. Nie, "An efficient approach for synthesizing irregularly shaped patterns based on 4D arrays," in *2015 IEEE Int. Conf. Commun. Probl. ICCP 2015.* IEEE, October 2015, pp. 133–136.

[4.5] L. Poli, P. Rocca, L. Manica, and A. Massa, "Handling Sideband Radiations in Time-Modulated Arrays Through Particle Swarm Optimization," *IEEE Trans. Antennas Propag.*, vol. 58, no. 4, pp. 1408–1411, Apr 2010.

[4.6] Y. Tong and A. Tennant, "Simultaneous control of sidelobe level and harmonic beam steering in time-modulated linear arrays," *Electron. Lett.*, vol. 46, no. 3, p. 200, 2010.

[4.7] C. Dolph, "A Current Distribution for Broadside Arrays Which Optimizes the Relationship between Beam Width and Side-Lobe Level," *Proc. IRE*, vol. 34, no. 6, pp. 335–348, June 1946.

[4.8] S. Horst, D. E. Anagnostou, G. E. Ponchak, E. Tentzeris, and J. Papapolymerou, "Beam-Shaping of Planar Array Antennas Using Integrated Attenuators," in *2007 Proc. 57th Electron. Components Technol. Conf.* IEEE, 2007, pp. 165–168.

[4.9] S. Yang and Z. Nie, "Time modulated planar arrays with square lattices and circular boundaries," *Int. J. Numer. Model. Electron. Networks, Devices Fields*, vol. 18, no. 6, pp. 469–480, November 2005.

[4.10] A. Bresler, "A new algorithm for calculating the current distributions of dolph-chebyshev arrays," *IEEE Trans. Antennas Propag.*, vol. 28, no. 6, pp. 951–952, November 1980.

[4.11] Y. Tong and A. Tennant, "A Two-Channel Time Modulated Linear Array With Adaptive Beamforming," *IEEE Trans. Antennas Propag.*, vol. 60, no. 1, pp. 141–147, January 2012.

5 | Implementation

M<small>OST</small> of the work presented so far has been demonstrated numerically, however there are many factors that need to be considered and properties of the real world need to addressed before implementation. This chapter considers the practical aspects of time-modulated arrays and outlines suggestions when using hardware to implement the techniques described in the previous chapters.

5.1 Introduction

One major benefit to using TMAs is the reduction of device complexity. Phase shifters found in conventional beam scanners can be expensive and have can have significant power consumption [5.1]. To make the most out of this advantage, considerable care needs to be taken in designing a system capable of both switching and processing the output of the array. With each of the techniques described in this thesis, the following issues are of importance and are addressed in this chapter:

- The software architecture used for time modulation.

- The accuracy and reliability of the time modulation technique.

- The time taken to process the signal to find signal parameters.

- The hardware capabilities for time modulation.

- Environmental factors that need to be taken into consideration.

5.2   Design of a generalised TMA simulation

A tool that allows a user to design a time-modulated array and explore its potential outputs would be beneficial. A simulation that allows the user to input a large number of parameters concerning arrays was developed to aid with understanding of the theory and to design an array for practical use in the future. This simulation and its user-interface was designed using LabVIEW [5.2] and built into an standalone executable program. The goal of the simulation's design was to allow the user (or a script using the interface) to specify a custom switching pattern for an array of elements of arbitrary size. This simulation should be able to:

- Allow the user to specify a custom switching pattern, or select between the switching patterns demonstrated in Chapters 3 and 4.

- Allow the user to input a signal frequency and direction, either in terms of Azimuth and Elevation or using a pair of broadside angles using equations (4.19) and (4.20) defined in Chapter 4.

- Calculate and show the time-series and frequency responses of the array.

- Have the ability to define data acquisition parameters such as sampling frequency, signal-to-noise ratio etc..

- Demonstrate the effectiveness of the DoA algorithm proposed in Chapter 4.

5.2.1   Switching Frames

To simplify the process of switching elements, a switching frame can be defined as a two-dimensional boolean array that marks which elements are supposed to be switched on at a specific instance in time. A switching frame can have any number of elements in the array set, with the expectation that the output of each element is summed together.

A set of these frames can be used inside a three-dimensional "frame matrix" denoted by F, and indexed by m, n (the element indexes in the x and y axes) and frame index i.

$$F[1] = \begin{bmatrix} 1 & 0 & 0 & 0 & 0 \\ 0 & 0 & 0 & 0 & 0 \\ 0 & 0 & 0 & 0 & 0 \\ 0 & 0 & 0 & 0 & 0 \\ 0 & 0 & 0 & 0 & 0 \end{bmatrix} \qquad F[2] = \begin{bmatrix} 0 & 0 & 0 & 0 & 0 \\ 1 & 0 & 0 & 0 & 0 \\ 0 & 0 & 1 & 0 & 0 \\ 0 & 0 & 0 & 0 & 0 \\ 0 & 0 & 1 & 0 & 0 \end{bmatrix} \qquad F[3] = \begin{bmatrix} 1 & 0 & 0 & 0 & 0 \\ 0 & 1 & 0 & 0 & 0 \\ 0 & 0 & 1 & 0 & 0 \\ 0 & 0 & 0 & 1 & 0 \\ 0 & 0 & 0 & 0 & 1 \end{bmatrix}$$
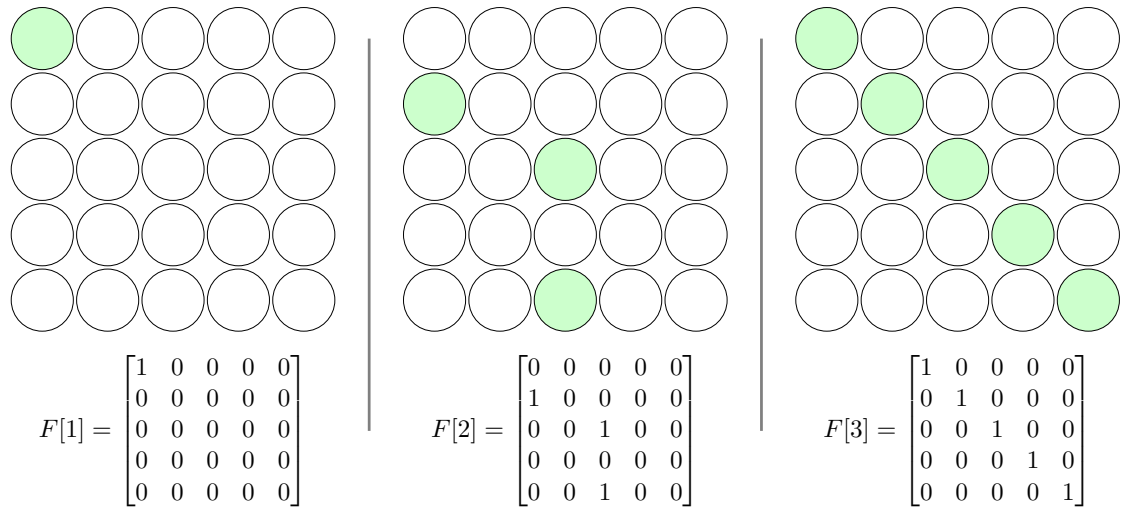
Figure 5.1: Example of a sequence of three 5×5 switching frames, and its equivalent in matrix notation. A shaded element represents an element that is to be switched on during the frame's timespan.

These frames can have a specific duration in time allocated to them, and a process or method for defining switching sequences in software can readily be achieved.

Figure 5.1 shows a set of three switching frames. As an example using this figure, if a single frame described the state of elements for a single millisecond ($T_{frame} = 0.001$) then the total switching period T_s would be 3 milliseconds ($f_s = 333Hz$), and harmonics would be expected in multiples of f_s. In mathematical terms this harmonic frequency is simply:

$$f_s = \frac{1}{FST_{frame}} \tag{5.1}$$

where S is the total number of frames.

This notation allows for a simplified method for understanding other expected properties of the array. Assuming that the array is formed of identical isotropic elements with a maximum individual output of 1, then the expected maximum amplitude of the output signal $y(t)$ obtained from the array will be the maximum sum of all elements within a frame:

$$\max(y(t)) = \max_{i=1}^{S} \left(\sum_{m=0}^{M} \sum_{n=0}^{N} F[m, n, i] \right) \tag{5.2}$$

Using Figure 5.1 as an example, the maximum expected amplitude of the array at the broadside would equal 5, as there are at most five elements on in a single frame (occurring at $F[3]$).

The calculation of the switching function is therefore straightforward. As $U_{mn}(t)$ at any point in time is simply mapped to an index within a switching frame.

5.2.2 Generating Samples

A simulation would only need to iterate through the above switching frames in order to generate output. For each element within each frame, a TMA output signal $y(t)$ can be generated based on the calculated delay:

$$y(t) = x(t) \sum_{m=0}^{M-1} \sum_{n=0}^{N-1} U_{mn}(t) \times D[m,n] \tag{5.3}$$

where D is an $M \times N$ matrix containing the delays of each element:

$$D = \begin{bmatrix} 1 & e^{jkd_x \sin \beta_x} & \cdots & e^{jk(M-1)d_x \sin \beta_x} \\ e^{jkd_y \sin \beta_y} & e^{jk(d_x \sin \beta_x + d_y \sin \beta_y)} & \cdots & e^{jk((M-1)d_x \sin \beta_x + d_y \sin \beta_y)} \\ \vdots & \vdots & \ddots & \vdots \\ e^{jk(N-1)d_y \sin \beta_y} & e^{jk(d_x \sin \beta_x + (N-1)d_y \sin \beta_y)} & \cdots & e^{jk((M-1)d_x \sin \beta_x + (N-1)d_y \sin \beta_y)} \end{bmatrix} \tag{5.4}$$

If a set number of samples L_F are specified for a single frame, then the switching frequency can be calculated using the sampling frequency f_s and number of frames S:

$$f_m = \frac{f_s}{FL_F} \tag{5.5}$$

For example, for receiving a single-tone signal of 40 kHz, sampling a three-element TMA at 500 kHz with 5 defined switching frames and 100 samples per frame would create a switching frequency of 1 kHz. Power would therefore be expected to be distributed to 39 kHz, 40 kHz, and 41 kHz, with levels depending on the signal's position. To simplify the output of the simulation, it is assumed that $x(t)$ is a single frequency sinusoid.

Figure 5.2 shows the steps needed in order for a simulation to generate these samples.
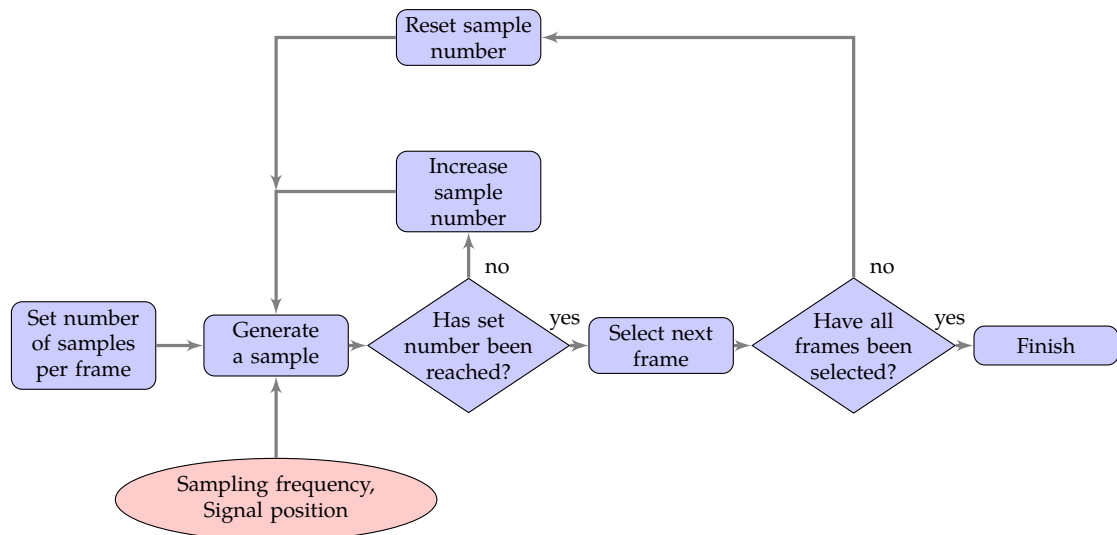
Figure 5.2: Process of generating signal samples

5.2.3 Generating Weighting Systems

Time-modulated weighting systems as explained by Tong and Tennant [5.3] for TM-LAs and in Chapter 4 for TMPAs can also be implemented with the concept of binary weighting frames. The ratio of consecutive "on frames" to the number of following "off frames" would exactly describe the element's weighting. Since each frame contains the same number of samples as each other then the weighting distributions would stay constant if another value of L_F is chosen. In a basic example, a set of frames that keep an element on, followed by the same number of frames keeping that element off would give that element a time-weighting of 0.5 over the sequence.

A relative weighting is set by continuing the switching sequence for other elements. Elements have a relative weighting of 1 if they have an identical sequence of switching frames, regardless of where the sequence starts in the switching period. Section 4.2.4 gave examples of 2D time-weighting systems for a 5×5 element array, but the simulation used was developed to generate the response from an array of any size.

The following sections explain the process used to generate the frames needed for specific weighting systems. For each pattern, the element with the largest weighting has a sequence of frames, all of which turn that element on. The other elements' relative weightings are then adjusted by turning on an element for a number of frames, and then by turning all elements off for as many frames are needed to match the weighting ratio.

Table 5.1: The minimum number of frames needed to produce a binomial weighting for a TMPA of different sizes. Even if the number of samples per frame was set to 1, the total samples needed for a perfect binomial pattern is unrealistic.

Size ($M \times N$)	Number of Frames for Each Element	Total Frames for array
5×5	36	900
6×6	100	3600
7×7	400	19600
8×8	1225	78400
9×9	4900	396900
10×10	15876	1587600
12×12	213444	30735936
15×15	11778624	2650190400

Generating Binomial Frames

The binomial series is a set of integer values and is therefore trivial to implement in terms of switching-frames, as the number of on-frames is the same number as the binomial weighting. This is calculated by:

$$F_{on,mn} = \binom{M-1}{m} \times \binom{N-1}{n} \tag{5.6}$$

After each element is switched on for the above number of frames, they are immediately switched off and the next element in the sequence turns on after multiples of the largest weighting. This is calculated by:

$$F_{mn} = \binom{M-1}{\lfloor \frac{M}{2} \rfloor} \times \binom{N-1}{\lfloor \frac{N}{2} \rfloor} \tag{5.7}$$

For example in a 5×5 array switching using same pattern as shown in Figure 4.2, the first element on the first row would be on for a single frame then all elements are off for the next 35 frames. Following this, the second element would be on for 4 frames and then all elements are off for 32 frames. The central element in the array is on for 36 frames (as calculated in (5.7)), and there are no associated "off frames". The next element in the pattern switches on immediately after.

As can be seen from Table 5.1, the required number of frames increases exponentially when the number of elements is increased. The computational requirement is therefore significantly impacted by using a binomial distribution with a large number of elements.

Table 5.2: The relative weightings achieved by a switching system that uses an integer number of frames to obtain a 15 dB Dolph-Chebyshev pattern for a 5×5 array.

Minimum number of frames	Number of frames for each element	Ratio between largest and smallest weighting
1	2	2.00000
10	18	1.80000
25	44	1.76000
40	71	1.77500
75	133	1.77333
100	177	1.77000

Generating Dolph-Chebyshev Frames

The Dolph-Chebyshev coefficients are more difficult to implement than the binomial weightings as the calculations are non-integer. The ratios between the largest and smallest weightings are also much smaller. This means that in the context of frames, the accuracy of the actual weightings depend on how close the calculated ratios can be using integer numbers. In summary, accuracies in the Dolph-Chebyshev weightings are lost when fewer frames are used in the signal generation as the ratios of two different weightings will not exactly equal the required amount.

In this weighting system, Bresler's method [5.4] was used to calculate the coefficients for each axis on the planar array, then the element weighting is calculated as a multiple of the two coefficients based on its position on each axis as shown in Chapter 4.

In a 5×5 array with a sidelobe suppression target of -15 dB relative to the mainbeam, the element with the largest weighting will have a weighting of 1.77417 times larger than the smallest element. Clearly, a system where the smallest element is on for a single frame would not work, as the necessary weightings will be impossible to obtain. Instead, it is possible to define a minimum number of frames to be "on" and scale the other elements accordingly. Using a 5×5 array as an example, Table 5.2 shows how accurate the weighting system is when the minimum number of frames is increased.

If 75 frames are chosen as the minimum value of "on frames", then Table 5.3 shows that the required number of frames increases non-linearly when the number of elements is increased but at a much less significant rate when compared with the binomial weight-

Table 5.3: The minimum number of frames needed for each element to produce a 15 dB Dolph-Chebyshev weighting for a TMPA of different sizes, given that the minimum number of "on" frames is set as 75.

Size ($M \times N$)	Number of frames for each element	Total frames for array
5×5	133	3325
6×6	109	3924
7×7	126	6174
8×8	135	8640
9×9	160	12960
10×10	197	19700
12×12	286	41184
15×15	452	101700

ing system.

Not only is the Dolph-Chebyshev system an optimised solution for reducing sidebands and minimizing beam-width, but it is also a good weighting system to use to reduce the computational requirement of the frame generation.

5.2.4   Application

With the considerations outlined above. A simulation with the theories introduced in Chapters 3 and 4 has been created.

Figure 5.3 shows the user interface for the simulation developed with the concepts described above. It can be seen that time and frequency data has been performed on the signal. And on any changes to the input of signal or array parameters (such has signal position or noise level, and array size or switching pattern) the program will calculate the output.

For use as a teaching tool, the program will also attempt to calculate the frequencies that need to be measured by the DFT algorithm, as well as the signal positions on which each of the harmonics are maximized. Since these calculations are made using Equations 4.16 and 4.17.

The example in Figure 5.3 shows the output of a signal approaching the broadside of a 5×5 array with the switching pattern set to "Row by Row Switching (Planar)". If a

user tries to change the number of elements for the array in this mode, the program will automatically generate the required switching frames to match the switching pattern described in Chapter 4. The output is automatically updated to reflect the new number of DFT bins and associated beam positions.

When the switching pattern is set to "Custom Pattern Input", the user is able to click on each element per frame to switch them on or off. Figure 5.4 repeats the same example given in Figure 5.1 and displays the generated output.

Figure 5.5 shows the DoA display window, where the DoA estimation algorithms shown in Equations 4.24 and 4.26 are tested against the actual simulated signal direction, and errors are displayed. As with the main page, these values are recalculated on any change of input or array configuration which allows the user so see in real-time how the algorithms can be used to track a moving targets position or how the parameter estimations vary with Gaussian distributed noise.
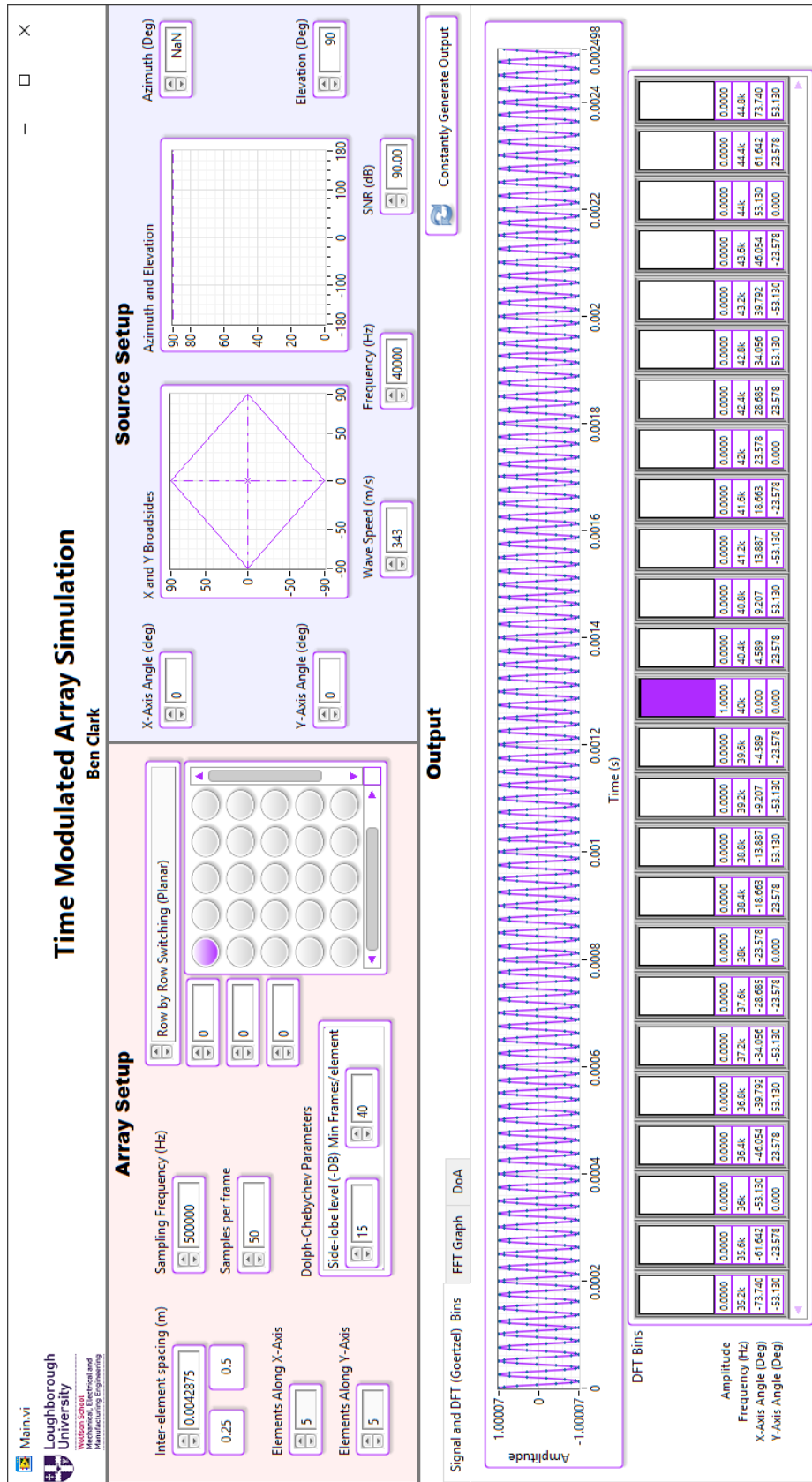
Figure 5.3: The front panel user interface for the simulation program. A user may interact with any object on screen and the program will update the output of the signal.
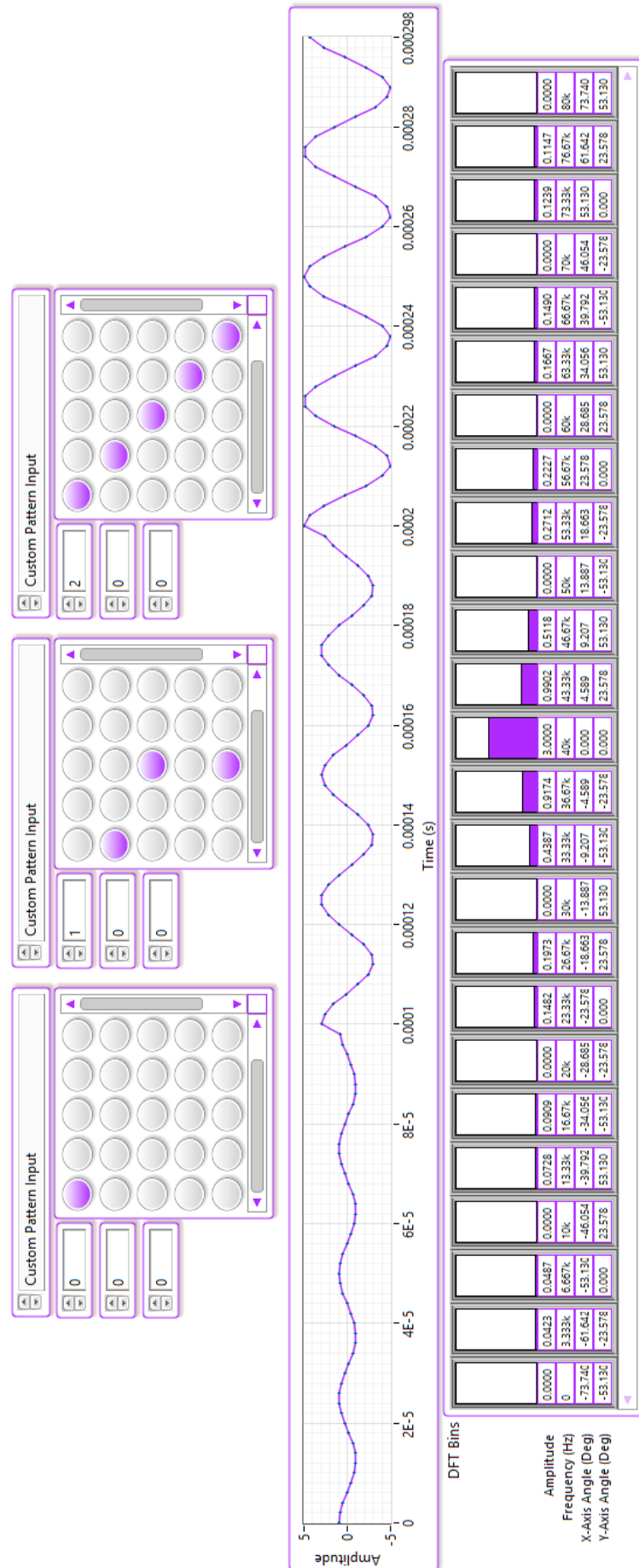
Figure 5.4: Results of inputting the switching sequence in the example shown in Figure 5.1
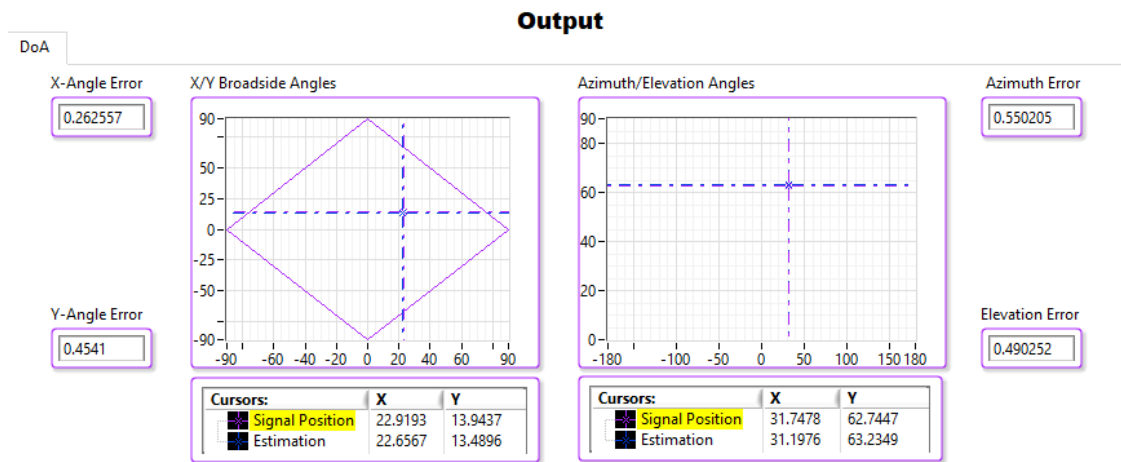
Figure 5.5: An example of the theory in Chapters 3 and 4 being used to obtain a simulated DoA estimation for two dimensional arrays.

5.3 DFT Analysis of TMA Input

The methods and algorithms explained in this thesis heavily depend on the accuracy and speed of performing DFT calculations on the array sidebands. For the DFT Analysis to be accurate, the signal should be oversampled at a rate greater than signal frequency plus the bandwidth of the signal [5.5].

5.3.1 Considerations for Multi-tone Signals

The considerations so far have assumed that the target consists of a single frequency tone. In reality, applications in the real-world will have to handle more complex signals. Signals of multiple tones will generate more than one set of sidebands (i.e. one for each frequency).

Using a 4 kHz square-wave as an example, harmonic frequencies of the signal will exist at odd harmonics (12 kHz, 20 kHz, 28 kHz etc.). If the sampling frequency is low, then the sidebands will exist far away from the signal harmonics. Figure 5.6 shows an example in this situation where the switching frequency is 50 Hz for a five-element array. As can be seen in the figure, which shows the frequency spectrum of a signal impinging the array at $90°$, the harmonics of the square wave have a minimal effect.

However, if we have a signal composed of two frequencies — one at 4 kHz and one
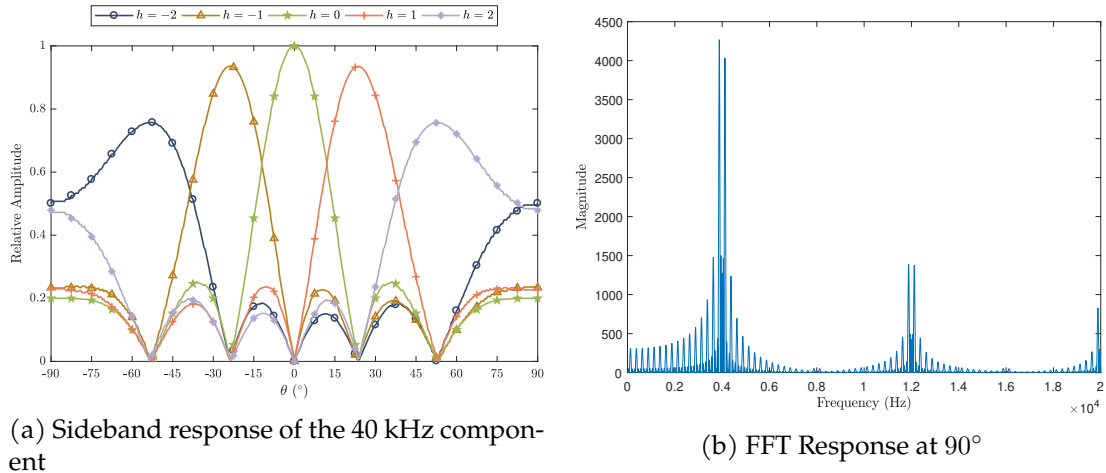
(a) Sideband response of the 40 kHz component

(b) FFT Response at $90°$

Figure 5.6: The response of a five element TMLA switched at 50 Hz receives a square-wave signal operating at 4 kHz. (a) shows the sideband response of the 40 kHz component from any signal angle, while (b) shows an example frequency spectrum when the signal is impinging on the array at a broadside angle of $90°$

at 3.9kHz —, then multiple sidebands will be produced. At a switching frequency of 50 Hz, Figure 5.7 clearly shows that the frequencies of the relative outer sidebands of both of these tones interfere with each other.

5.3.2   Goertzel Algorithm

The Goertzel algorithm is an algorithm that performs efficient calculations of DFT bins when it is useful to extract individual frequencies [5.6]. The calculation of the amplitude X at frequency f can be written as:

$$
\begin{aligned}
G_2 &= G_1 = 0 \\
G_N &= x(s) + 2\cos(f)G_{N+1} - G_{N+2} \\
X &= x(0) + G_1 \cos f - G_2
\end{aligned}
\tag{5.8}
$$

where $x(s)$ is the signal value at sample s and G is the Goertzel buffer which passes the result of the previous result and the earlier previous result to G_{N+1} and G_{N+2} respectively.

The algorithm performs calculations per sample with buffered input, enabling the system designer to feed sampled input directly into the input of the algorithm without having to store the full set of the sampled data. This feature reduces the memory require-

(a) Sideband response of the 40 kHz component

(b) FFT Response at $90°$
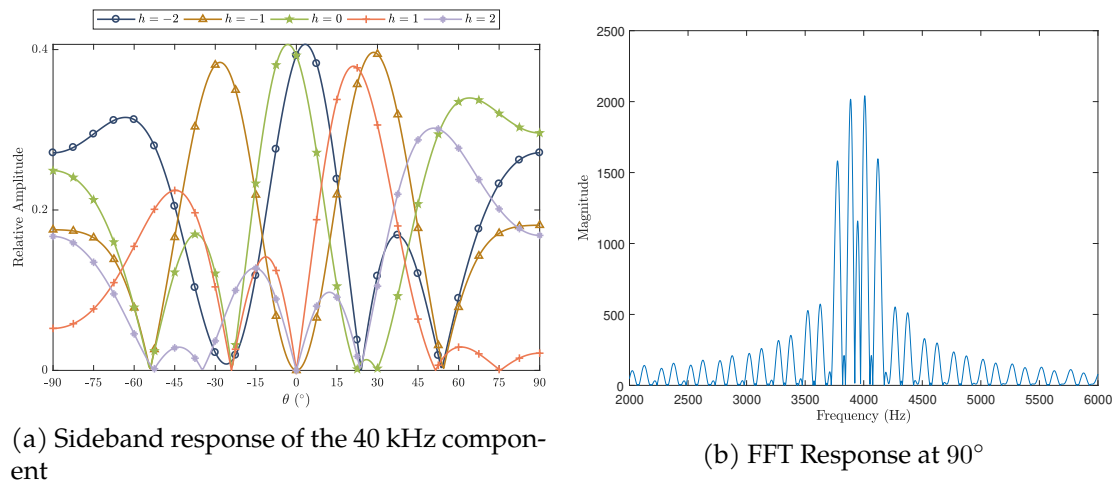
Figure 5.7: The response of a 5-element TMLA switched at 50 Hz when receiving a dual-tone signal containing frequencies at 4 kHz and 3.9 kHz. (a) shows the sideband response of the 40 kHz component from any signal angle, while (b) shows an example frequency spectrum when the signal is impinging on the array at a broadside angle of $90°$

ment of the device and is therefore attractive in embedded systems [5.7, 5.8, 5.9]. The use of real valued, fixed point arithmetic has also been demonstrated for the purposes of low-cost, embedded systems [5.9].

5.4   Controller Considerations

In addition to the physical requirements of an array and its elements, the utilization of devices capable of controlling the array must be considered. The choice of controller depends the importance of cost and performance. In this section, the use of both high performing controllers and low-cost implementations are considered.

5.4.1   Using Field Programmable Gate Arrays (FPGAs)

FPGAs are a set of Configurable Logic Blocks (CLBs) that can be programmed on-the-fly to implement a specific function. They offer a middle ground between the performance of an Application Specific Integrated Circuit (ASIC) and programmability of Digital Signal Processor (DSP) [5.10]. In the signal processing domain, it has been shown that FPGAs can significantly out perform DSPs [5.11] and therefore have received a high-
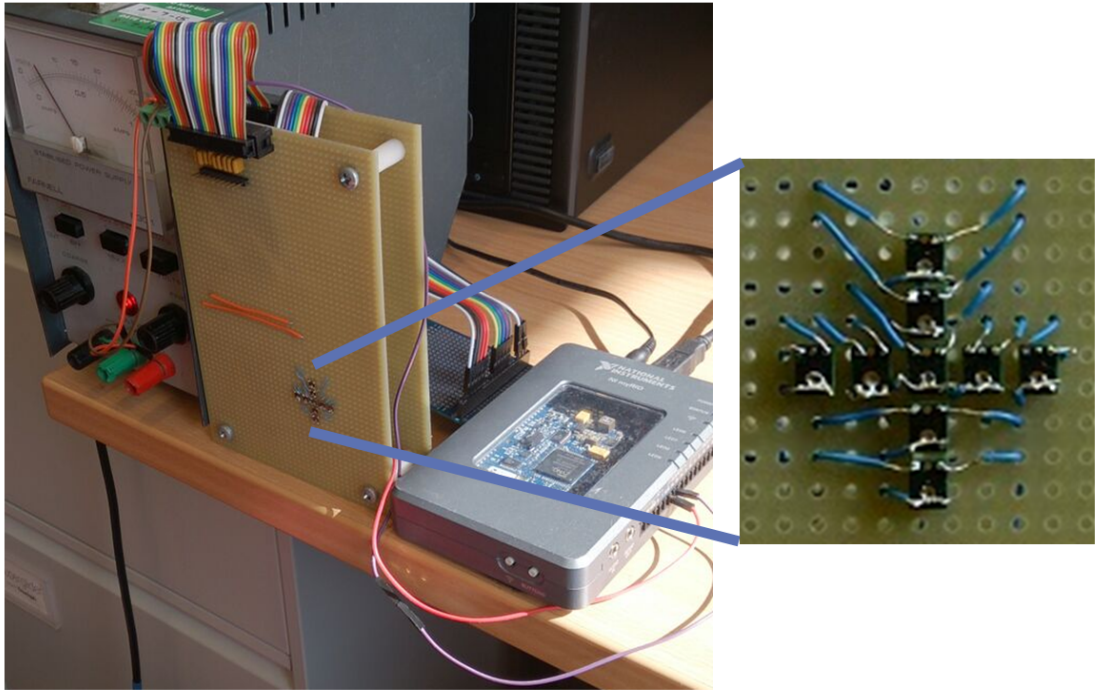
Figure 5.8: The testing device, each of the 9 microphone elements were digitally switched on and off using a port connected to the FPGA. Analogue samples were collected using the ADC on board the myRIO and pushed to its real-time processor for signal processing.

level of interest in the sensor array fields [5.12, 5.13, 5.14].

A major benefit to using FPGAs is that they can perform a very large number of processes concurrently and can be programmed with very strict timing constraints. Due to these features, conventional arrays using the MUSIC algorithm have recently been developed using FPGAs [5.15, 5.16]. For TMAs this means that the switching patterns and sampling timings can be built into the chip, and the implementation methods discussed in Section 5.2 become simpler to realise.

The myRIO used in Chapter 3 utilizes an FPGA described using LabVIEW to control the switching and sampling and demonstrates both the potential of using FPGAs for TMAs, as well demonstrating how they can be used to implement direction finding strategies.

Figure 5.8 shows how a cross array consisting of nine MEMS microphones and a set of digitally controlled analogue switches developed for ultrasonic signals [5.17] was connected to the myRIO. For each of the nine elements, a single digital signal was used directly through the FPGA. The output of each microphone was summed into the same

analogue input port, which was then converted digitally and connected to the FPGA using the myRIOs on board ADC the maximum sample frequency being 500 KHz. Appendix Figure A.1 shows how the code compiled onto the FPGA was written.

The FPGA on the myRIO operates by default using a 40 MHz clock but this can be divided for faster frequencies. This means that between samples at the maximum analogue input rate, there will be 80 ticks for the FPGA to action the next stage of a switching pattern. By determining that a digital switch between elements occurs well before the analogue sample is taken it can be guaranteed that the same number of samples for each element are taken at a consistent rate.

The costs of FPGAs are decreasing steadily over time [5.18], however systems with FPGAs such as the myRIO are considerably more expensive than the rest of the array design.

5.5   Very Low-cost Design for DoA Estimation

The techniques described in 3 and 4 were developed with some mindfulness of reducing computational complexity, and whilst FPGAs are capable of performing time modulation tasks exactly as requested it would not be practical to utilize one for a low-cost or low profile implementation. Many small, low cost devices with specific functionality use an embedded microcontroller to handle specific tasks. A major issue with using controllers such as these is their slow data-acquisition speed. In time-modulation, great care needs to be taken in order sample the analogue channel at regular intervals, as not to distort the result of the DFTs.

There a numerous low-cost "off the shelf" data acquisition devices that are able to sample at the speed required for acoustical TMAs. For RF applications, low-cost implementations require mixing of the signal into a lower intermediate frequency (IF) so that it can be sampled by an Analogue to Digital Converter (ADC). Due to this difference, RF implementations may be more expensive than a similar acoustic implementation and therefore the example given in this section continues to focus on sound detection.

The mbed LPC1768 is a prototyping microcontroller [5.19] containing readily available accessories, such as a USB connector for serial communication, digital ports, an ADC capable of sampling speeds of up to 200 kHz and a set of four Light Emitting Diodes. The board is controlled by an ARM Cortex-M3 microprocessor and is compatible with the lightweight mbed online compiler. Such a system is common in low-cost data-acquisition and processing tasks, but literature showing examples of using one for time-modulation is severely limited. The following sections describe an implementation of a five-element TMA using the LPC1768.

5.5.1 Software Design

The LPC1768 runs code through the mbed platform and uses its lightweight online compiler [5.20] to compile C++ code into a binary file used by the device. The use of this compiler allowed for rapid development of a C++ implementation of the DoA algorithm as seen in Chapter 3. Figure 5.9 shows a flow diagram of the program written onto the device to test the TMA. The onboard LEDs of the LPC1768 were turned on in relation to the estimated signal DoA. The device was also set up to send a numerical value through the onboard USB serial interface. The code running on the LPC1768 can be found in Appendix Section A.

5.5.2 Results

As can be seen in Figure 5.10, the microcontroller correctly indicates the general position of the source through the LEDs and shows a great potential for the use of this technology in applications such as low-cost robotics and guidance systems.

Although consistent, the numerical values given (as can be seen in Figure 5.11) are inaccurate and skewed towards a particular end-fire angle depending on the sample frequency set. This is thought to be due to the sampling function not being called at consistent periods, or due to a number of periodic misreadings seen on the device.
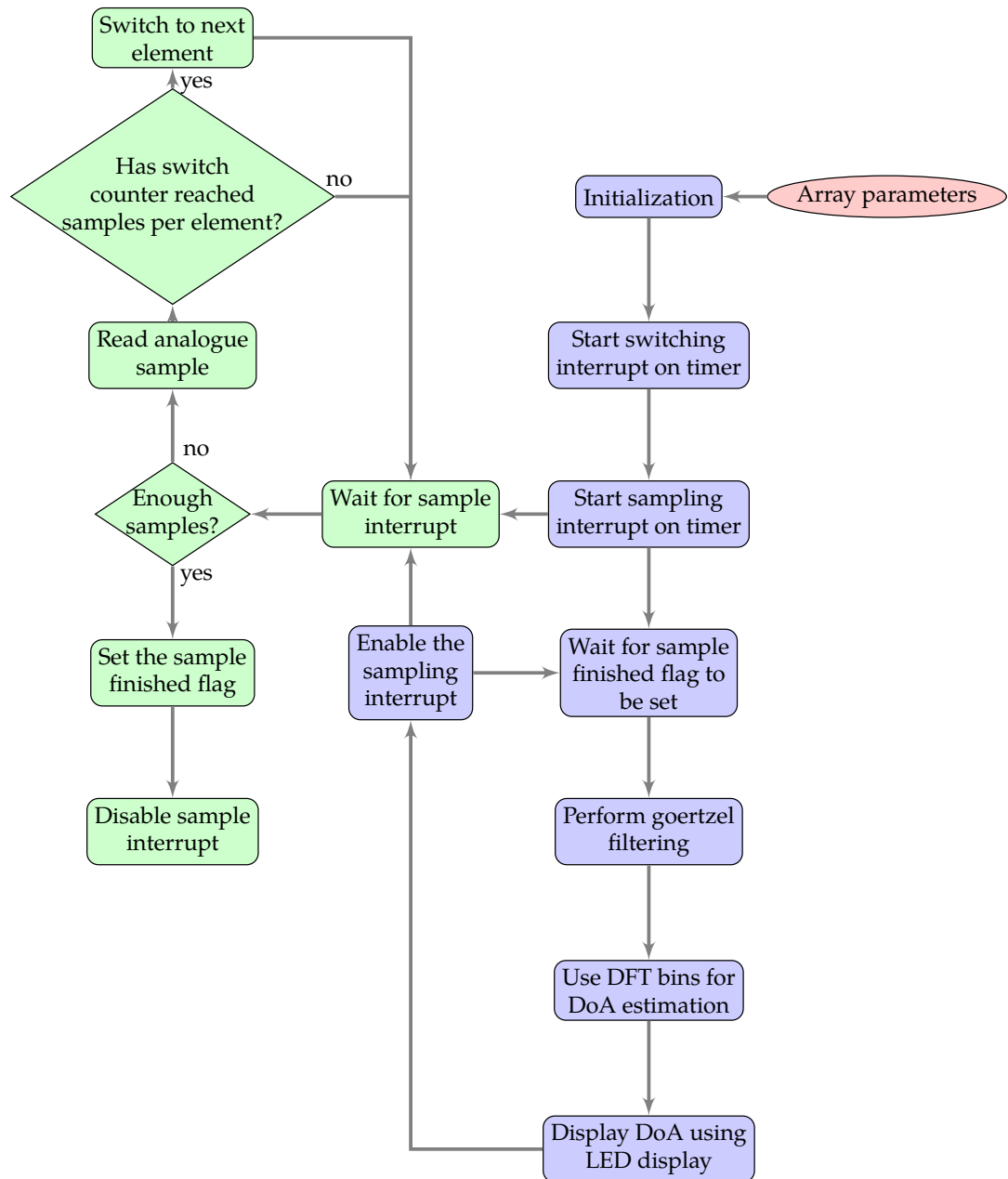
Figure 5.9: Software diagram of time-modulation integration on an LPC1768 Microcontroller
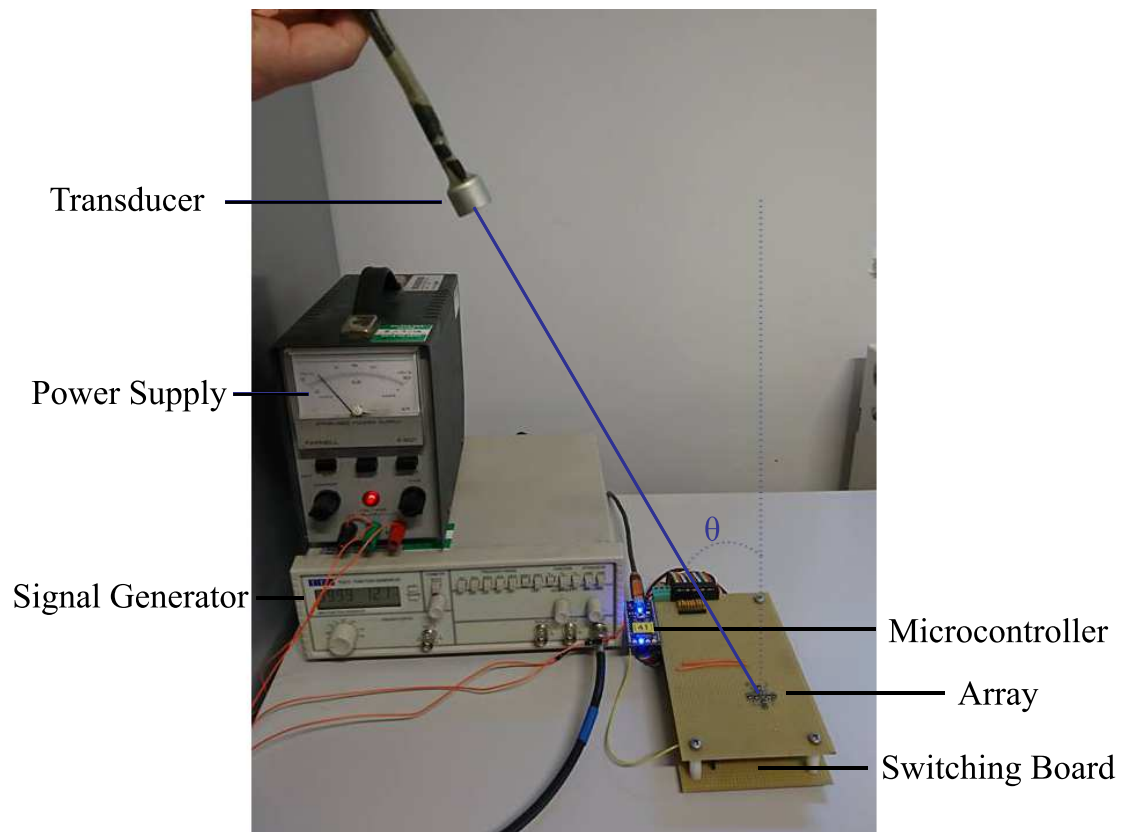
Figure 5.10: The linear array of 5 microphones being sampled and switched using a LPC1768 running code compiled on the mbed online compiler. The photo shows the source propagating towards the array at an angle θ and the LED on the microcontroller has turned on to indicate the source is slightly to the left of the array.
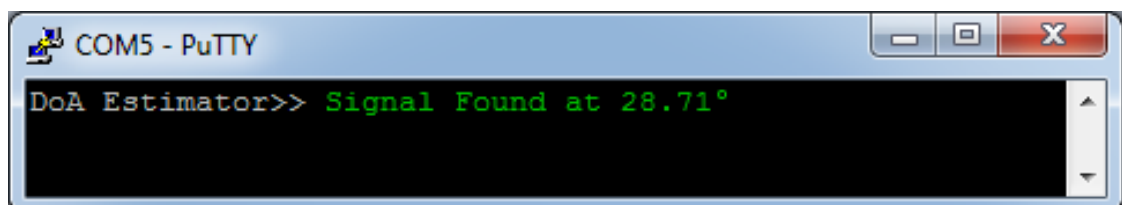
Figure 5.11: Using the USB serial port to transmit the DoA estimation to a terminal.

5.6   Conclusion

Aspects of software and hardware have been considered and a simulation which demonstrates the concepts developed in this thesis has been created. The simulation and its user interface can be used as a tool for demonstrating how one or two dimensional TMAs behave with a given set of parameters.

Once a TMA design has been conceptualised numerically, the next stage in implementation is to use suitable hardware, and it has been shown that the algorithms demonstrated in this thesis are suitable for use on FPGAs or low-cost microcontrollers.

When designing TMAs for DoA applications, a choice between performance and cost needs to be considered. The use of FPGAs for controlling and sampling the array is recommended when numerical precision is required. However if only a rough estimate is required, the use of low-cost microcontrollers are sufficient. When designing a bespoke system, a low-cost microcontroller paired with a high-speed ADC may offer the best compromise between the two criteria.

References

[5.1] H. Al-Saedi, W. M. Abdel-Wahab, S. Gigoyan, A. Taeb, and S. Safavi-Naeini, "A low-cost wideband phase shifter for two-way mm-wave phased array antenna system," *Int. J. Microw. Wirel. Technol.*, vol. 10, no. 01, pp. 77–86, February 2018.

[5.2] National Instruments, "LabVIEW," 2015.

[5.3] Y. Tong and A. Tennant, "Simultaneous control of sidelobe level and harmonic beam steering in time-modulated linear arrays," *Electron. Lett.*, vol. 46, no. 3, p. 200, 2010.

[5.4] A. Bresler, "A new algorithm for calculating the current distributions of dolph-chebyshev arrays," *IEEE Trans. Antennas Propag.*, vol. 28, no. 6, pp. 951–952, November 1980.

[5.5] J. M. Blackledge, *Digital Signal Processing - Mathematical and Computational Methods, Software Development and Applications*, 2nd ed.   Horwood Publishing, 2006.

[5.6] G. Goertzel, "An Algorithm for the Evaluation of Finite Trigonometric Series," *Am. Math. Mon.*, vol. 65, no. 1, pp. 34–35, January 1958.

[5.7] R. Y. Tara and T. B. Adji, "Robust and low-cost proximity sensor for line detection robot using goertzel algorithm," in *2011 2nd Int. Conf. Instrum. Control Autom.* IEEE, November 2011, pp. 340–343.

[5.8] S. N. Bhavanam, P. Siddaiah, and P. R. Reddy, "FPGA based efficient DTMF detection using Split Goertzel algorithm with optimized resource sharing approach," in *2014 Elev. Int. Conf. Wirel. Opt. Commun. Networks.* IEEE, September 2014, pp. 1–8.

[5.9] T. Lysaght, J. Timoney, and S. Brown, "An Evaluation of the Goertzel Algorithm for Low-Power, Embedded Systems," in *25th IET Irish Signals Syst. Conf. 2014 2014 China-irel. Int. Conf. Inf. Communities Technol. (ISSC 2014/CIICT 2014).* Institution of Engineering and Technology, 2014, pp. 357–361.

[5.10] S. R. Chowdhury, "Signal Processing through Field Programmable Gate Arrays: Prospects and Challenges," *Recent Patents Signal Process.*, vol. 2, pp. 1–5, 2010.

[5.11] S. Dikmese, A. Kavak, K. Kucuk, S. Sahin, A. Tangel, and H. Dincer, "Digital signal processor against field programmable gate array implementations of space–code correlator beamformer for smart antennas," *IET Microwaves, Antennas Propag.*, vol. 4, no. 5, p. 593, 2010.

[5.12] T. W. Nuteson, J. S. Clark, D. S. Haque, and G. S. Mitchell, "Digital Beamforming and Calibration for Smart Antennas using Real-Time FPGA Processing," in *2002 IEEE MTT-S Int. Microw. Symp. Dig. (Cat. No.02CH37278)*, Seattle, WA, USA, 2002, pp. 307–310.

[5.13] A. Izquierdo, J. J. Villacorta, L. Del Val, L. Suárez, and D. Suárez, "Implementation of a virtual microphone array to obtain high resolution acoustic images," *Sensors*, vol. 18, no. 1, 2018.

[5.14] C. He, L. Wang, J. Chen, and R. Jin, "Time-Modulated Arrays: A Four-Dimensional Antenna Array Controlled by Switches," *J. Commun. Inf. Networks*, vol. 3, no. 1, pp. 1–14, Mar 2018.

[5.15] M. Devendra and K. Manjunathachari, "Direction of Arrival Estimation Using MUSIC Algorithm in FPGA: Hardware Software Co-Design," *Int. J. Appl. Eng. Res.*, vol. 11, no. 5, pp. 3112–3116, 2016.

[5.16] K. Huang, J. Sha, W. Shi, and Z. Wang, "An Efficient FPGA Implementation for 2-D MUSIC Algorithm," *Circuits, Syst. Signal Process.*, vol. 35, no. 5, pp. 1795–1805, May 2016.

[5.17] B. Clark, "Acoustic tracking of a moving bat using linear arrays," MEng Project Report (Unpublished), Loughborough University, 2014.

[5.18] S. M. Trimberger, "Three Ages of FPGAs: A Retrospective on the First Thirty Years of FPGA Technology," *Proc. IEEE*, vol. 103, no. 3, pp. 318–331, March 2015.

[5.19] Mbed, "mbed LPC1768," 2017. [Online]. Available: https://developer.mbed.org/platforms/mbed-LPC1768/

[5.20] Arm Limited, "mbed Compiler - handbook." [Online]. Available: https://os.mbed.com/handbook/mbed-Compiler

6 | Conclusion

By making comparisons between the components in the harmonic content generated by the distributed switching of an array, a good approximation of the signal's arrival angle can be obtained. The use of analysing real-valued sideband amplitudes and simple linear approximations means that the DoA techniques can be made low cost.

6.1 Summary of Contributions in this Thesis

This thesis has shown how time-modulated planar arrays can be used to obtain a two-dimensional direction of arrival estimation. A novel technique was first demonstrated using a one-dimensional variant for time-modulated linear arrays. This technique has then been developed further to show its potential for two-dimensional estimations using time-modulated planar arrays. The work has demonstrated this using a physical microphone array consisting of five-elements, but verified the two-dimensional case with use of a novel, run-time configurable simulation.

It has also been shown that the algorithms can be made to run on low-end processors, and the resolution of a DoA estimate can be maintained provided that the signal is sampled and switched sufficiently.

The caveat of the techniques outlined in this work is that they require a larger number of elements than other TMA techniques to maintain high levels of accuracy. However, the extra sideband content generated by arrays of larger sizes means that the DoA algorithms are more immune to noise and multipath interference, even when using the same number of total samples.

6.2   Further Research

The work in this thesis has given rise to additional work that requires further research.

6.2.1   Printed Circuit Board Implementations

Printed circuit boards (PCBs) can be designed and manufactured using computer aided software. This allows an electronic system to be constructed with precise dimensions. For TMAs this is a benefit for two reasons: First, the array can be constructed in such a way that more sensors can be placed within a small footprint, even whilst having the switching systems built-in. Secondly, the the ability to be precise with component placement will make sure that the array is equally spaced, making the techniques mentioned in this thesis more accurate.

Whilst an array of 5 elements has been demonstrated, the techniques could be further verified using an array with a greater number of elements and with more precise construction. It is expected that even when utilizing five elements, using a PCB will show better DoA estimation performance.

Furthermore, a planar array that achieves 2D estimation should be constructed so that the contents of Chapter 4 can be verified with a real implementation. This work will also put into context the scalability of time-modulated arrays using many elements.

6.2.2   Time-Modulated Speaker Arrays

The majority of this thesis has focused on TMAs as a receiver only. However, the effect of switching an array of transmitters has the same effect on harmonic power spreading and directivity.

Further exploring the use of time modulation in the acoustics domain, a time-modulated array of loud speakers has not been fully explored. Work was carried out by Paulo Westphal-Caetano[6.1] using the guidance and information detailed in this thesis, and
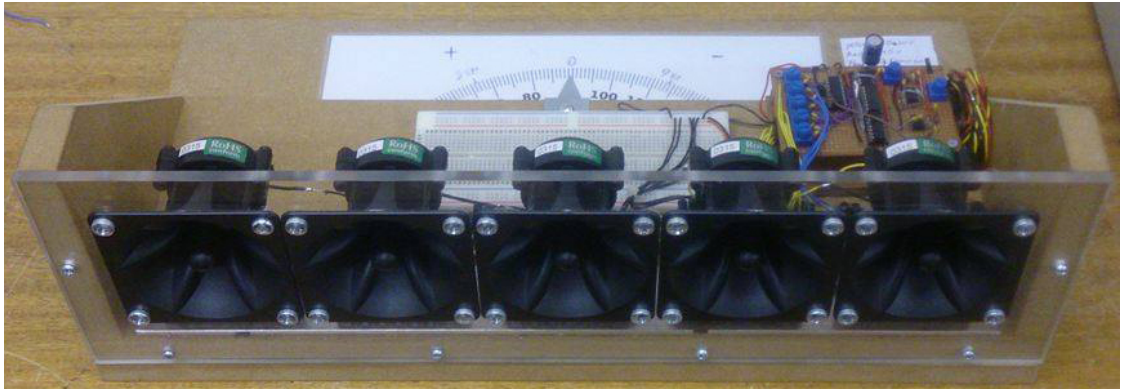
Figure 6.1: Photo of the Speaker Array Configuration, showing the types of speakers used and their spacing.

was able to construct a Time-Modulated speaker array which transmitted a high-frequency audible signal into five speakers spaced out equally in a line.

Whilst the expected sidebands of the time-modulated array were generated, there was a high level of unexpected frequency content. More analysis into the phenomena is needed, but a receive/transmit pair of TMAs would be an interesting study, especially for research in communication applications.

Using the theories discussed in this thesis, the ratio of harmonic content received by a microphone listening to a signal transmitted by a TMA may be able to calculate certain properties. If the angular heading of the transmitting object is known then its orientation can be calculated. Likewise, if the orientation of the object is known, then its angular heading can be calculated.

References

[6.1] P. Westphal-Caetano, "Speaker Array for Human Navigation," MEng Project Report (Unpublished), Loughborough University, 2016.

A | Programming Samples

A.1 LPC1768 TMLA DoA Code

```cpp
1   ////////////////////////////////////////////////////////////////
2   // Main - C++ File                                           //
3   // Ben Clark, Wolfson School - Lougborough University        //
4   ////////////////////////////////////////////////////////////////
5   // This function  uses a LPC1768 to continously obtain samples  //
6   // for a TMLAs and then requests an estimation of an angle. It   //
7   // displays this on the LEDs on the device or through the USB   //
8   // serial port.                                              //
9   ////////////////////////////////////////////////////////////////
10
11  ////////////////////////////////////////////////////////////////
12  // Includes              ////////////////////////////////////
13  ////////////////////////////////////////////////////////////////
14
15  //mbed specific libs
16  #include "mbed.h"
17  #include "FastAnalogIn.h"
18
19  //General C/C++ libs
20  #include "math.h"
21  #include "string.h"
22
23  #define SAMPLE_FREQ         150000          //Analogue input frequency
24  #define TARGET_FREQ         40000           //Incident signal main frequency
25  #define SAMPLES_PER_SENSOR 50
26  #define NUMBER_OF_SENSORS   5
27  #define TOTAL_SAMPLES       (SAMPLES_PER_SENSOR * NUMBER_OF_SENSORS)
28  #define NUMBER_OF_BINS      5
29  #define HARMONIC_FREQ       (SAMPLE_FREQ / TOTAL_SAMPLES)
30  #define D_SPACING           0.5
31  #ifndef PI
32      #define PI              3.14159265359   //Pi used in DFT calculations
33  #endif
34
35  ////////////////////////////////////////////////////////////////
36  // Global Variables                //////////////////////////
37  ////////////////////////////////////////////////////////////////
38
39  Serial  pc(USBTX, USBRX); // tx, rx
40
41  unsigned int      samplecount = 0;
```

```cpp
42  unsigned int      sensorcount = 0;
43  unsigned int      sensorcountprev = 0;
44  volatile bool     samplerFinished = false;
45  float             sample[TOTAL_SAMPLES] = {0};
46  uint64_t          takenat[TOTAL_SAMPLES] = {0};
47
48
49  DigitalOut        DigitalLine[NUMBER_OF_SENSORS] = {p21, p22, p23, p24, p25};
50  DigitalOut        d5(p26), d6(p27), d7(p28), d8(p29), d9(p30), d10(p10), d11(p11);
51  FastAnalogIn      ain(p15,1);
52  DigitalOut        led[4] = {LED1, LED2, LED3, LED4};
53
54  /////////////////////////////////////////////////////////////////
55  // Functions                        /////////////////////////////////
56  /////////////////////////////////////////////////////////////////
57
58  /////////////////////////////////////////////////////////////////
59  // Take a single sample and switch to the next sensor if necessary
60  void sampler()
61  {
62      //Only process if sampler hasn't finished
63      if (!samplerFinished) {
64          //Value is floating at around 2.5V, ain is a scaled value from 0-1
65          sample[samplecount] = (ain - 0.722);
66
67          //Evaluate which sensor is supposed to be switched on next sample
68          sensorcount = ++samplecount / SAMPLES_PER_SENSOR;
69
70          //Set the digital line accordingly
71          if ((sensorcount != sensorcountprev)
72                  && (sensorcount != NUMBER_OF_SENSORS)) {
73              DigitalLine[sensorcountprev] = 0;
74              DigitalLine[sensorcount] = 1;
75              //In the specific electronics case, sensor2 is also sensor7
76              if (sensorcount == 2) d7=1;
77              else d7=0;
78          }
79          sensorcountprev = sensorcount;
80
81          //Check to see if next iteration should do anything
82          samplerFinished = (samplecount == TOTAL_SAMPLES);
83      }
84      //Clear the interrupt so that it can flag again
85      LPC_TIM0->IR = 1;
86  }
87
88  /////////////////////////////////////////////////////////////////
89  //Set up the internal registers of the LPC1768
90  void initTimer()
91  {
92      // Enable TIMER0
93      LPC_SC->PCONP |= 1 << 1;
94
95      // Reset and set TIMER0
96      LPC_TIM0->TCR = 0x2;
97      LPC_TIM0->CTCR = 0x0;
98
99      // No prescaler
100     LPC_TIM0->PR = 0;
101
102     // Set match register
```

```
103      LPC_TIM0->MR0 = (SystemCoreClock / 4)/SAMPLE_FREQ; // timer speed
104      LPC_TIM0->MCR |= 1 << 0;                              // interrupt on match
105      LPC_TIM0->MCR |= 1 << 1;                              // reset on match
106
107      // Use the sample function when interrupt is matched
108      NVIC_SetVector(TIMER0_IRQn, (uint32_t)&sampler);
109      NVIC_EnableIRQ(TIMER0_IRQn);
110  }
111
112  /////////////////////////////////////////////////////////////////
113  //Displays DoA to inbuilt LED and as a specific number to USB
114  void displayDoA(double estimate, double maxBin)
115  {
116      //Disable the console, and print at the start of the line
117      pc.printf("\x1b[?25l\x1b[0mDoA Estimator>> ");
118
119      //Check to see if any signal is present
120      if (maxBin > 0.01) {
121
122          //Set an LED depending on the DoA
123          led[3] = (estimate > 26.5);
124          led[2] = (estimate > -13.25) && (estimate < 39.75);
125          led[1] = (estimate < 13.25) && (estimate > -39.75);
126          led[0] = (estimate < -26.5);
127
128          //Print the specific number (in green) on a terminal
129          pc.printf("\x1b[32mSignal Found at %05.2f\xB0            \r", estimate);
130      } else {
131          //Otherwise, LEDs should be off
132          led[0] = led[1] = led[2] = led[3] = 0;
133
134          //Print a warning message (in red) on a terminal
135          pc.printf("\x1b[31mNo Signal found!                    \r", estimate);
136      }
137  }
138
139  /////////////////////////////////////////////////////////////////
140  // Main                           /////////////////////////////////
141  /////////////////////////////////////////////////////////////////
142  int main()
143  {
144      //Initialise the arrays used in the calculation once
145      double  DFT_Bin[NUMBER_OF_BINS] = {};
146      double  coeff[NUMBER_OF_BINS] = {};
147      double  S[NUMBER_OF_BINS][3] = {};
148
149      //These belong to other sensors on a specific setup
150      d5 = d6 = d7 = d8 = d9 = d10 = d11 = 0;
151
152      //Initialise the sample interupt timer
153      initTimer();
154
155      //Initialise any calculated variables
156      for (unsigned int i = 0 ; i < NUMBER_OF_BINS ; i++) {
157          int m = (int)i - (int)floor((double)(NUMBER_OF_BINS/2));
158          double bin_freq = TARGET_FREQ + (m*HARMONIC_FREQ);
159
160          coeff[i] = 2*cos(2*PI*(bin_freq/SAMPLE_FREQ));
161      }
162
163      //Loop forever
```

```
164        while(true) {
165
166            //Reset each variable on loop
167            double        maxBin, cmpBin = 0;
168            unsigned int index = 0;
169            int maxIndex,cmpIndex = 0;
170            memset(DFT_Bin,0,NUMBER_OF_BINS*sizeof(double));
171            samplecount = sensorcount = sensorcountprev = 0;
172            samplerFinished = false;
173
174            //Set the first microphone on
175            DigitalLine[0] = 1;
176            for (unsigned int i = 1 ; i < NUMBER_OF_SENSORS ; i++)
177            DigitalLine[i] = 0;
178
179            //Start sampling!
180            LPC_TIM0->TCR = 1;              //Start the sampler
181            while(!samplerFinished);       //Wait until done
182            LPC_TIM0->TCR = 0;             //Stop the sampler
183
184            //Begin Goertzel Algorithm
185            for (unsigned int x = 0 ; x < TOTAL_SAMPLES ; x++) {
186                for (unsigned int i = 0 ; i < NUMBER_OF_BINS ; i++) {
187
188                    //Reset second-order filter on first iteration
189                    if (x == 0) {
190                        S[i][1] = 0;
191                        S[i][2] = 0;
192                        maxBin = cmpBin = 0;
193                    }
194
195                    //Filter the signal
196                    S[i][0] = sample[x] + (coeff[i] * S[i][1]) - S[i][2];
197                    S[i][2] = S[i][1];
198                    S[i][1] = S[i][0];
199
200                    //After the last iteration of the filtering
201                    if ((x + 1) == TOTAL_SAMPLES) {
202
203                        //Calculate the final part
204                        double partone = (S[i][1] * S[i][1]) + (S[i][2] * S[i][2]);
205                        double parttwo = S[i][1] * S[i][2] * coeff[i];
206                        DFT_Bin[i] = sqrt(partone-parttwo); //no need to scale.
207
208
209                        //Determine the largest harmonic
210                        if (DFT_Bin[i] > maxBin) {
211                            maxBin = DFT_Bin[i];
212                            index = i;
213                            maxIndex = i-(int)floor((double)(NUMBER_OF_BINS/2));
214                        }
215                    }
216                }
217            }
218
219            //Find the next appropriate frequency bin to use in the estimation
220            //If the largest harmonic is at the end, there is only one adjacent
221            if (index == 0) {
222                cmpBin = DFT_Bin[1];
223                cmpIndex = maxIndex+1;
224            } else if (index == NUMBER_OF_BINS-1) {
```

```
225            cmpBin = DFT_Bin[NUMBER_OF_BINS−2];
226            cmpIndex = maxIndex − 1;
227
228        //Otherwise find which of the two adjacent bins is larger
229        } else if (DFT_Bin[index+1] > DFT_Bin[index−1]) {
230            cmpBin = DFT_Bin[index+1];
231            cmpIndex = maxIndex + 1;
232        } else {
233            cmpBin = DFT_Bin[index−1];
234            cmpIndex = maxIndex−1;
235        }
236
237        //Perform the estimation
238        float estimateIndex = (((maxBin * (float)maxIndex) + (cmpBin * (float)cmpIndex))
239                        /(maxBin + cmpBin));
240
241        float estimate=asin(estimateIndex/(D_SPACING*NUMBER_OF_BINS))*180.0/PI;
242
243        //Display the estimation
244        displayDoA(estimate,maxBin);
245    }
246 }
```
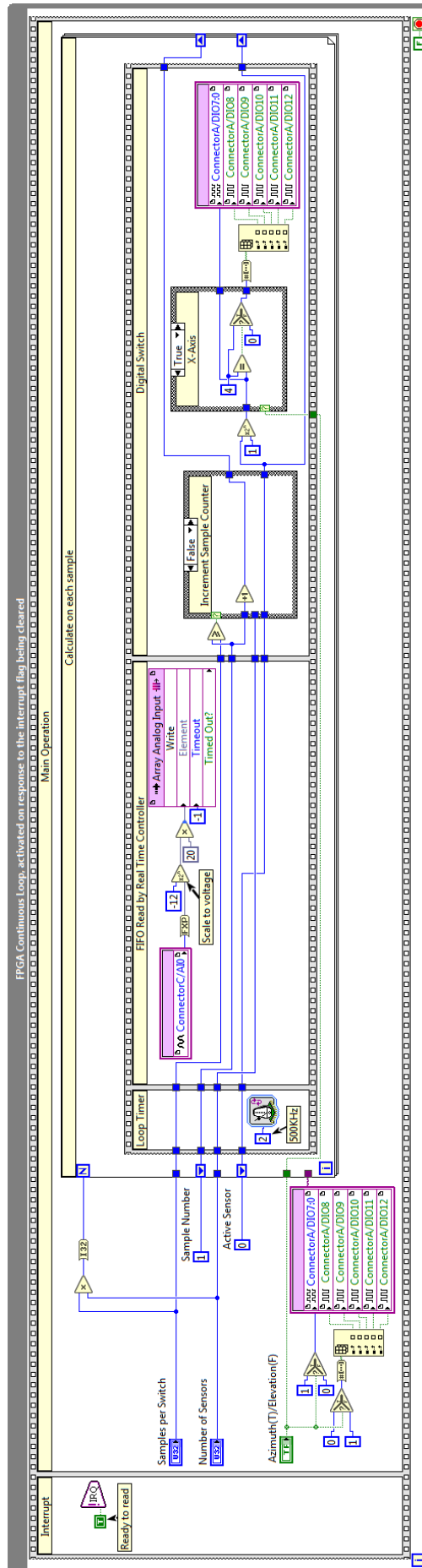
A.2   LabVIEW FPGA Code

Figure A.1: Screenshot of the LabVIEW code written for switching and sampling through the nine-element cross array.